Astron Astrophys Rev (2023) 31:1
https://doi.org/10.1007/s00159-022-00146-x

REVIEW ARTICLE

Origin of the elements

Almudena Arcones[1,2] · Friedrich-Karl Thielemann[2,3]

Received: 31 May 2022 / Accepted: 26 October 2022 / Published online: 13 December 2022
© The Author(s) 2022

Abstract

What is the origin of the oxygen we breathe, the hydrogen and oxygen (in form of water H_2O) in rivers and oceans, the carbon in all organic compounds, the silicon in electronic hardware, the calcium in our bones, the iron in steel, silver and gold in jewels, the rare earths utilized, e.g. in magnets or lasers, lead or lithium in batteries, and also of naturally occurring uranium and plutonium? The answer lies in the skies. Astrophysical environments from the Big Bang to stars and stellar explosions are the cauldrons where all these elements are made. The papers by Burbidge (Rev Mod Phys 29:547–650, 1957) and Cameron (Publ Astron Soc Pac 69:201, 1957), as well as precursors by Bethe, von Weizsäcker, Hoyle, Gamow, and Suess and Urey provided a very basic understanding of the nucleosynthesis processes responsible for their production, combined with nuclear physics input and required environment conditions such as temperature, density and the overall neutron/proton ratio in seed material. Since then a steady stream of nuclear experiments and nuclear structure theory, astrophysical models of the early universe as well as stars and stellar explosions in single and binary stellar systems has led to a deeper understanding. This involved improvements in stellar models, the composition of stellar wind ejecta, the mechanism of core-collapse supernovae as final fate of massive stars, and the transition (as a function of initial stellar mass) from core-collapse supernovae to hypernovae and long duration gamma-ray bursts (accompanied by the formation of a black hole) in case of single star progenitors. Binary stellar systems give rise to nova explosions, X-ray bursts, type Ia supernovae, neutron star, and neutron star–black hole mergers. All of these events (possibly with the exception of X-ray bursts) eject material with an abundance composition unique to the specific event and lead over time to the evolution of elemental (and isotopic) abundances in the galactic gas and their imprint on the next generation of stars. In the present review, we want to give a modern overview of the nucleosynthesis processes involved, their astrophysical sites, and their impact on the evolution of galaxies.

Keywords Element abundance · Big Bang nucleosynthesis · Stellar evolution · Core collapse · Supernovae · Compact binary mergers · Galactic evolution

Extended author information available on the last page of the article

Contents

1 Introduction

The origin of the elements has been an essential question in the history of mankind. In its modern form, since the creation of the periodic table of chemical elements, the understanding of their possible sources in the universe has been an open question.

What do we know at present? What are the key challenges and opportunities? The seminal works of Burbidge et al. (1957) (B^2HF) and Cameron (1957b, 1957a) provided a first summary of the different nuclear processes producing all elements and isotopes found in nature. Most of their original ideas are still valid, but since then our understanding has tremendously improved. Here we attempt to review the nucleosynthesis processes, their astrophysical sites, and how they affect the evolution of galaxies. Before starting with a detailed discussion, we want to present the motivation asking for combined explanations, based essentially on observations (a) of individual events and (b) their integrated features in the evolution of galaxies. Therefore, in this introduction, we address first the approaches to observe nucleosynthesis sites in Sect. 1.1, the imprint of these sites on galactic evolution and specifically on solar abundances in Sect. 1.2, before starting with an introductory overview of the individual nucleosynthesis processes in Sect. 1.3. In the following sections, we will pass through the individual sites from the Big Bang to stars, stellar evolution, and stellar explosions in single and binary systems, before returning at the end to the understanding of the evolution of galaxies with the knowledge of the previous sections.

1.1 Abundance observations of individual astrophysical sites

In the abstract, we listed already many astrophysical sites, from the Big Bang, via stellar winds from evolving stars, stellar explosions like novae, core-collapse and type Ia supernovae, compact binary stellar mergers—leading to kilonovae, to very massive stars leading to collapsars and hypernovae, or even pair-instability supernovae. How can we address the question which abundances these events eject?

The Big Bang cannot be observed directly, but its results can be viewed in low metallicity gas at high redhifts, probing conditions early in the universe before extensive star formation took place. The ^{2}H/H ratio can be deduced from absorption lines seen in cold intergalactic clouds (through the light of bright background galaxies—quasars) as a function of their redshift. Therefore, the best constraints on the deuterium abundance come from these quasar absorption lines. This is an excellent application of the JWST with near to mid-infrared capabilities, launched only very recently. The primordial He determination is based on detecting He emission lines in low metallicity H II regions in dwarf galaxies.

Nova abundance observations can be undertaken in the visible and UV with optical telescopes and UV Explorer Satellites. It is more difficult to make use of more powerful explosions like supernovae, because the fast expansion leads to Doppler broadening and associated blending of spectral features, which make line identifications of specific elements not easy. However, sophisticated radiation hydrodynamics modelling, combined with observational spectra, can provide further insight, especially for the more compact type Ia supernovae (without an extended H envelope). As a function of time during the expansion the spectra scan through the element abundances from outer to inner layers. A further view comes from light curve observations, which indicate the amounts of radioactive decay energy from ^{56,57}Ni and Co (as well as ^{44}Ti in core-collapse supernovae). Direct gamma-ray

observations of these radioactive decays in supernovae and their remnants are another tool to get access to their abundance features. Here, the COMPTEL and INTEGRAL satellites played/play a leading role, also observing the spread of long-lived isotopes like ^{26}Al in the galaxy. The spatial and spectral resolutions of X-ray observations of supernova remnants (e.g. from Chandra or XMM Newton satellites) have also presented the opportunity to study the chemical and physical structure of the explosion debris. Supernova remnants can thus put strong constraints on the fundamental aspects of supernova explosion physics. This view of the supernova phenomenon is completely independent of, and complementary to, the study of distant extragalactic supernovae at optical wavelengths. A further important fact is that stellar winds lead to dust formation, which also takes place in supernova explosions. Isotopic abundance properties in meteoritic inclusions can directly point back to dust grains from such events.

New challenges have come with gravitational wave observations of compact binary mergers, which reveal the details of involved merging masses. Optical and IR observations of the resulting kilonova event bear the possibility to hint at the element content with the help of radiation transport simulations, requiring as input opacities of very heavy elements. Until now, only a Sr line identification has been achieved; however, the light-curve decline can be related to integrated decay energy of the involved heavy elements.

This has been only a quick survey of direct observational features related to individual nucleosynthesis sites; for a more detailed discussion of all these aspects, see a parallel review by Diehl et al. (2022). Here, we want to focus more on observations of old stars as witnesses for integrated nucleosynthesis contributions as a function of galactic evolution time. The event frequencies, and even their first emergence, determine the composition of the evolving interstellar medium. Our solar system composition represents only a snapshot in time and position in the galaxy. The understanding of this evolution needs observational backing. Old (lower mass, still unevolved) stars, going back to the first epochs in our galaxy, have surface compositions that are identical to the composition of gas out of which they formed. Thus, they are witnesses of the galactic evolution in time. There exist already a multitude of observations with terrestrial telescopes with the aim to determine such stellar surface abundances. These will be extended by major ongoing and future spectroscopic surveys such as Gaia-ESO, APOGEE, GALAH, LAMOST, WEAVE, and 4MOST. The HST with its optical and UV capabilities has been a working horse for stellar abundance determinations. Its scientific successor, the JWST, has no UV, but high-resolution capabilities in the mid and far infrared. The identification of element lines in the IR could thus provide additional clues to the operation of important nucleosynthesis processes. Progress in this quite interdisciplinary field includes the individual disciplines entering nucleosynthesis compositions, involving (a) nuclear physics in terms of reactions and also the high-density equation of state, (b) modelling and observations of stellar evolution, stellar explosions and their remnants up to observations of low metallicity stars, and (c) the combination of knowledge at the interface of these fields. The overall aim is an improved understanding of the evolution of our galaxy and its abundance content.

1.2 Element abundances in the Sun and galactic stars

This topic divides into two different aspects: (i) to find out and understand the composition of the abundances in the solar system and (ii) to understand their evolution in our galaxy the Milky Way and surrounding dwarf galaxies, giving possible clues for the different components that contributed, apparently also on different timescales.

Figure 1 shows a snapshot in time, i.e. the element composition of the interstellar medium that formed the Sun about 4.57 Gyr ago. The reason that we can identify the surface abundances of stars with the composition of the gas out of which they formed is due to the fact that nuclear transformations take place only in the central parts [understood exceptions relate to giants where dredge-up processes via the deep-convective envelope cause modifications of the surface abundances]. This way one can actually follow a time evolution in the galaxy when looking at stars of different Fe/H abundance ratios, representing stars of different ages in the Milky Way. Figure 2 shows such a collection as a function of $[Fe/H] = \log_{10}[\,(Fe/H)_{star}/\,(Fe/H)_{\odot}]$, with [X/Y] standing for the logarithm of the stellar to solar X/Y element ratio. If the enrichment of the galaxy with heavy elements like Fe increases as a function of time, [Fe/H] is also a measure of the element evolution as a function of time.

Opposite to the impression from Fig. 2 that all elemental abundances seem to vanish for the oldest stars in the galaxy, there exist exceptions for the light elements He and Li as well as the apparently well abundant H. It appears that while most of the elements we know on Earth are produced during the evolution of galaxies (probably

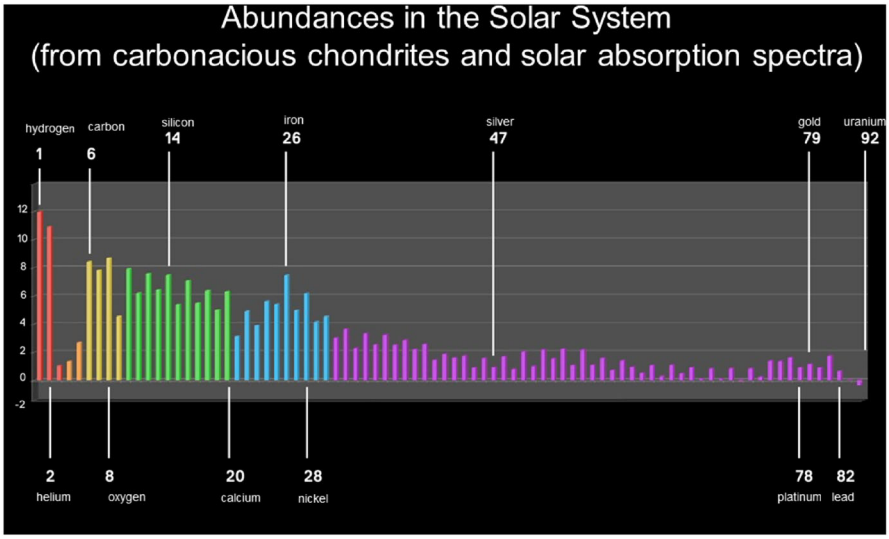

Fig. 1 Abundances of the elements in the solar system from solar absorption spectra and carbonaceous chondrites (primitive meteorites, which show no fractionation) on a logarithmic scale. Hydrogen is normalized to 10^{12} (based on Lodders 2021).

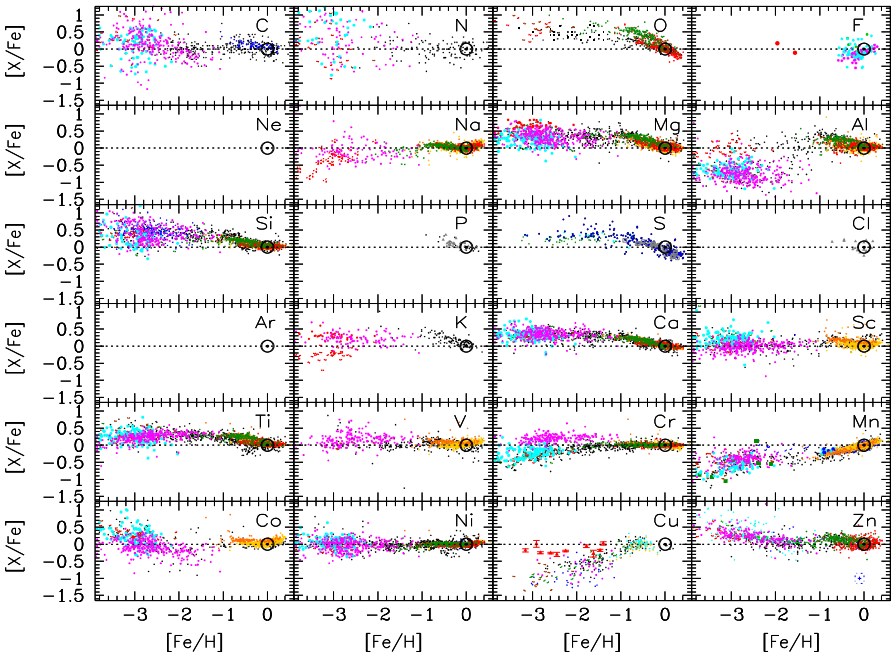

Fig. 2 Abundance ratios of various elements X in comparison to Fe [X/Fe] as a function of "metallicity" [Fe/H]. We will later discuss what causes the kinks in [X/Fe] ratios for O, Mg, Si, S, K, Ca, Ti and Mn at [Fe/H]$= -1$. However, what can be realized is that for the lowest metallicities, most of the [X/Fe] ratios become constant or even decline. Thus, with Fe abundances going to zero, the other abundances vanish as well, leading to the impression that all elements started out with initially vanishing but gradually augmenting abundances during the evolution of the galaxy. Image courtesy of N. Prantzos

due to the activity of stars), these light elements are inherited from preceding phases of the universe, we assign to the Big Bang.

In addition to the abundant information resulting from stellar spectra as shown in Fig. 2, which only provide knowledge about the sum of events that contributed to the galactic gas up to that time/metallicity, observations of individual events can help to characterize their distinct ejecta contributions. As already discussed in Sect. 1.1, these include, e.g. novae, stellar winds, supernovae, hypernovae, kilonovae, etc. To understand these individual events not only spectra are of importance, but also resulting dust condensations from ejecta can be found in meteoritic inclusions, and multi-messenger observations, including gravitational waves, neutrinos, gamma-rays, and X-rays can constrain the underlying mechanisms, and—when combined with theoretical modelling—provide a complete understanding of all these stellar sources. This requires further input from theory, terrestrial experiments, and, last but not least, sufficient computational power for modelling all these environments.

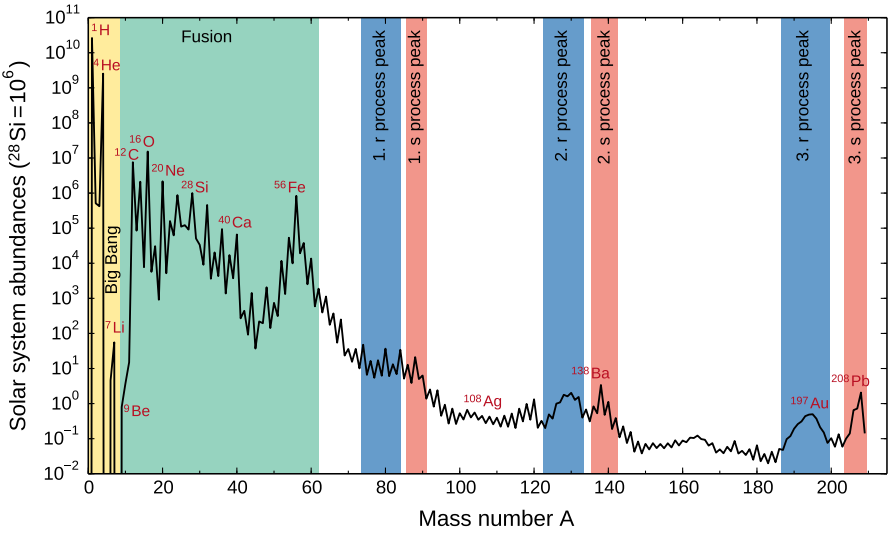

Fig. 3 Solar system abundances based on Lodders (2021) as a function of mass number A ($A = Z + N$), with Z being the number of protons and N the number of neutrons), normalized to Si at 10^6

1.3 Nucleosynthesis processes and their imprint on isotopic abundances

Elemental and isotopic abundances in the solar system contain the fingerprint of the nuclear processes involved in their production. Already in B^{2}HF (Burbidge et al. 1957), eight processes were identified. Most of them are still valid, others have changed slightly and there are new processes that have been discovered. To understand the origin of different isotopes, one can look at the solar system abundances (Fig. 3). The various features and trends in the solar system abundances are strongly related to the nuclear physics involved in the different nucleosynthesis processes shown in Fig. 4. In the nuclear chart, every square represents an isotope and those in the same horizontal line correspond to an element with given number of protons, Z. Therefore, the different squares along a line are various isotopes of the same element that have different number of neutrons, N. The stable isotopes are marked with black boxes, the grey region show the nuclei that have been produced already in the laboratory, and the light blue region covers the exotic isotopes where FAIR, FRIB, RIKEN, HIAF, RAON, ISOLDE, TRIUMF and SPES[1] will investigate their discovery. The various nucleosynthesis processes are schematically indicated by colored lines.

In the solar system and in the universe, the most abundant elements are hydrogen and helium that were produced already in the Big Bang (see Sect. 3). In the **Big Bang nucleosynthesis,** only hydrogen (with its isotopes ^{1,2}H), helium (with its isotopes ^{3,4}He) and ^{7}Li were created. Because of the absence of stable or even only long-lived nuclei with $A = 5$ and 8, the production of heavier nuclei is inhibited. Therefore, from an observational perspective, astronomers divided elements into H (often

[1] Worldwide leading and new/planned facilities for rare radioactive isotope beams.

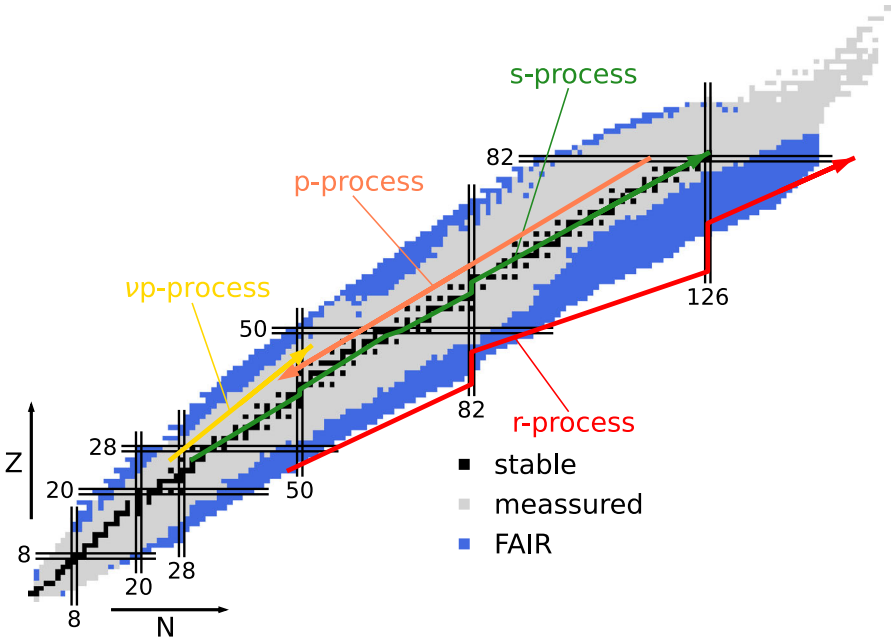

Fig. 4 In the nuclear chart, every square represents an isotope and those in the same line correspond to an element with a given number of protons, Z. Therefore, the different squares along a line are various isotopes of the same element that have a different number of neutrons, N. The stable isotopes are marked with black boxes, the grey region demarcates the nuclei that have been produced already in the laboratory, and the light blue region shows the exotic isotopes that rare isotope facilities will discover. The various nucleosynthesis processes are schematically indicated by coloured lines

abbreviated as X), He (often abbreviated as Y) and metals (everything beyond He and abbreviated as Z). All metals are made in stars during their life and death.

Different burning phases in the stellar interiors produce elements up to the iron group. These **stellar fusion stages** will be discussed in Sect. 4 and include hydrogen burning through pp chains and CNO cycles, He burning, and further burning phases. In the late burning stages for massive stars, the temperature in the centre becomes extremely high. Therefore, photons have sufficient energy to dissociate the freshly produced nuclei and a chemical equilibrium is reached. This is known as nuclear statistical equilibrium (NSE) and will be discussed in Sect. 2. If we look at the solar system abundances in the region from $A = 12$ to $A = 60$, there are two clear features: (i) a fast drop of the abundances with increasing proton number and (ii) a pronounced peak around iron. For low mass numbers, the abundance curve drops very fast due to the increasing Coulomb barriers, when nuclei with a larger number of protons are involved in the fusion reactions. These reactions involve alpha captures and create even–even nuclei with higher binding energies than their neighbors, thus the abundances are higher for the so-called alpha elements (^{12}C, ^{16}O, ^{20}Ne, ^{24}Mg, ^{28}Si, ^{32}S, ^{36}Ar, and ^{40}Ca). The other feature, namely the iron-group peak, is due to the stability of those nuclei that have the highest binding energy per nucleon.

The abundance curve presents a completely different trend beyond iron with a close to flat slope in three steps between double-peak structures related to neutron-shell closures. This points to different nuclear processes that do not involve protons. Indeed most of the isotopes beyond iron are produced by neutron capture processes as already reviewed by B^2HF (Burbidge et al. 1957; Cameron 1957a, b): the s-process and the r-process. When a nucleus captures a neutron, this includes a shift by one unit to the right in the nuclear chart (Fig. 4). If the new nucleus is unstable, the further evolution will depend on the amount of available neutrons. For low neutron densities, the newly formed unstable isotope will in most cases beta decay to a stable isotope before a new neutron is captured. In this case, we talk about the **s-process** where the neutron capture is **s**low compared to the beta decay. In contrast, if the neutron density is very high, many neutrons can be captured, leading to nuclei with very short beta-decay lifetimes. Due to small neutron-capture Q-values far from stability, even small photon energies—attained already for temperatures just above 10^9 K—cause sufficiently high photodisintegration rates (see Eq. (11)), determining in competition with neutron captures a path (see Eq. (29) in Sect. 4.2.3) where maximum abundances in each isotopic chain result (see Fig. 4). This path connects the so-called waiting point nuclei, and their beta decays control the progress towards heavier nuclei. This is the **r**apid neutron capture process (**r-process**) that reaches extreme and unknown neutron-rich nuclei. Both processes leave a fingerprint in the solar system abundances, namely the double peak structure around $A = 80$, 130–140, and 195–208. These are produced by accumulation of matter at nuclei with closed neutron shells (the magic neutron numbers $N = 50, 82, 126$), but related to different proton numbers and therefore different mass numbers, for each of these processes (see Fig. 4).

Here we discuss the solar system abundances via different processes, but it should be considered that these processes do not need to result from unique contributions. They can in fact be the result of many superpositions during galactic evolution until the formation of the solar system. In this respect, it should also be pointed out that so-called **primary and secondary nucleosynthesis processes** exist. The secondary processes require pre-existing nuclei in the starting composition that were produced in previous stellar generations. The s-process, where the neutrons can be captured on pre-existing Fe, is an example of a secondary process. Primary processes synthesize elements starting from the burnt hydrogen and helium of the initial stellar starting composition or from nucleons and nuclei produced in nuclear statistical equilibrium in the same astrophysical site, not in a previous event.

The solar system abundances of Fig. 3 seem to show double peaks above $A = 80$ (i.e. at around 130 and 197, which is at $A = 80$ not yet that clearly visible). The s-process experiences abundance pile-ups due to small neutron capture rates at closed neutron shells at or near stability. The r-process speed is determined by beta-decay half-lives, the longest being close to stability. Therefore pile-ups occur at the top of the kinks in the r-process path at neutron-shell closures far from stability. After beta-decay back to stability, this causes peaks at lower mass numbers than the s-process peaks, e.g. the peak at $A \sim 130$ is due to $N = 82$ and $Z \sim 50$. The required high

neutron densities in the r-process point to an explosive astrophysical scenario, involving matter that is as neutron rich as in neutron stars.

While in this section we discuss mainly the different nucleosynthesis processes and not their astrophysical sites, we want to sidestep here for a moment to give a brief history on suggested sites for this process under extreme condition. In 1957, supernovae were suggested as the perfect site to produce heavy elements by the r-process. Many investigations afterwards have shown that this is very challenging, even if neutron-rich matter is ejected from a neutron star. As matter expands, neutrino reactions can change neutrons into protons, preventing an r-process. In the 1970s, the merger of a neutron star and a black hole was suggested as a potential candidate. This scenario has been also investigated in detail, especially in recent years in combination with gravitational wave detection. Our understanding today is that the r-process occurs in neutron star mergers, (Sect. 7.2) and probably also in some rare supernovae driven by magnetic fields and rotation (Sect. 6) as well as very massive stars leading to black hole forming collapsars and hypernovae. We have observed the radioactive decay of the neutron-rich nuclei produced by the r-process after the neutron star merger GW170817, and also freshly synthesized Sr was observed (Watson et al. 2019). Therefore, this is a proof that the r-process occurs in neutron star mergers. However, the abundances of heavy elements observed in the oldest stars and galactic chemical evolution models (Sect. 8) suggest that an additional contribution is needed at early times before mergers could significantly contribute to the chemical inventory.

Variations of the above mentioned processes are occasionally given different names, i.e. the **weak r-process** works similar to the strong r-process, occurring for moderate neutron densities. It starts also from neutrons and protons that build seed nuclei, but the neutron-to-seed ratio is smaller than in the full/strong r-process, which is characterized by a ratio exceeding 100. The implications are that it does not proceed beyond $N = 82$ or the second peak, its path moves closer to stability with longer beta-decay half-lives. The **i-process (intermediate process) is a variety of the s-process,** but more neutrons are available and thus the path passes a few nuclei away from stability. Still pre-existing seed nuclei are required. During the late stages of stellar evolution, convection in stellar envelopes triggers mixing that can lead to the production of a varying amount of neutrons by specific reactions that are then captured by iron group nuclei, present already in the star when it was born. This abundance of neutrons in excess of typical s-process conditions, but also much below those for an r-process, is responsible for the synthesis of heavy elements up to Pb. This is similar to the s-process, but especially responsible for producing specific isotopes (see Sect. 5.4).

In addition to these, there exist other processes producing some isotopes beyond iron that are not accessible by neutron capture processes. They include the **p-process** or γ-process and the νp-process (Fig. 4), responsible for proton-rich stable nuclei up to $A = 80$–90. Already discussed in B^2HF (Burbidge et al. 1957), the p-process consist mainly of photo dissociation of existing heavy isotopes. This moves matter from nuclei previously produced by the s- and r-process to the proton-rich side of stability. The initial suggestion was that conditions in a hydrodynamic shock wave

triggers this process when running through layers of an exploding star that contain already heavy nuclei from previous generations. We will discuss this with respect to core-collapse as well as type Ia supernova explosions, including an additional option to produce light p-nuclei in the so-called *v*p-process in neutrino-driven, proton-rich ejecta (for details see the Sects. 6 and 7.1). A summary of all these processes and their actions in specific regions of the nuclear chart is given in Fig. 4.

2 Nuclear reactions and NSE

In the previous subsection, we had a first glance on the nucleosynthesis processes and their link to the observed abundances in our solar system. Before we go into more details about all these processes and their astrophysical sites in the next sections, we want to present here a short overview of the tools used to calculate abundances: nucleosynthesis networks and nuclear statistical equilibrium (NSE).

The matter in an astrophysical environment is composed of different nuclei and the mass fraction (X_i) indicates the percentage of mass m_i (or density ρ_i) of nucleus i with respect to the total mass (density):

$$X_i = \frac{\rho_i}{\rho} = \frac{n_i}{\rho N_\mathrm{A}} m_i N_\mathrm{A}. \tag{1}$$

Here, n_i is the number density, ρ the density of the astrophysical environment, and N_A the Avogadro number. The term $m_i N_\mathrm{A}$ is the total mass of a mole of nucleus i and defines the atomic weight. The abundance of a nucleus or isotope is defined as:

$$Y_\mathrm{i} = \frac{n_\mathrm{i}}{\rho N_\mathrm{A}}. \tag{2}$$

The mass number of a nucleus is given by the sum of protons and neutrons $A_i = N_i + Z_i$. With the new definition of the nuclear mass unit, changing from 1/12 of the mass of a ^{12}C atom to $m_u = 1/N_\mathrm{A}$ g, the term $m_i N_\mathrm{A}$ can be rewritten with a high precision as $A_i m_u N_\mathrm{A}$, i.e. it is identical with A_i; therefore, $X_i = A_i Y_i$. As a result of the definition of the mass fraction, all mass fractions must add up to 1:

$$\sum_i X_i = \sum_i A_i Y_i = 1. \tag{3}$$

In addition to this constraint of mass conservation, astrophysical environments are also neutrally charged, which implies that

$$\sum_i Z_i Y_i = Y_\mathrm{e} = \frac{n_\mathrm{e}}{\rho N_\mathrm{A}} = \frac{\sum_i Z_i Y_i}{\sum_i A_i Y_i}, \tag{4}$$

with electron fraction (Y_e) being on the one hand defined by the electron number density, but also equal to the number of protons per nucleon (i.e. protons plus neutrons).

After introducing these general definitions, we can now enter the calculation of abundances (Y_i). The simplest conditions occur in case of an equilibrium between production and destruction of nuclei. At high temperatures, the photons are very energetic and can photodissociate nuclei. If these temperatures are also sufficient for the bombarding energies to overcome Coulomb barriers and, at the same time, the density is sufficiently high, nuclear reactions can occur at the same speed and rebuilt nuclei. In case such chemical equilibria do not only hold for specific reactions, but involve essentially all nuclei of the astrophysical plasma, this leads to

$$(Z, A) + \gamma \longleftrightarrow Zp + Nn. \tag{5}$$

We talk then about a **nuclear statistical equilibrium (NSE)** and can simplify the calculation of the abundances by using the chemical potential

$$\mu_{(Z,A)} = Z\mu_{\mathrm{p}} + N\mu_{\mathrm{n}} \tag{6}$$

with a vanishing chemical potential of photons. Assuming that nucleons and nuclei follow a Maxwell–Boltzmann distribution, this leads to

$$\mu_i = m_i c^2 + k_{\mathrm{B}} T \ln\left[\rho N_{\mathrm{A}} \frac{Y_i}{G_i}\left(\frac{2\pi\hbar^2}{m_i k_{\mathrm{B}} T}\right)^{3/2}\right]. \tag{7}$$

From these two equations, the so-called Saha equation follows for the abundance of nucleus (Z, A):

$$Y(Z,A) = G(Z,A)(\rho N_{\mathrm{A}})^{A-1}\frac{A^{3/2}}{2^A}\left(\frac{2\pi\hbar^2}{m_{\mathrm{u}} k_{\mathrm{B}} T}\right)^{\frac{3}{2}(A-1)} \exp[B(Z,A)/(k_{\mathrm{B}}T)]\, Y_n^{A-Z} Y_p^{Z}, \tag{8}$$

with $m_n \approx m_p \approx m_{\mathrm{u}}$, $m_{(Z,A)} \approx A m_{\mathrm{u}}$, and $B(Z,A) = (A-Z)m_n c^2 + Z m_p c^2 - m_{(Z,A)}c^2$. Therefore, at a given temperature (T) and density (ρ), the NSE abundance of nucleus (Z, A) with binding energy $B(Z, A)$, and partition function $G(Z, A)$ depends only on the neutron (Y_{n}) and proton (Y_{p}) fractions. Together with the mass ($\sum_i X_i = \sum_i A_i Y_i = 1$) and charge ($\sum_i Z_i Y_i = Y_{\mathrm{e}}$) conservation, we have two equations with two unknowns (Y_{n}, Y_{p}), when utilizing Eq. (8) for $Y_{\mathrm{i}}(Z_{\mathrm{i}}, A_{\mathrm{i}})$. With the solution for Y_{n} and Y_{p} all other abundances $Y_{\mathrm{i}}(Z_{\mathrm{i}}, A_{\mathrm{i}})$ can be expressed.

When temperature and density are not very high or when matter expands very fast, the variation of the thermodynamic quantities (dynamical timescale) is faster than the nuclear reactions and an equilibrium is not possible. Outside equilibrium, the individual abundances are calculated with a nuclear reaction network based essentially on r, the number of reactions per volume and time between reaction partners i and j, which can be expressed, when targets and projectiles follow specific distributions dn, by

$$r_{i;j} = \int \sigma \cdot |\mathbf{v}_i - \mathbf{v}_j| dn_i dn_j. \tag{9}$$

The evaluation of this integral depends on the type of particles and distributions that are involved. For nuclei i and j in an astrophysical plasma, obeying a Maxwell–Boltzmann distribution, we find $r_{ij} = n_i n_j \langle \sigma v \rangle_{i;j}$ where $\langle \sigma v \rangle$ is integrated over the relative bombarding energy and is only a function of temperature T

$$\langle \sigma v \rangle_{i,j} = \left(\frac{8}{\pi\mu}\right)^{1/2} (k_B T)^{-3/2} \int_0^\infty E\sigma(E) \exp\left(-\frac{E}{k_B T}\right) \mathrm{d}E, \tag{10}$$

where $\mu = m_i m_j/(m_i + m_j)$ is the reduced mass. For a reaction with photons, we have $j = \gamma$, i.e. in this case the projectile j is a photon. The relative velocity is the speed of light c, the distribution dn_j is the Planck distribution of photons. As the relative velocity between the nucleus and the photon is a constant (c), and the photodisintegration cross section is only dependent on the photon energy E_γ, the integration over dn_i can be easily performed, resulting in

$$\begin{aligned} r_{i\gamma} &= n_i \frac{1}{\pi^2 c^2 \hbar^3} \int \frac{\sigma_i(\gamma; E_\gamma) E_\gamma^2}{\exp(E_\gamma/kT) - 1} dE_\gamma = n_i \lambda_{i;\gamma}(T), \\ \lambda_{i;\gamma}(T) &= \frac{1}{\pi^2 c^2 \hbar^3} \int \frac{\sigma_i(\gamma; E_\gamma) E_\gamma^2}{\exp(E_\gamma/kT) - 1} dE_\gamma. \end{aligned} \tag{11}$$

Contrary to the reactions among nuclei or nucleons, where both reaction partners are following a Boltzmann distribution, this expression has only a linear dependence on number densities. The integral acts like an effective (temperature dependent) decay constant of nucleus i. Electron captures behave in a similar way because the mass difference between nucleons/nuclei and electrons is huge and the relative velocity is with high precision given by the electron velocity. This leads to

$$r_{i;e} = n_i \int \sigma_e(v_e) v_e dn_e = \lambda_{i;e}(\rho Y_e, T) n_i. \tag{12}$$

This is an expression similar to that for photodisintegrations, but now we have a temperature- and density-dependent "decay constant". In principle, neutrino reactions with nuclei would follow the same line, because the neutrinos, propagating essentially with light speed, would lead to a simple integration over the neutrino energies. However, as neutrinos, interacting very weakly, do not necessarily obey a thermal distribution for local conditions, their spectra depend on detailed transport calculations, leading to

$$r_{i;\nu} = n_i \int \sigma_e(E_\nu) c dn_\nu(E_\nu) = \lambda_{i;\nu}(\text{transport}) n_i. \tag{13}$$

Finally, for normal decays, like beta- or alpha-decays or ground-state fission with a half-life $\tau_{1/2}$, we obtain a similar equation with a decay constant $\lambda_i = ln2/\tau_{1/2}$ and

$$r_i = \lambda_i n_i. \tag{14}$$

In this case, the change in the number density due to decay is $\dot{n}_i = -\lambda_i n_i$, with the solution $n_i = n_i(0)e^{-\lambda_i t}$ and $n_i(\tau_{1/2}) = \frac{1}{2}n_i(0)$. The decay half-life of a nuclear ground state is a constant. Adding all these different kinds of reactions, we can describe the time derivative of abundances $Y_i = n_i/\rho N_A$ as the difference of production and destruction terms with a differential equation for each species:

$$\frac{\mathrm{d}Y_i}{\mathrm{d}t} = \mathrm{production_i} - \mathrm{destruction_i}. \tag{15}$$

Both the production and destruction channels include particle-induced reactions, decays, photodissotiation, electron capture, etc. For every nucleus i, the abundance is given by a differential equation:

$$\begin{aligned}\dot{Y}_i = &\sum_j N_j^i \lambda_j Y_j + \sum_{j,k} \frac{N_{j,k}^i}{1+\delta_{jk}} \rho N_\mathrm{A} \langle \sigma v \rangle_{j,k} Y_j Y_k + \\ &\sum_{j,k,l} \frac{N_{j,k,l}^i}{1+\Delta_{jkl}} \rho^2 N_\mathrm{A}^2 \langle \sigma v \rangle_{j,k,l} Y_j Y_k Y_l,\end{aligned} \tag{16}$$

where the factors $1/(1+\delta_{jk})$ and $1/(1+\Delta_{jkl})$ prevent double counting of reactions in two- and three-body reactions, respectively. Δ_{jkl} has the value 0, 1 or 5, so that, dependent on the multiplicity of identical partners, the denominators are equal to 1!, 2!, or 3!. λ's stand for reactions that can be written as one-body rates, including decays, photodisintegrations, electron captures as well as neutrino interactions with nuclei. $\langle \sigma v \rangle_{i,j}$ stands for reactions between nuclei i and j, and $\langle \sigma v \rangle_{j,k,l}$ includes expression for three-body reactions as in Nomoto et al. (1985); Fushiki and Lamb (1987); Görres et al. (1995). The N^i's include integer (positive or negative) factors (appearing with one, two or three lower indices for one-body, two-body, or three-body reactions), describing whether (and how often) nucleus i is created or destroyed in this reaction. Consistent with the new definition of m_u mentioned above, the expressions ρN_A (and $(\rho N_A)^2$) can also be found as ρ/m_u (and $(\rho/m_u)^2$) in the literature (Cowan et al. 2021).

To find the solution of the reaction network, one has to solve the system of coupled non-linear differential equations. The timescales of the strong, electromagnetic, and weak reactions span a wide range and lead to a very stiff set of equations. A survey of computational methods to solve nuclear networks is given in Hix and Thielemann (1999b); Timmes (1999); Hix and Meyer (2006); Lippuner and Roberts (2017).

All the above considerations would not have been possible without the experimental and theoretical input for the nuclear reactions involved. We do not discuss this here in detail, but much of it has been presented in depth in textbooks

(Rolfs and Rodney 1988; Iliadis 2007). The present understanding has been based on tremendous efforts in experimental determinations of cross sections for the involved nuclear reactions, starting from those mentioned by Bethe and von Weizsäcker in H burning and going beyond. A first breakthrough was a compilation based on experimental cross section determinations (Fowler et al. 1967) with continuing efforts via the European NACRE compilation plus investigations in hydrogen burning reactions (Angulo et al. 1999; Adelberger et al. 2011; Xu et al. 2013). Ongoing investigations in underground laboratories like, e.g. LUNA[2], CASPAR[3] and JUNA (Liu et al. 2022) avoid background noise and permit cross section measurements down to the energies in the 50 keV region, which are probed in stellar interiors. This has been complemented by determinations of neutron-capture reactions, which started with Cameron and the nuclear reactor community (Macklin and Gibbons 1965) and continues to present-day efforts (Bao et al. 1997, 2000; Käppeler et al. 2011; Reifarth et al. 2014, and further efforts at nToF at Cern). Predictions for nuclear reaction cross sections of medium and heavy nuclei, based on statistical model approaches, have been provided (Truran et al. 1966; Arnould 1972; Holmes et al. 1976; Woosley et al. 1978; Cowan et al. 1991; Rauscher and Thielemann 2000; Goriely et al. 2008, 2009; Panov et al. 2010; Rauscher 2011), some of them including neutron-induced fission reactions. Weak interactions, such as beta-decays, electron captures, and neutrino interactions have been pioneered experimentally (Kratz et al. 1986), followed by theoretical predictions (Möller et al. 1997; Fuller et al. 1985; Langanke and Martínez-Pinedo 2003; Langanke et al. 2004, 2008, 2011; Martínez-Pinedo et al. 2012; Marketin et al. 2016; Langanke et al. 2021; Giraud et al. 2022) and ongoing investigations. Reactions involving short-lived radioactive targets are/will be investigated with radioactive ion beam facilities such as FAIR, FRIB, RIKEN, HIAF, RAON, ISOLDE, TRIUMF, and SPES.[4]

3 Big Bang nucleosynthesis

3.1 Physics of the expansion

As discussed in the introduction, it appears that most of the elements we know on Earth are produced during the evolution of galaxies (probably due to the activity of stars). However, the light elements/isotopes ^{1,2}H, ^{3,4}He, and ^{7}Li are inherited from preceding phases of the universe, which we assign to the Big Bang. Their abundances are consistent with the observation of the cosmic microwave background. The measurements of the COBE, WMAP and PLANCK satellites clearly provided a proof that this expansion is isotropic in all directions (i.e. can be described in spherical symmetry) and homogeneous with tiny fluctuations in temperature and density of the order 10^{-5} (Planck Collaboration 2020, 2021). This

[2] https://luna.lngs.infn.it/index.php/new-about-us.

[3] https://caspar.nd.edu/.

[4] Combined information has entered complete reaction libraries that are presently publicly available at https://nucastro.org/reaclib.html or https://www.jinaweb.org/science-research/scientific-resources/data.

enormous degree of isotropy and homogeneity within our observational horizon points to a very early phase of extremely rapid expansion (inflation), initially outlined by Guth (2014) and described in understandable technical details by Baumann (2018). The discovery of general relativity by Einstein (1915) Friedmann (1922, 1924) and Lemaître (1927, 1931) led to the formulation of the Friedmann–Lemaitre equations of a spatially homogeneous and isotropic universe. The three Friedmann–Lemaitre equations, originating from the Einstein field equations when utilizing the Robertson–Walker metric (Weinberg 1972), govern the evolution of the early universe:

$$\left(\frac{\ddot{R}}{R}\right) = -\frac{4\pi}{3c^2}(\rho_\epsilon + 3P)G + \frac{1}{3}\Lambda c^2, \tag{17a}$$

$$\left(\frac{\dot{R}}{R}\right)^2 = H(t)^2 = \frac{8\pi G}{3c^2}\rho_\epsilon - \frac{kc^2}{R^2(t)} + \frac{1}{3}\Lambda c^2, \tag{17b}$$

$$0 = \frac{d(\rho_\epsilon R^3)}{dt} + P\frac{dR^3}{dt}. \tag{17c}$$

Whenever $\dot{R} \neq 0$, two of them imply the third. In the following, we will only make use of Eqs. (17b) and (17c). ρ_ϵ denotes the total relativistic energy density $\rho_\epsilon = u + \rho c^2$ and ρ the mass density. Equation (17b) can be, in the non-relativistic limit, interpreted as an energy conservation equation. The related constant k can take only three integer values ($k = 0, \pm 1$), which in general relativity stand for the space curvature (see e.g. Weinberg 1972; Peebles 1993). The third term contains the so-called cosmological constant. It can be identified with a vacuum energy density $\rho_V = (\Lambda c^4/8\pi G)$. When replacing ρ_ϵ by $\rho_\epsilon + \rho_V$ in the first term of Eq. (17b), the third term comes out automatically. The vacuum pressure is related to ρ_V via $P_V = -\rho_V$ (Kolb and Turner 1990). If replacing ρ_ϵ by $\rho_\epsilon + \rho_V$ and P by $P + P_V$, also the second term in Eq. (17a) follows automatically. Thus, if one utilizes consistently the total energy density and pressure (including the vacuum energy density), the Friedmann–Lemaitre equations can be written without the terms for the cosmological constant $\Lambda c^2/3$. The total energy density of a flat universe with $k = 0$, i.e. the so-called critical density, is given by

$$\rho_{\epsilon,c} = \frac{3H(t)^2c^2}{8\pi G}. \tag{18}$$

Within the concordance Λ-CDM cosmological model (cold dark matter with a cosmological constant Λ), this leads to a consistent picture from CMB observations, type Ia supernovae (to be explained in later sections) distance measurements (Riess 2012; Perlmutter 2012) and baryon acoustic oscillations BAO (Beutler et al. 2011) of a flat universe with $\Omega = \rho_\epsilon/\rho_{\epsilon,c} = 1$ (the total relativistic energy density of the universe divided by the critical energy density to obtain a vanishing curvature) with a division of the total energy density into matter $\Omega_m = 0.315$ and a cosmological constant part $\Omega_\Lambda = 0.685$. Ω_m includes a superposition of cold dark matter and

baryonic matter with a ratio of about 5.56 or $\Omega_b \approx 0.048$. This also leads to a Hubble expansion parameter $H_0 \approx 67\,\mathrm{km\,s^{-1}\,Mpc^{-1}}$ from the global PLANCK analysis. The Hubble parameter determined from type Ia supernovae distance measurements (a method pioneered by G.A. Tammann and his students, standing for the more local universe) suffers from a necessary calibration (performed with two methods: "pulsating Cepheid stars" or "tip of the red giant branch fitting") with different (still debated) results of about 74 (Riess et al. 2021) or 70 (Freedman 2021). An independent method based on the recent neutron star merger event GW170817 results also in a value of about 70 (Hotokezaka et al. 2019). To explain the debate, the errors given with all of these methods are quoted to be less than 2, except for the one determined from neutron star mergers, giving an error bar of 5.

Equation (17c) can be interpreted as the first law of thermodynamics $dQ = TdS = dU + PdV = 0$ in an adiabatic expansion of an ultra-relativistic gas. In such a case, $\rho_\epsilon = u$, i.e. in the very early and hot phase of an expanding universe, the temperature is so high that the rest mass of particles is negligible in comparison to the kinetic energies. In this relativistic limit, i.e. $kT \gg mc^2$, which is the case for the whole early radiation-dominated phase, we have $P = u/3 = \rho_\epsilon/3$. Utilizing Eqs. (17c) and 17b) and $k = 0$, the solution for a flat universe is $R(t) = \alpha t^{1/2}$ with a proportionality constant α.

In the very early phases for $kT > 100 - 200$ MeV or $T > 10^{12}$K, free quarks still exist. During the further expansion quarks combine to baryons. All particles with masses $mc^2 < kT$ exist, because particle–antiparticle pairs can be created in photon collisions. At $kT > 1$ MeV , the hot plasma is composed of nucleons, photons, electrons, positrons, electron-, muon-, and tau-neutrinos (dependent of their actual mass) and their antiparticles. We have scatterings that thermalize all constituents to the same temperature, as well as reactions like $\gamma + \gamma \rightleftharpoons e^+ + e^-$, $\nu_e + \nu_e \rightleftharpoons e^+ + e^-$, $e^- + p \rightleftharpoons n + \nu_e$, and $e^+ + n \rightleftharpoons p + \bar{\nu}_e$ (and other scattering reactions involving μ and τ neutrinos), which are all in chemical equilibrium. The physical quantities needed in Eqs. (17b) and (17c) are P and ρ_ϵ, they are easily expressed for ultra-relativistic particles, i.e. when the rest mass energy is negligible in comparison to the total relativistic energy (Kolb and Turner 1990).

Except for nucleons ($m_u c^2 = 931$ MeV), all particles are ultra-relativistic. At temperatures of about 1 MeV, nucleons follow a Maxwell–Boltzmann distribution. Their pressure contribution will be nkT. This linear temperature dependence is negligible in comparison to T^4 for ultra-relativistic gases, and thus this pressure term is not important in a radiation-dominated regime.

The ultra-relativistic particles have chemical potentials $\bar{\mu}_i = 0$. Therefore, the electron and positron captures on protons and neutrons, producing neutrons and protons via

$$e^- + p \rightleftharpoons n + \nu \qquad e^+ + n \rightleftharpoons p + \bar{\nu}, \tag{19}$$

lead to $\bar{\mu}_n = \bar{\mu}_p$ in chemical equilibrium. Making use of the Maxwell–Boltzmann expressions for their chemical potentials $\bar{\mu} = kTln[(nh^3/g)(2\pi mkT)^{-3/2}] + mc^2$ results in

$$\frac{n_n}{n_p} = \frac{X_n}{X_p} = \exp\left(-m_{np}c^2/kT\right), \tag{20}$$

where m_{np} is the neutron–proton mass difference, and the number densities n_i can be expressed by abundances Y_i or mass fractions X_i via $n_i = \rho N_A Y_i = \rho N_A X_i/A_i$, where N_A stands for Avogadro's number, and A_i for the mass number of the nucleus.

Equations (17b) and (17c) lead to a uniquely predicted evolution of the expansion, once the initial value problem is set up or a relation between density and temperature is determined. Ultra-relativistic particles are only related to the temperature, like e.g. photons with $n_\gamma = 2.404/\pi^2(kT/\hbar c)^3$. The baryon (or nucleon) properties depend on density and temperature. Thus, the global $n_b/n_\gamma = \eta$ provides a relation between density and temperature and determines a unique solution of the expanding early universe. Different solutions can be described as a function of the parameter η.

Once $kT \approx 1$ MeV ($T \approx 10^{10}$ K or slightly lower, as the thermal distributions have high energy tails) electrons are not energetic enough anymore to overcome the mass difference between protons and neutrons via electron capture. Photons are also not energetic enough anymore to produce electron–positron pairs for the positron capture on neutrons. These weak interactions, which also produced neutrinos and antineutrinos, will cease to exist. They were, however, also the channel through which neutrinos communicated thermally with nucleons, electrons, positrons and photons. This phase of weak freeze-out or weak decoupling causes the neutron/proton ratio of Eq. (20) to be frozen at $\exp(-m_{np}c^2/kT_{\rm weak})$, in case this freeze-out occurs abruptly at $T_{\rm weak}$). Afterwards, it can only change via beta-decay of neutrons $n \rightarrow p + e^- + \bar{\nu}$. If all reactions, e.g. via Eq. (19) plus the above-mentioned reactions including photons, electrons. positrons, and neutrinos are followed correctly, a fixed proton/neutron or proton/nucleon ratio (for charge neutrality identical to the electron/nucleon ratio, the latter also dubbed Y_e) is set for the onset of nucleosynthesis, which will only change via beta-decays.

Detailed analysis during the phase of weak decoupling leads to the determination of the energy density u, due to a mix of fermionic and bosonic degrees of freedom resulting in $g = 3.3626$ (Kolb and Turner 1990)

$$u = \frac{g}{2} a T_\gamma^4. \tag{21}$$

With $g = 3.3626$ after weak decoupling, the energy density and pressure can be expressed in terms of the photon and nucleon temperature that later on determines nuclear reactions.

Equation (17c) leads to $\rho_\epsilon R^4 = \text{const}$ in the radiation-dominated phase and a solution of Eq. (17b) is $R(t) = \alpha t^{1/2}$, $\dot{R}(t) = (\alpha/2)t^{-1/2}$ and $\dot{R}/R = 1/(2t)$. Thus, when utilizing Eq. (17b) for a flat universe with $k = 0$, $(\dot{R}/R)^2 = 1/(4t^2)$, and $\rho_\epsilon = (g/2)aT^4$ with $g = 3.3626$ in this still radiation-dominated phase after weak decoupling, one obtains a relation between $1/t^2$ and T^4, with its precise form being

$$t = \left(\frac{3c^2}{16\pi G a}\right)^{1/2} \mathrm{g}^{-1/2} \frac{1}{T^2} \tag{22a}$$

$$T_9 = 13.336/t^{1/2}. \tag{22b}$$

This relation for $T_9 = T/10^9\,\mathrm{K}$ is plotted in Fig. 5.

With a global $n_b/n_\gamma = \eta$ and $n_\gamma = 2.404/\pi^2(kT/\hbar c)^3$, one can express the baryon number density and the baryon matter density as a function of temperature, and accordingly the baryon matter density ρ_b

$$n_b = \eta n_\gamma = 2.404\eta/\pi^2(kT/\hbar c)^3 = 2.029 \times 10^{28}\eta T_9^3\ \mathrm{cm}^{-3} \tag{23a}$$

$$\rho_b = n_b m_u = 3.376 \times 10^4 \eta T_9^3\,\mathrm{g\,cm}^{-3}, \tag{23b}$$

when we neglect the small effect of binding or neutron–proton mass difference in comparison to the nuclear mass unit. This relation provides also the total neutron and proton densities, when introducing the neutron to proton ratio after weak freeze-out and decay before the onset of nucleosynthesis.

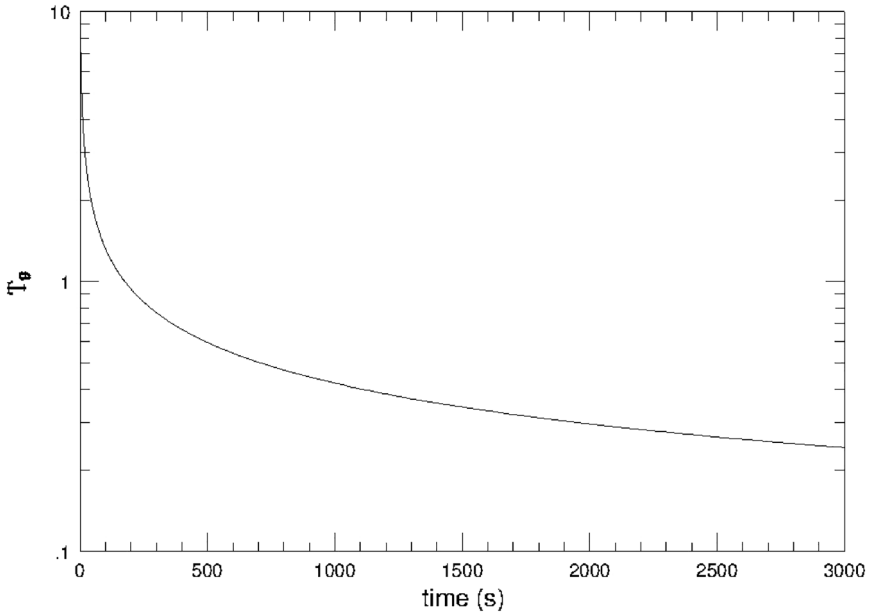

Fig. 5 The photon temperature (responsible for Big Bang nucleosynthesis) as a function of time, $T_9 = T/10^9$ K, according to Eq. (22)

3.2 Primordial nucleosynthesis

During the expansion from high temperatures, after the quark–hadron phase transition at 100–200 MeV, baryonic matter is in a chemical equilibrium with essentially only free neutrons and protons. During further temperature decline, the photodisintegration of ^{2}H, which is constantly produced via neutron capture on protons, eventually slows down and nucleosynthesis proceeds when a substantial abundance of ^{2}H at $T_{D\gamma} \simeq 0.1\,\mathrm{MeV} \hat{=} 1.2 \times 10^9\,\mathrm{K}$ enables further neutron, proton and light-nuclei capture to form ^{3}H, ^{3}He, ^{4}He and even heavier nuclei. The onset of nucleosynthesis is due to the Q-value of the reaction $^1\mathrm{H}\,(n,\gamma)^2\mathrm{H}$ ($Q = 2.3$ MeV). Typically, photodisintegrations are active and winning for temperatures beyond $kT \approx Q/20$. That means that we had initially a complete nuclear statistical equilibrium, but because of very high temperatures—and relatively low densities—as we will see later on, only neutrons and protons are abundant. At temperatures of $T \approx 10^9\,\mathrm{K}$ ($kT \approx 0.1$ MeV), the photodisintegration of deuterium ceases and the path is free to the production of heavier elements.

On the way to heavier nuclei, the gaps existing among stable nuclei at $A = 5$ and $A = 8$, where only highly unstable nuclei with extremely short lifetimes exist, can only be overcome by three-body terms in Eq. (16), which require high densities that do not exist under Big Bang conditions. This inhibits the formation of nuclei beyond the latter mass number. Therefore, the standard Big Bang can produce only ^{2}H, ^{3}He, ^{4}He and ^{7}Li in appreciable amounts.

The neutron-to-proton (n/p) ratio, which constrains primordial nucleosynthesis, is determined by the conditions during weak decoupling, when the electrons are no longer energetic enough to ensure an equilibrium by the reaction $p(e^-, \nu)n$ due to the neutron–proton mass difference of 1.3 MeV, and the positrons needed for the inverse reaction $n(e^+, \bar{\nu})p$ are no longer produced by pair creation. Primordial nucleosynthesis conditions are then determined by the particles remaining in thermal equilibrium, initial conditions at time t (e.g. the onset of nucleosynthesis) and global adiabatic expansion. The initial conditions are set by neutrons, protons, electrons and photons with densities n_n, n_p, n_e and $n_\gamma = 2.404/\pi^2(kT/\hbar c)^3$. From charge neutrality, it follows that $n_e = n_p$; n_p/n_n is given by the equilibrium ratio at weak freeze-out ($\approx 1/6$). When following correctly all reactions involving nucleons,

Table 1 Important reactions

$^1\mathrm{H}\,(n,\gamma)^2\mathrm{H}$
$^2\mathrm{H}\,(d,\ p \text{ or } n,\gamma)^3\mathrm{H}$
$^2\mathrm{H}\,(d,\ n \text{ or } p,\gamma)^3\mathrm{He}$
$^3\mathrm{H}\,(d,\ n \text{ or } p,\gamma)^4\mathrm{He}$
$^3\mathrm{He}\,(d,\ p \text{ or } n,\gamma \text{ or } ^3He,2p)^4\mathrm{He}$
$^3\mathrm{H}\,(\alpha,\gamma)^7\mathrm{Li}$
$^7\mathrm{Li}\,(\mathrm{p},\alpha)^4\mathrm{He}$
$^3\mathrm{He}\,(\alpha,\gamma)^7\mathrm{Be}$

electrons, positions, neutrinos and photons, in addition to Eq. (19) those listed in Table 1 of Grohs et al. (2016), the $Y_e = n_p/(n_p + n_n) = X_p/(X_p + X_n) = X_p$ emerges as shown in the bottom part of Fig. 6, being very close to that resulting from Eq. (20) at $T_{\rm weak}$.

The strength of the standard Big Bang scenario is that only one free parameter, the baryon-to-photon ratio $\eta = n_b/n_\gamma$, must be specified to determine all of the primordial abundances, ranging over 10 orders of magnitude (see e.g. for early references Peebles 1966; Wagoner et al. 1967, more advanced ones Yang et al. 1984; Boesgaard and Steigman 1985; Kawano et al. 1988; Olive et al. 1990; Walker et al. 1991; Smith et al. 1993, and more recent publications Cyburt et al. 2016; Coc and Vangioni 2017; Pitrou et al. 2018 when also COBE, WMAP and PLANCK results could be included). The parameter η, already introduced in Eq. (23), can also be utilzed to determine the baryon fraction of the total critical density at present. Eq. (23b) can be written for the present baryon mass density as a function of the present photon temperature $T_{\gamma,0}$ (in K)

$$\rho_{b,0} = n_{b,0} m_u = \eta_{10} 10^{-10} n_{\gamma,0} m_u = 3.376 \times 10^{-33} \eta_{10} T_{\gamma,0}^3 \,\mathrm{g\,cm^{-3}}. \tag{24}$$

The baryon energy density at present, making use of a negligible kinetic energy at this point in comparison to the rest mass, is dominated by the latter and therefore given by $\rho_{\epsilon,b,0} = \rho_{b,0} c^2$ with the present value of the Hubble constant H_0. Both expressions permit determining the baryon fraction $\Omega_b = \rho_{\epsilon,b,0}/\rho_{\epsilon,c,0}$, which is proportional to H_0^{-2}. Expressing H_0 in terms of $H_0 = h \times 100$ km $\times$ s^{-1} Mpc^{-1}, we find the following expression, using all quantities at the present time:

$$\Omega_b h^2 = (\rho_{\epsilon,b,0}/\rho_{\epsilon,c,0}) h^2 \tag{25a}$$

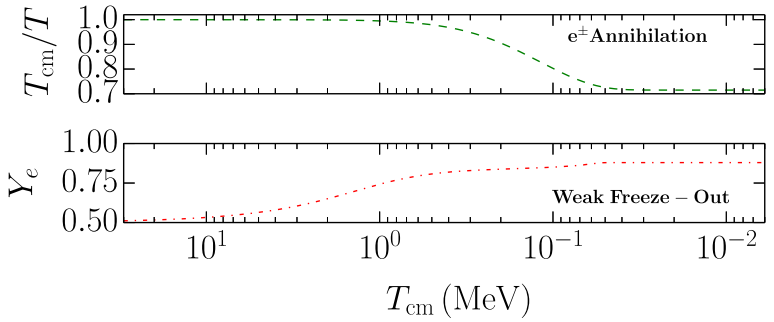

Fig. 6 Top: the evolution of the ratio T/T_γ (labeled as $T_{\rm cm}/T$) as a function of decreasing temperature, given on the abcissa in units of MeV from 10 down to 0.01 MeV. Bottom: the correct treatment of all weak reactions, plus their energetic feedback into the expansion dynamics, leads to the final proton/nucleon ratio Y_e after weak decoupling and freeze-out. Image reproduced with permission from Grohs et al. (2016), copyright by APS

$$= 0.364 \times 10^{-2} (T_{\gamma,0}/2.726\mathrm{K})^3 \eta_{10}. \quad (25b)$$

While in the early days, η_{10} could only be derived from fitting Big Bang nucleosynthesis predictions to observed primordial abundances (and determining Ω_b this way), in the light of COBE, WMAP, and Planck results on observations of the cosmic microwave background, one can obtain η_{10} more precisely from the latter procedure. Utilizing a CMB temperature of $T_{\gamma,0} = 2.726\,\mathrm{K}$ and $\Omega_b h^2 = 0.02233$ (with an error of less than 1%, see Planck Collaboration 2020), one obtains $\eta_{10} = 6.135$. Taking a Hubble constant of $H_0 = 67.37$, i.e. $h = 0.6737$, from the same source leads to $\Omega_b = 0.048$. Planck also results in a matter density fraction $\Omega_m = 0.315$ (including baryonic and dark matter), while $\Omega_\Lambda = 1 - \Omega_m$ stands for the fraction of the energy density related to the vaccum energy density (dark energy) corresponding to a cosmological constant. We will confront these values, especially for η, with those obtained from Big Bang nucleosynthesis.

Before starting to discuss this issue, we should consider which result we intend to match. As we do not yet predict η from basic principles, we have to take it as an initial condition for big bang nucleosynthesis. The idea is to determine η by obtaining a best fit to observed primordial element abundances. For that reason, we present a short review of such abundance observations.

It was already noticed in Fig. 2 that for essentially all elements X beyond Li, their ratio X/H declines in step with, e.g. of O/H or Fe/H. One finds according to these determinations that for all elements X beyond Li [X/H] and [O/H] or [Fe/H] go jointly to $-\infty$ for the oldest stars, being witnesses of the earliest instances in the evolution of the galaxy.

The existing exceptions are D (= ^{2}H), ^{3}He, ^{4}He, and ^{7}Li. Fig. 7, based on the observations of old galactic stars, shows that Li seems to approach a value at [Fe/H]= -2, which stays constant for lower "metallicities", indicating that this is a value inherited from the Big Bang and not obtained during galactic evolution, which increases Fe and the other elements (but see Korn 2020; Fields and Olive 2022, for further discussions on this issue). Fig. 8 displays the primordial He mass fraction X (He), among cosmologists also known as Y_p (based on early conventions for hydrogen (X), helium (Y) and the sum of all heavier elements "metals" Z). Its determination is based on detecting He emission lines in low metallicity H II regions in dwarf galaxies.

These are the latest constraints and limits from recent literature for all primordial abundances (Cooke and Fumagalli 2018; Bania et al. 2002; Sbordone et al. 2010; Aver et al. 2015, 2021):

$$\begin{aligned}
(^2\mathrm{H/H}) &= 2.527 \pm 0.030 \times 10^{-5} \\
(^3\mathrm{He/H}) &\leq 1.1 \pm 0.2 \times 10^{-5} \\
(^7\mathrm{Li/H}) &\leq 1.58 \pm 0.31 \times 10^{-10} \\
0.2419 &\leq X_\alpha \leq 0.2487.
\end{aligned}$$

The major reactions that determine these abundances during Big Bang nucleosynthesis in the build-up of the elements discussed are displayed in Table 1. We have to

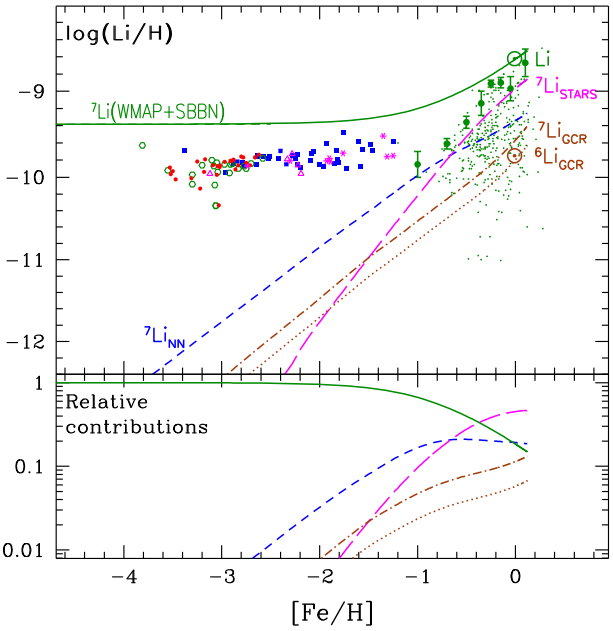

Fig. 7 [Li/H] as a function of [Fe/H]. This figure shows observations as well as abundance predictions related to other possible origins, like galactic cosmic rays. It can be seen that a plateau of constant values is observed for [Fe/H]<-2, pointing to an early inherited value from the Big Bang, i.e. before any possible contribution from stars. Image reproduced with permission from Prantzos (2012), copyright by APS; also see references therein

incorporate all these reactions, their inverse reactions, and the beta-decays of neutrons, ^{3}H, and ^{7}Be in the nuclear reaction network. Reaction networks with a special focus whether also heavier elements can be produced in the Big Bang have been utilized by quite a number of authors, but for a best fit to primordial abundances only the ones of Table 1 are important (see also Fig. 9). After the update of all relevant reaction rates by Pitrou et al. (2018), new measurements have been undertaken, especially for the ^{2}H (p,γ)^{3}He reaction, which contained the largest uncertainty of all reactions involving ^{2}H production or destruction. This resulted in a highly improved precision, leaving only a 3% uncertainty in relevant S-factor (Mossa et al. 2020; Moscoso et al. 2021).

A typical result for a specific η, neutron half-life of 609.5 s (corresponding to a mean lifetime of τ_n = 879.5 s, and three neutrino species is shown in Fig. 10 in the left column, while on the right the dependence on the choice of η is shown in comparison with $\Omega_b h^2$ determined by the Planck satellite, corresponding to a value of η; see Eq. (25).

The abundances of individual nuclei depend on η in the following way. A high (baryon) density during the nucleosynthesis phase, i.e. a large η, gives rise to a larger number of capture reactions on ^{2}H and ^{3}He, and consequently leaves less ^{2}H and ^{3}He, but increases the ^{4}He abundance. Therefore, the ^{2}H abundance is a test for the baryon density; however, a change in the related reaction rates in Table 1, resulting

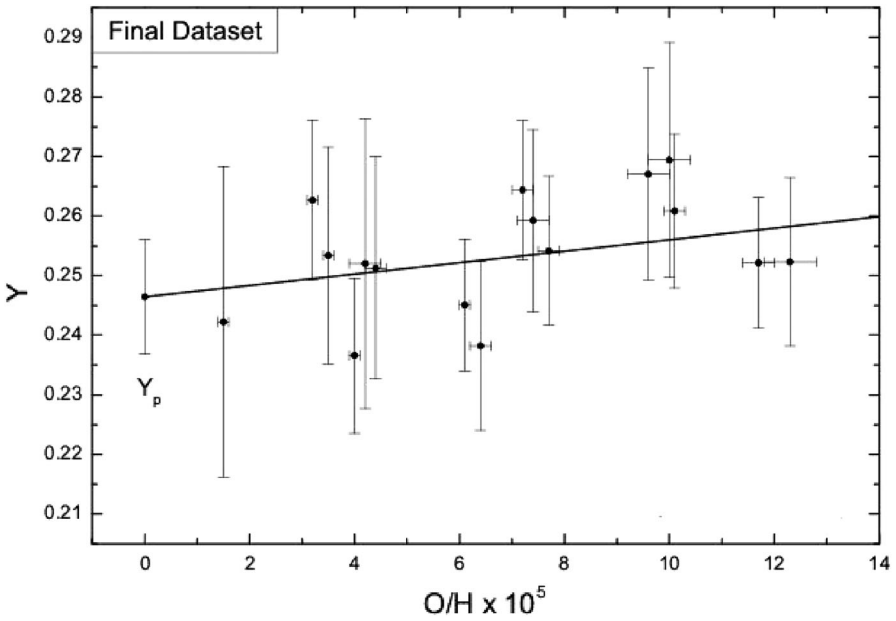

Fig. 8 Y (standing for the helium mass fraction X (He) as a function of O/H, based on observations of He emission lines in low metallicity H II regions in dwarf galaxies. Image reproduced with permission from Aver et al. (2013), copyright by IOP/SISSA

also in a changed (^{2}H/H) abundance ratio, feeds back into the interpretation in terms of the baryon density. The behaviour of the ^{7}Li-abundance is more complex. At low densities, ^{7}Li is produced via ^{3}H $(\alpha,\gamma)^7$Li, but is destroyed at higher densities by ^{7}Li $(p,\alpha)^4$He. However, increasing densities lead also to a larger production of ^{7}Be via ^{3}He $(\alpha,\gamma)^7$Be, which is preserved during the nucleosynthesis period and subsequently decays to ^{7}Li. The (^{7}Li/^{1}H)-ratio has a minimum of about 10^{-10} for $2<\eta_{10}<3$ due to the complicated origin from ^{7}Li and ^{7}Be. In addition to the η dependence, the abundances resulting from Big Bang nucleosynthesis are also dependent upon the number of existing neutrino species and the neutron half-life. In the standard scenario the (n/p)-ratio, resulting from weak decoupling, is always smaller than 1 because of the smaller proton mass. In addition, the neutron decays from $T_{\rm weak}$ $(n/p \approx 1/6)$ to $T_{D\gamma} \approx 0.1$MeV at the onset of nucleosynthesis for about 130s. This leads to an increase of $Y_e = X_p$. If we assume that all neutrons, which are less abundant than protons, combine with available protons to form ^{4}He, then the He-mass fraction is given by

$$X_\alpha = 4Y_\alpha = 4\frac{1}{2}Y_n = 2Y_n = 2X_n \tag{26a}$$

$$= 2(1 - X_p) = 2(1 - Y_e). \tag{26b}$$

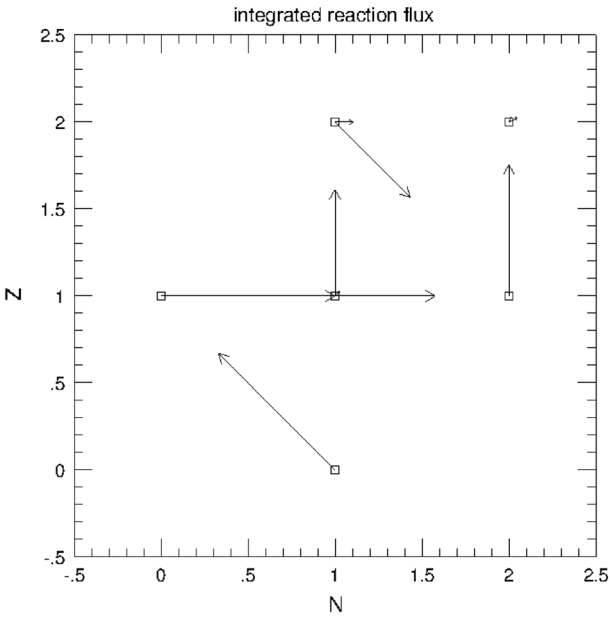

Fig. 9 For typical Big Bang conditions only the reactions shown in the figure are of importance, and display integrated reaction flows $f_{ij} = \int [\dot{Y}_i(i \rightarrow j) - \dot{Y}_i(j \rightarrow i)]dt$ for the conditions and reactions as discussed above. Different reactions with the same starting point and leading to the same final nucleus are added. The lengths of the vectors are scaled logarithmically, and a factor of 1/100 in f_{ij} reduces the vector length by a factor of 5. It can be recognized that the reaction flux beyond ^{4}He is minute

In Fig. 6, the rise of Y_e, due to the neutron decay after weak decoupling, can be recognized, approaching final values beyond $Y_e = 0.875$. The latter corresponds to $X_\alpha = 0.25$ when utilizing Eq. (26b). Here, we made use of the standard notation for the mass fraction $X = AY$ of a nucleus with mass number A and abundance Y. This notation is more useful for a world that is more complex than one consisting only of hydrogen (X), helium (Y) and 'metals' (Z), as often found in the astronomical literature. This makes the He mass fraction X_α a function of the (n/p) ratio or Y_e at the time of nucleosynthesis after weak freeze-out and decay.

Combining theoretical model predictions with primordial abundance information, utilizing three neutrino families ($N_\nu = 3$) leads to the following conclusions from Big Bang nucleosynthesis alone (within 68% confidence limit, Pitrou et al. 2018).

$$\Omega_b h^2 = 0.0219 \pm 0.002. \tag{27}$$

This result is shown in Fig. 27 of Pitrou et al. (2018) for a 68% confidence limit and marginally outside the CMB limits of 0.02233 ± 0.00015. According to Eq. (25), this corresponds to limits on $\eta_{10} = 6.01 \pm 0.06$. The shift to smaller values in comparison to the CMB results is mainly due to ^{7}Li. If one takes the constraints on D and ^{4}He alone, Cyburt et al. (2016) find a value almost coincident with the Planck results of $\eta_{10} = 6.1 \pm 0.2$. Detailed Monte Carlo simulations, varying nuclear reaction rates and the neutron lifetime within their experimental uncertainies, led to

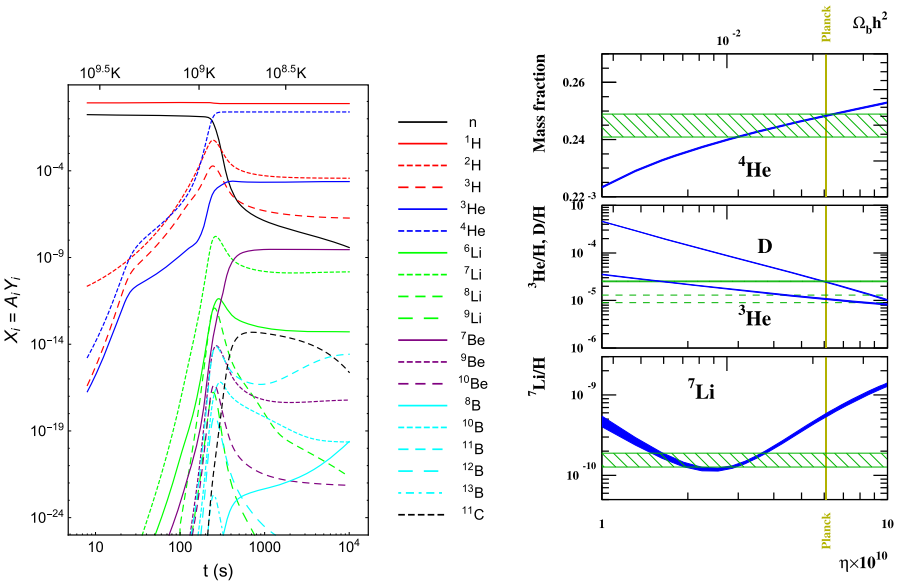

Fig. 10 Left: Mass fractions of various nuclei and helium mass as produced during Big Bang nucleosynthesis as a function of time or decreasing temperature. Right: variations of abundance results with the choice of η and comparison with the η obtained from the Planck satellite, related to the cosmic microwave background. Images reproduced with permission from [left] Pitrou et al. (2018), copyright by Elsevier; and from [right] Coc and Vangioni (2017), copyright by World Scientific

respective uncertainties for the predictions of the individual abundances to 0.068% for ^{4}He, 1.49% for D (^{2}H), 2.43% for ^{3}He, and 4.39% for ^{7}Li (see updates in the next Sect. 3.3). The latter is much smaller than the discrepancy seen in Fig. 10, being larger than a factor of 3. Thus, two questions arise: (a) is there a problem with the primordial abundance determination of ^{7}Li or (b) are extensions to the standard Big Bang model required, which would bring the CMB and BBN in accordance? There are indications that the determination of primordial ^{7}Li abundances is hampered by a number of stellar physics issues: (i) atomic diffusion transports Li down to deeper/hotter layers where it is destroyed, (ii) in addition to diffusion, additional mixing processes might be at work, supported by observations of metal-pour globular clusters, (iii) the plateau shown in Fig. 7 seems to change into an increased spread for metallicities below [Fe/H] = −3. This is contradictory to the notion of a primordial abundance enherited from the Big Bang. This suggests that ^{7}Li cannot be utilized anymore for constraints on the Big Bang nucleosynthesis, and thus the only remaining discrepancy between the standard Big Bang, including determinations from the CMB, and Big Bang nucleosynthesis is vanishing. However, one might nevertheless look into further options and uncertainties.

3.3 Uncertainties and further aspects

Increasing the number of neutrino species has an effect equivalent to that of a faster expansion due to a larger pressure. Utilizing 3.3 rather than 3 neutrino families would lead to an earlier weak decoupling at higher $T_{\rm weak}$. This results in a higher (n/p)-ratio and consequently to a higher ^{4}He abundance. While the number of neutrino families can only be an integer number, a weak decoupling occurring not in complete thermal equilibrium can also be described by an effective number of neutrino families.

Utilizing Big Bang nucleosynthesis constraints alone, Pitrou et al. (2018) obtained an $N_{\nu,\rm eff}$ of 2.88 ± 0.27, and when combining it with cosmic microwave background information this resulted in 3.01 ± 0.15, i.e. the effective value is almost identical with three neutrino families. Yeh et al. (2022) obtained with recent updates more constrained values of 2.95 ± 0.22.

A longer lifetime for the neutron beta-decay would have a similar effect, leaving a higher (n/p)-ratio once nucleosynthesis sets in. The uncertainty left presently by different experiments is claimed to be in less than the permille range (e.g. 877.75 ± 0.28s; Gonzalez et al. 2021), but there is still a debate based on two different methods (Witze 2019). Nevertheless, this leaves less than a 1% uncertainty.

There remain further nuclear uncertainties that enter BBN abundance predictions. While the reaction rates for ^{1}H $(n,\gamma)^2$H, ^{2}H $(d,p)^3$H, and ^{2}H $(d,n)^3$He are known within 1% (Ando et al. 2006; Gómez Iñesta et al. 2017), the uncertainty for the $^2H(p,\gamma)^3$He rate has only in very recent LUNA experiments been reduced down to the 3% level (Mossa et al. 2020; Moscoso et al. 2021). This led to the conclusion (Yeh et al. 2021; Pisanti et al. 2021) on a baryon density in very good agreement with CMB data, while Pitrou et al. (2021); Moscoso et al. (2021) find a 1.8σ tension between predicted and observed primordial D/H ratios, when utilizing different reaction rates for ^{2}H $(d,p)^3$H and ^{2}H $(d,n)^3$He. These latter reactions are presently looked at in new LUNA experiments. With the existing variations in the above-mentioned reaction rates, the abundance predictions come with the following uncertainties: ^{7}Li (4%), ^{2}H (1.5%), ^{3}He (1.3%), and ^{4}He (0.57%) (Pitrou et al. 2021). This should be compared with the presently existing observational uncertainties: ^{7}Li (22%), ^{2}H (1.2%), ^{3}He (18%), and ^{4}He (1.4%) (Pitrou et al. 2021), which underlines why at present ^{2}H and ^{4}He provide the best constraints for precision cosmology, utilizing those elements with the highest available observational and theoretical abundance precision. Additional aspects, which we did not mention here, are discussed by Pitrou et al. (2018), like e.g. weak rates in medium, zero-temperature radiative corrections, finite nucleon mass corrections, finite temperature radiative corrections, weak magnetism, QED plasma effects, and incomplete neutrino decoupling.

^{7}Li observations come with the doubt whether the observed so-called Spite plateau really corresponds to primordial abundances of ^{7}Li. Presently predicted Li abundances are a factor of 3 beyond the Spite plateau. Certainly stellar effects, depleting Li, have to be considered (Dumont et al. 2021) and there exist clear indications that this is the case (Korn 2020; Fields and Olive 2022), but physics

beyond the standard model might also be required on the theory side, for details see the white paper by Grohs et al. (2019).

In the not too recent past, there have been a number of investigations into the possible nucleosynthesis signature of Big Bang nucleosynthesis with density inhomogeneities (Reeves 1991; Thielemann et al. 1991; Malaney and Mathews 1993; Rauscher et al. 1994; Lara et al. 2006). This was extended more recently to stochastic variations in magnetic field strength (Mathews et al. 2017; Luo et al. 2019). While it seems not ruled out that such scenarios could be a solution to the Li-problem, the initial idea to also produce heavy elements during Big Bang nucleosynthesis has been completly ruled out (consistent with our present knowledge from observations).

4 Nuclear burning processes in stellar environments

Following the motivation to describe burning in stellar environments, we will discuss here the ingredients for their modelling. Thermonuclear energy generation is one of the key aspects. It shapes the interior structure of the star, and thus its evolutionary timescale, and the generation of new chemical elements and nuclei. Without understanding these, the feedback from stars as it determines the evolution of galaxies cannot be understood in astrophysical terms. Thermonuclear burning, nuclear energy generation, and resulting nuclear abundances are determined by thermonuclear and weak interactions. The treatment of the nuclear/plasma physics required and a detailed technical description of reaction rates, their determination, and the essential features of composition changes in reaction networks have been presented in Sect. 2. Here, we want to discuss which types of reactions are involved specifically in the evolution of stars and their end stages. Nuclear burning can in general be classified into two categories: (1) hydrostatic burning stages on timescales dictated by stellar energy loss and (2) explosive burning due to hydrodynamics of the specific event.

Massive stars (as opposed to low- and intermediate-mass stars) are the ones that experience explosive burning (2) as a natural outcome at the end of their evolution, and they undergo more extended hydrostatic burning stages (1) than their low- and intermediate-mass cousins. Therefore, we want to address some of these features here in a general way, before describing the evolution and explosion in more detail in the following sections.

The important ingredients for describing nuclear burning and the resulting composition changes (i.e. nucleosynthesis) are (i) strong interaction cross sections, (ii) photodisintegrations, (iii) weak interactions related to decay half-lives, electron or positron captures, and finally (iv) neutrino-induced reactions. They will now be discussed.

4.1 Nuclear burning during hydrostatic stellar evolution

Charged-particle reactions, i.e. a subset of strong interactions, are—opposite to neutron-induced reactions—highly dependent on the Coulomb repulsion of the

interacting nuclei/particles, requiring minimum energies to overcome Coulomb barriers. Hydrostatic burning stages are therefore characterized by temperature thresholds, permitting thermal Maxwell–Boltzmann distributions of (charged) particles (nuclei) to penetrate increasingly larger Coulomb barriers of electrostatic repulsion. These are generally two body reactions as discussed in Eq. (16).

4.1.1 H burning

The "fuel" with the lowest charge is hydrogen, permitting nuclear burning at the lowest possible temperatures among all nuclear burning stages. **H burning** converts ^{1}H into ^{4}He via *pp chains* or the *CNO cycles*. The simplest PPI chain is initiated by ^{1}H (p,$e^{+}\nu$)^{2}H (p,γ)^{3}He and completed by ^{3}He (^{3}He,2p)^{4}He, with the first pp-reaction having as alternative the pep-reaction ^{1}H (pe^{-}, ν)^{2}H. PPII acts as a branching on ^{3}He via ^{3}He (α, γ)^{7}Be (e^{-}, ν)^{7}Li (p,α)^{4}He, and PPIII branches off at ^{7}Be via ^{7}Be (p,γ)^{8}B ($e^{+}\nu$)^{8}Be*(α)^{4}He. Finally, PPIV (or the Hep-reaction) also branches off at ^{3}He via ^{3}He (p,$e^{+}\nu$)^{4}He. The pep reaction is the slowest of all, because a three-body reaction is a very rare event, but it is relatively unimportant because the pp-reaction procedes faster, although being the slowest reaction of the whole set of pp cycles, controlling the speed of all sub-cycles, converting ^{1}H into ^{4}He (see Table 2, we give the individual sub-cycle name, the Q-value, and a lifetime for each reaction at $T \approx 10^{7}$ K).

The alternative CNO cycle of H burning acts if C, N, or O nuclei are already present, and, in addition, at higher temperatures than the pp cycles, due to the fact that they permit overcoming Coulomb barriers of the larger charge numbers of these nuclei. How and for which stars this applies in stellar evolution will be subject of the following section, concentrating on stellar evolution. The dominant CNOI cycle ^{12}C (p,γ)^{13}N($e^{+}\nu$)^{13}C(p,γ)^{14}N(p,γ)^{15}O($e^{+}\nu$) ^{15}N(p,α)^{12}C contains branchings at ^{15}N, ^{17}O, and ^{18}O, opening reaction chains to sub-cycles. It is controlled by the slowest reaction ^{14}N(p,γ)^{15}O. Sub-cycles are CNOII: ^{15}N(p,γ)^{16}O(p,γ)^{17}F($e^{+}\nu$)^{17}O(p,α)^{14}N, CNOIII: ^{17}O(p,γ)^{18}F($e^{+}\nu$) ^{18}O(p,α)^{15}N, and CNOIV: ^{18}O(p,γ)^{19}F(p,α)^{16}O (see Table 3). In the case of pre-existing heavier elements (similar to C, N, and O) also other proton-induced reaction cycles can take place. A specific case is the so-called NeNaMg cycle that proceeds via a similar sequence of three proton captures, two beta-decays, and one final (p,α) reaction as in the CNOI cycle.

For presently utilized compilations for hydrogen burning reactions and updates by recent investigations, see the references given at the end of the following subsubsections for He burning and the s-process.

4.1.2 He burning

The next burning stage, **He burning**, acts on the ashes of H burning, i.e. ^{4}He. The major reactions are the triple-alpha reaction ^{4}He ($2\alpha, \gamma$)^{12}C and ^{12}C(α, γ)^{16}O (deBoer et al. 2017), followed to some extent by ^{16}O(α, γ)^{20}Ne. The triple-alpha reaction, being essentially a sequence of two two-body reactions with an extremely short-lived

Table 2 The PP cycles in hydrogen burning

cycle	reaction	τ (years)	Q (MeV)
PPI	^{1}H (p,$e^{+}\nu$)^{2}H	7.9×10^{9}	0.420
(pep reaction)	^{1}H (pe^{-}, ν)^{2}H	3.7×10^{12}	1.442
	^{2}H (p,γ)^{3}He	5.9×10^{-8}	5.493
	^{3}He (^{3}He,2p)^{4}He	$1.4/Y_3$	12.859
PPII	^{3}He (α, γ)^{7}Be	1.1×10^{6}	1.586
	^{7}Be (e^{-}, ν)^{7}Li	2.9×10^{-1}	0.861
	^{7}Li (p,α)^{4}He	4.3×10^{-5}	17.347
PPIII	^{7}Be (p,γ)^{8}B	1.8×10^{2}	0.135
	^{8}B ($e^{+}\nu$)^{8}Be*(α) ^{4}He	3.5×10^{-8}	18.078
PPIV (Hep reaction)	^{3}He (p,$e^{+}\nu$)^{4}He	3.7×10^{7}	19.795

Table 3 The CNO cycles in hydrogen burning

cycle	reaction sequence
CNOI	^{12}C(p,γ)^{13}N($e^{+}\nu$)^{13}C(p,γ)^{14}N(p,γ)^{15}O($e^{+}\nu$)^{15}N(p,α)^{12}C
CNOII	^{15}N(p,γ)^{16}O(p,γ)^{17}F($e^{+}\nu$)^{17}O(p,α)^{14}N
CNOIII	^{17}O(p,γ)^{18}F($e^{+}\nu$)^{18}O(p,α)^{15}N
CNOIV	^{18}O(p,γ)^{19}F(p,α)^{16}O

intermediate nucleus ^{8}Be, is an example for "apparent" three-body terms in Eq. (16), which include the product of three abundances. A side reaction, acting on ^{14}N (the dominant CNO-nucleus remaining after H burning, because of experiencing the slowest proton capture reaction in the whole cycle) is given by ^{14}N(α, γ)^{18}F ($e^{+}\nu$)^{18}O(α, γ)^{22}Ne, where neutrons can be produced via ^{22}Ne (α,n)^{25}Mg. The CNO cycle in H burning leaves an equilibrium abundance of ^{13}C, which can act as a neutron source via the ^{13}C(α,n)^{16}O reaction before ^{22}Ne becomes active. However, this mechanism produces a much smaller neutron flux than ^{22}Ne. Alternatively, when hydrogen (protons) is mixed into He burning zones, this creates via ^{12}C(p,γ)^{13}N ($e^{+}\nu$)^{13}C also ^{13}C as an alternative and much stronger neutron source. As will be discussed in the following Sect. 5, the H- and He burning stages are encountered in essentially all stars, while low and intermediate-mass stars will only undergo H- and He burning, leaving white dwarfs as central objects.

Most of the reactions listed here and in the preceding H burning section have been studied experimentally, but the extrapolation to low energies in the keV range is

important to understand the behaviour at Gamow peak energies (Angulo et al. 1999; Adelberger et al. 2011; Xu et al. 2013). The slowest reaction in the CNO cycle has experienced a recent update (Gyürky et al. 2022). A major uncertainty has been the $^{17}O(p,\alpha)/^{17}O(p,\gamma)$-branching between the CNOII and CNOIII cycle, related mostly to a low-lying 65keV resonance (Rolfs and Rodney 1988), which has recently been determined in a direct measurement (Bruno et al. 2016).

4.1.3 The s-process during He burning

The two neutron sources ^{22}Ne and ^{13}C, mentioned above, can, again in the case of pre-existing heavier nuclei from earlier stellar generations, lead to a sequence of neutron captures and beta-decays. In the case of low neutron densities, as they result from these sources, it causes the production of heavy nuclei up to Pb and Bi in the slow neutron capture or **s-process** (see Fig. 4). This process encounters dominantly nuclei close to stability (with small exceptions at branching points where neutron capture and beta-decay are in competition (see Fig. 11).

The reason that such a process can take place during the relatively low temperatures of He burning is that neutron capture reactions are not hampered by Coulomb barriers like charged-particle reactions. The process is only terminated by alpha-decay or (n,α)-reactions beyond Pb and Bi, cycling in each case back to lighter nuclei. The status of understanding the nuclear input is well discussed in the present literature (Reifarth et al. 2014). The outcome of an s-process can depend on the amount of heavy elements already available during these phases of He burning,

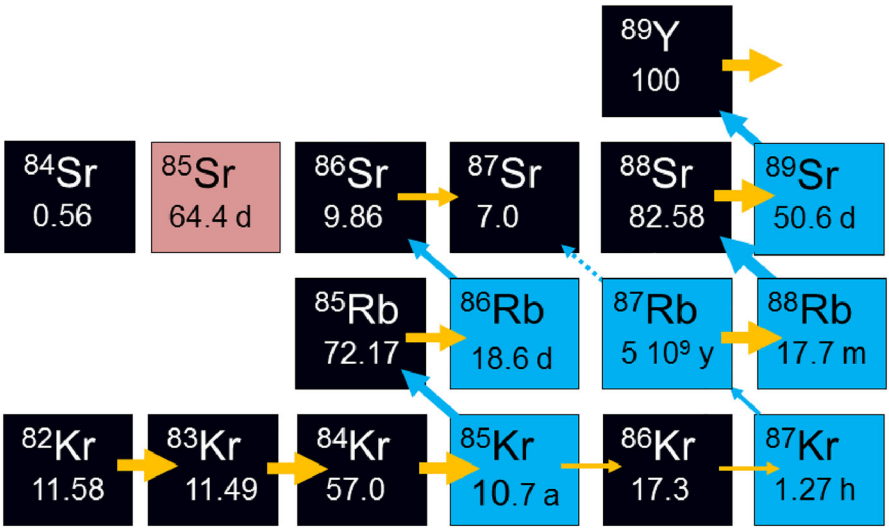

Fig. 11 Neutron captures connect isotopes with neutron number N and $N + 1$ of the same element with charge number Z until a β^--unstable nucleus decays to the next isotopic chain with $Z + 1$. For very long-lived nuclei, a further neutron capture can win against beta-decay and a branching in the s-process path occurs. A pure s-nucleus is ^{86}Sr, as nuclei that would be produced by other more neutron-rich processes would end up via beta-decay in ^{86}Kr, blocking any contribution to ^{86}Sr. Image courtesy of F. Käppeler

usually measured via [Fe/H] = $\log_{10}$ (He/H)$_{star}$/ (Fe/H)$_{\odot}$, which measures the ratio of Fe (but also the other "metals") in comparison to the solar ratios. The amount of ^{22}Ne originates from ^{14}N, which is, like Fe, related in a similar way to the metallicity. Therefore the s-process based on the ^{22}Ne neutron source should not depend on the metallicity in the resulting relative abundance pattern (although the total amount of s-processed matter will do). In a different way, if the ^{13}C results from admixtures of protons into He burning zones, this is in principle not dependent on metallicity. Thus, the ratio of the amount of neutrons produced by ^{13}C with respect to the existing Fe depends on the metallicity and can affect the produced abundance pattern. A higher neutron/Fe ratio at lower metallicities produces preferentially an abundance pattern tilted towards heavy nuclei up to Pb and Bi (as shown nicely already in Cristallo et al. 2009), while this tendency weakens for higher metallicities.

The neutrons released by ^{13}C and ^{22}Ne can be affected by competing (charged-particle) reactions on these nuclei, preventing them from undergoing an (α,n)-reaction. In addition, independent of these neutron-releasing sources, the ratio of neutrons available for capture on heavy nuclei to ensure an s-process, so-called neutron poisons, can also affect the outcome. While on average, the neutron capture cross sections and rates increase with the mass number of nuclei (due to higher level or resonance densities), the amount of neutrons consumed in such reactions is also affected by the product of neutron densities/abundances with the abundance of a target nucleus. In a typical (seed) abundance pattern, the lighter heavy nuclei dominate against Fe and heavier nuclei, and thus their abundance and their capture cross sections can have a strong influence on the strength of an s-process.

In most cases, the beta-decays in the s-process are much faster than neutron captures for these low neutron densities, and the s-process passes through a path of stable nuclei with a unique identification of nuclei for each mass number A. In the case of very long-lived nuclei (longer than the typical neutron-capture timescales in the s-process of months to years), permitting a further neutron capture, also branchings can be noticed (see ^{85}Kr in Fig. 11). With a unique identification of mass number $A = Z + N$ with a specific nucleus (Z, N) in the s-process path (when beta-decays can be viewed as instantaneous), one can think of the s-process path as a chain of neutron captures, where the progress is only determined by the neutron exposure $\tau_n = \int n(t)dt$, which integrates the neutron density of the environment over time (first suggested in Seeger et al. 1965). With neutron capture cross sections known for stable nuclei, the abundances can be predicted as a function of A, dependent on the neutron exposure τ_n. What is shown in Fig. 12 is actually based on an exponential superposition of neutron exposures. In a steady flow of neutron captures, the flow from nucleus $A-1$ to nucleus A should be the same as the flow from A to $A+1$, resulting in $\langle \sigma v \rangle_{A-1} Y_{A-1} = \langle \sigma v \rangle_A Y_A = \text{const}$. With the same neutron velocity distribution in a given environment, this can also be written as $\sigma_A Y_A = \text{const}$. We see in Fig. 12 that this is essentially fulfilled for nuclei in between the neutron shell closures at $N = 50$, 82, and 126. The exceptions with multiple entries are branchings, like the ones in Fig. 11. At the shell closures $N = 50$, 82, 126 and for $A < 90$ (or $N < 50$), such an equilibrium is not attained, because the too small

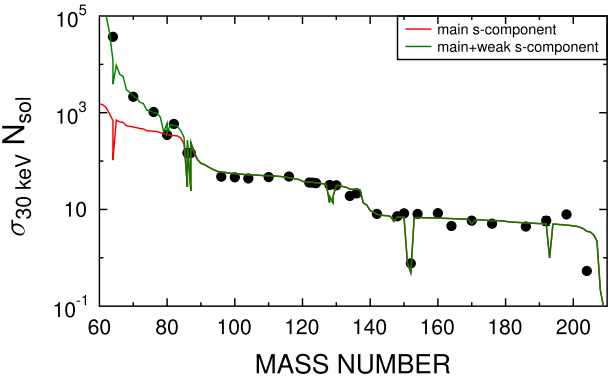

Fig. 12 Results of s-process simulations for pure s-process nuclei from two exponential superpositions of neutron exposures τ_n, showing the product of Y_A with the related neutron capture cross section σ_A. Horizontal lines with $\sigma_A Y_A = \text{const}$ show regions of a steady-flow equilibrium of neutron captures. The branch up to $A = 90$ requires smaller neutron exposures, introduced here as the weak s-process in comparison to the main s-process. Image reproduced with permission from Reifarth et al. (2014), copyright by the authors

capture cross sections do not permit a steady-flow equilibrium for the small neutron densities experienced.

Many of the reactions of importance in He burning and related to the strength of the s-process are presently investigated in deep underground laboratories, such as LUNA,[5], CASPAR,[6] and JUNA (Liu et al. 2022), where recent results can be found. Important reactions are, e.g. $^{18}O(\alpha,\gamma)$, producing the neutron source ^{22}Ne, the ratio of $^{17}O(p,\alpha)$ in comparison to $^{17}O(\alpha,n)$, affecting the strength of the neutron source, and also $^{25,26}Mg$ (α,n) as possible alternatives. For further aspects, how present-day nuclear input affects the s-process outcome, have a look at Vescovi and Reifarth (2021) and the detailed discussion in Sect. 5.4.

4.1.4 Advanced burning stages

Advanced burning stages beyond He burning are characterized by three ingredients: (i) heavy-ion fusion reactions, (ii) photodisintegrations, (iii) electron capture reactions, and partially also (iv) neutrino reactions as presented already in Sect. 2. C burning and O burning are dominated by the heavy-ion fusion reactions ^{12}C $(^{12}C,\alpha)^{20}Ne$ vs. $^{16}O(^{16}O,\alpha)^{28}Si$. Reactions going beyond these key reactions are provided in Tables 4 and 5. Further features, as well as the status of nuclear cross sections, have been discussed in a number of reviews on stellar burning stages (Käppeler et al. 1998; Wiescher et al. 2006, 2012; Moghadasi 2021; Aliotta et al. 2022).

The alternative to fusion reactions are photodisintegrations that start to play a role at sufficiently high temperatures T when $30\,kT \approx Q$ (the Q-value or energy release of

[5] https://luna.lngs.infn.it/index.php/scientific-output/publications.

[6] https://caspar.nd.edu/.

Table 4 Major reactions in carbon burning

(a) Basic energy generation
$^{12}C(^{12}C,\alpha)^{20}Ne$ $^{12}C(^{12}C,p)^{23}Na$
$^{23}Na\ (p,\alpha)^{20}Ne$ $^{23}Na\ (p,\gamma)^{24}Mg$ $^{12}C(\alpha,\gamma)^{16}O$
(b) Fluxes $> 10^{-2}\times$ (a)
$^{20}Ne\ (\alpha,\gamma)^{24}Mg$ $^{23}Na\ (\alpha,p)^{26}Mg\ (p,\gamma)^{27}Al$
$^{20}Ne\ (n,\gamma)^{21}Ne\ (p,\gamma)^{22}Na\ (e^{+}\nu)^{22}Ne\ (\alpha,n)^{25}Mg\ (n,\gamma)^{26}Mg$
$^{21}Ne\ (\alpha,n)^{24}Mg$ $^{22}Ne\ (p,\gamma)^{23}Na$ $^{25}Mg\ (p,\gamma)^{26}Al\ (e^{+}\nu)^{26}Mg$
(c) Low temperature, high density burning
$^{12}C(p,\gamma)^{13}N(e^{+}\nu)^{13}C(\alpha,n)^{16}O(\alpha,\gamma)^{20}Ne$
$^{24}Mg\ (p,\gamma)^{25}Al\ (e^{+}\nu)^{25}Mg$
$^{21}Ne\ (n,\gamma)^{22}Ne\ (n,\gamma)^{23}Ne\ (e^{-}\bar{\nu})^{23}Na\ (n,\gamma)^{24}Na\ (e^{-}\nu)^{24}Mg$ + s-processing

Table 5 Major reactions in oxygen burning

(a) Basic energy generation
$^{16}O(^{16}O,\alpha)^{28}Si$ $^{16}O(^{12}O,p)^{31}P$ $^{16}O(^{16}O,n)^{31}S\ (e^{+}\nu)^{31}P$
$^{31}P\ (p,\alpha)^{28}Si\ (\alpha,\gamma)^{32}S$
$^{28}Si\ (\gamma,\alpha)^{24}Mg\ (\alpha,p)^{27}Al\ (\alpha,p)^{30}Si$
$^{32}S\ (n,\gamma)^{33}S\ (n,\alpha)^{30}Si\ (\alpha,\gamma)^{34}S$
$^{28}Si\ (n,\gamma)^{29}Si\ (\alpha,n)^{32}S\ (\alpha,p)^{35}Cl$
$^{29}Si\ (p,\gamma)^{30}P\ (e^{+}\nu)^{30}Si$
Electron captures
$^{33}S\ (e^{-},\nu)^{33}P\ (p,n)^{33}S$
$^{35}Cl\ (e^{-},\nu)^{35}S\ (p,n)^{35}Cl$
(b) High temperature burning
$^{32}S\ (\alpha,\gamma)^{36}Ar\ (\alpha,p)^{39}K$
$^{36}Ar\ (n,\gamma)^{37}Ar\ (e^{+}\nu)^{37}Cl$
$^{35}Cl\ (\gamma,p)^{34}S\ (\alpha,\gamma)^{38}Ar\ (p,\gamma)^{39}K\ (p,\gamma)^{40}Ca$
$^{35}Cl\ (e^{-},\nu)^{35}S\ (\gamma,p)^{34}S$
$^{38}Ar\ (\alpha,\gamma)^{42}Ca\ (\alpha,\gamma)^{46}Ti$
$^{42}Ca\ (\alpha,p)^{45}Sc\ (p,\gamma)^{46}Ti$
(c) Low temperature, high density burning
$^{31}P\ (e^{-}\nu)^{31}S$ $^{31}P\ (n,\gamma)^{32}P$
$^{32}S\ (e^{-},\nu)^{32}P\ (p,n)^{32}S$
$^{33}P\ (p,\alpha)^{30}Si$

Table 6 Major reactions in neon burning

(a) Basic energy generation
^{20}Ne $(\gamma,\alpha)^{16}$O ^{20}Ne $(\alpha,\gamma)^{24}$Mg $(\alpha,\gamma)^{28}$Si
(b) Fluxes $> 10^{-2}\times$ (a)
^{23}Na (p,α)^{20}Ne ^{23}Na (α,p)^{26}Mg (α,n)^{29}Si
^{20}Ne (n,γ)^{21}Ne (α,n)^{24}Mg (n,γ)^{25}Mg (α,n)^{28}Si
^{28}Si (n,γ)^{29}Si (n,γ)^{30}Si
^{24}Mg (α,p)^{27}Al (α,p)^{30}Si
^{26}Mg (p,γ)^{27}Al (n,γ)^{28}Al ($e^-\bar{\nu}$)^{28}Si
(c) Low temperature, high density burning
^{22}Ne (α,n)^{25}Mg (n,γ)^{26}Mg (n,γ)^{27}Mg ($e^-\bar{\nu}$)^{27}Al
^{22}Ne left from prior neutron-rich carbon burning

Table 7 Electron capture

$p + e^- \rightarrow \nu_e + n$ or p (e^-, ν_e)n
$(A, Z) + e^- \rightarrow \nu_e + (A, Z-1)$ or ^{A}Z $(e^-, \nu_e)^A$Z-1
$E_F(\rho Y_e = 10^7$ g cm$^{-3}) = 0.75$ MeV
$E_F(\rho Y_e = 10^9$ g cm$^{-3}) = 4.70$ MeV

the inverse capture reaction). This ensures the existence of photons with energies $> Q$ in the Planck distribution and leads to Ne burning [^{20}Ne $(\gamma,\alpha)^{16}$O, ^{20}Ne $(\alpha,\gamma)^{24}$Mg] at $T > 1.5 \times 10^9$ K (preceding O burning) due to a small Q-value of $\approx$ 4 MeV and Si burning at temperatures in excess of 3×10^9 K [initiated like Ne burning by photodisintegrations]. Such photodisintegrations (after integrating over a thermal (Planck) distribution of photons at temperature T) enter as a temperature-dependent one-body reaction in Eq. (16) and act similar to decays, but with a temperature-dependent decay constant. In Table 6, we provide some of the main reactions of Ne burning, which is initiated by the photodisintegration of ^{20}Ne.

Stellar nucleosynthesis at high densities leads to electron-gas degeneracy, i.e. the Pauli exclusion principle for fermions determines the population of energy states rather than the Boltzmann statistics, valid only for low densities/high temperatures. The Fermi energy of electrons is

$$E_F = \hbar^2/2m_e(3\pi^2)^{2/3}n_e^{2/3}. \tag{28}$$

Here, n_e is the density of the electron gas $n_e = \rho N_A Y_e$, ρ denotes the matter density, and N_A the Avogadro's number. If in stellar late stages this Fermi energy of (degenerate) electrons increases to the level of nuclear energies (MeVs), electron captures can have a major impact. In a neutral, completely ionized plasma, the electron abundance Y_e is equal to the total proton abundance $Y_e = \sum_i Z_i Y_i$ (summing over all abundances of nuclei, including protons/hydrogen) and limited by the extreme values

Fig. 13 Burning timescales in ($\log_{10}$) seconds for fuel destruction of He, C, and O burning (top) and Ne and Si burning (buttom) as a function of temperature. Density-dependent timescales are labeled with a chosen typical density (in $\mathrm{g\,cm^{-3}}$). They scale with $1/\rho$ for C- and O burning and $1/\rho^2$ for He burning. Ne- and Si burning, initiated by photodisintegrations, are not density dependent. The almost constant He burning timescale beyond $T_9 = T/10^9\,\mathrm{K} = 1$ permits efficient destruction on explosive timescales only for high densities. Image reproduced with permission from Thielemann et al. (2018a), copyright by Springer

0 (only neutrons) and 1 (only protons) with typical values during stellar evolution close to 0.5 or slightly below. Such conditions permit electron captures on protons and nuclei, if the negative Q-value of the reaction can be overcome by the electron (Fermi) energy. The general features for typical conditions are presented in Table 7; example reactions are already given in Table 5.

Thus, at sufficiently high densities, electron captures—which are energetically prohibited—can become possible and lead to an enhanced *neutronization* of the astrophysical plasma, in addition to the role of beta-decays and electron captures with positive Q-values (Langanke et al. 2021). If after C burning Ne–O–Mg plasmas are degenerate, electron captures on ^{20}Ne and ^{24}Mg can cause a substantial loss of degeneracy pressure support (leading possibly to a fast collapse and so-called electron capture supernovae (EC supernovae; Leung et al. 2020; see also Sect. 6). In Si burning, electron capture on intermediate-mass and Fe-group nuclei becomes highly important and determines the neutronization (Y_e). Such rates contribute also to the one-body reaction terms in Eq. (16) with the effective decay constants being a function of T and $n_e = \rho N_A Y_e$, the electron number density.

As we discuss at this point weak interaction processes in stellar environments, we add here also neutrino interactions, although they are only of importance at much higher densities in the final stages of stellar collapse or explosive environments. Neutrino cross sections for reactions on nucleons, nuclei, and electrons are minute (Balasi et al. 2015). It therefore requires high densities of the order $\rho > 10^{12}\,\mathrm{g\,cm^{-3}}$ such that also the inverse process to electron/positron capture (neutrino capture) can occur on relevant timescales. The same is true for other processes such as, e.g. inelastic scattering, leaving a nucleus in an excited state that can emit nucleons and alpha particles in exit channels. Such neutrino-induced reactions can be expressed in a similar way as photon and electron captures, integrating now over the corresponding neutrino distribution. The latter is, however, not necessarily in thermal equilibrium and not just a function of temperature and neutrino densities. Neutrino distributions are rather determined by (neutrino) radiation transport calculations, discussed in later sections mostly related to stellar explosions.

Core Si burning, the final burning stage during stellar evolution, is initiated by the photodisintegration $^{28}\mathrm{Si}\,(\gamma,\alpha)^{24}\mathrm{Mg}$ close to 3×10^9 K—followed by a large number of fusion and photodisintegration reactions, as well as electron captures at high densities—and ends with nuclear reactions in a complete chemical equilibrium (all strong thermonuclear and photodisintegration reactions are equilibrated, while weak interaction reactions, changing Y_e, may occur on longer timescales). This "nuclear statistical equilibrium" (NSE) is reached via precursor quasi-equilibrium (QSE) phases (see below), with nuclei in the Si-group as well as Fe-group in local equilibria, but not a global equilibrium (see also Fig.13 in Chieffi et al. 1998) and

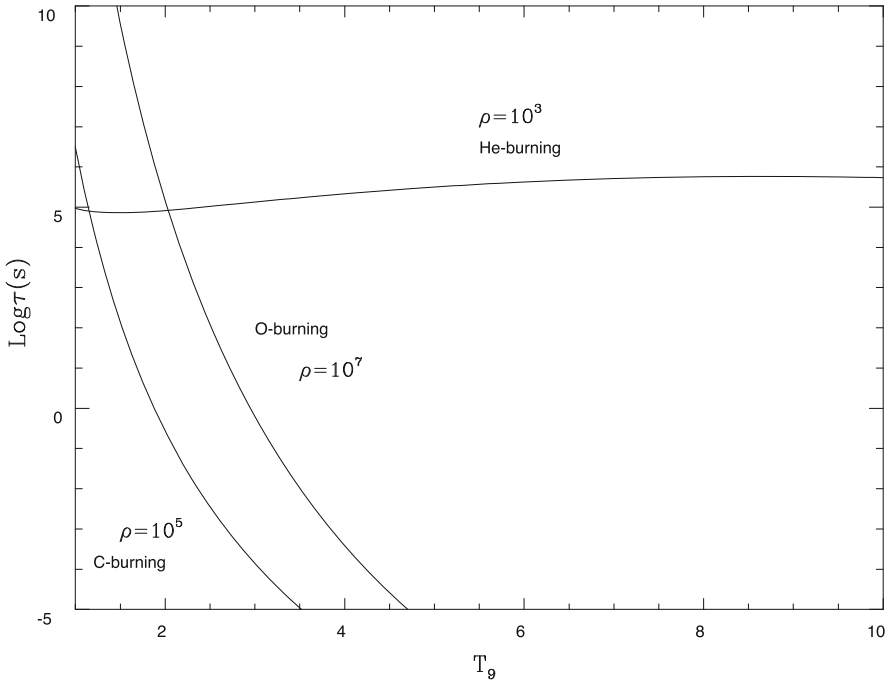
10
5
0
-5
2
4
6
8
10
$\rho=10^3$
He-burning
O-burning
$\rho=10^7$
$\rho=10^5$
C-burning
$\mathrm{Log}\tau(\mathrm{s})$
T_9

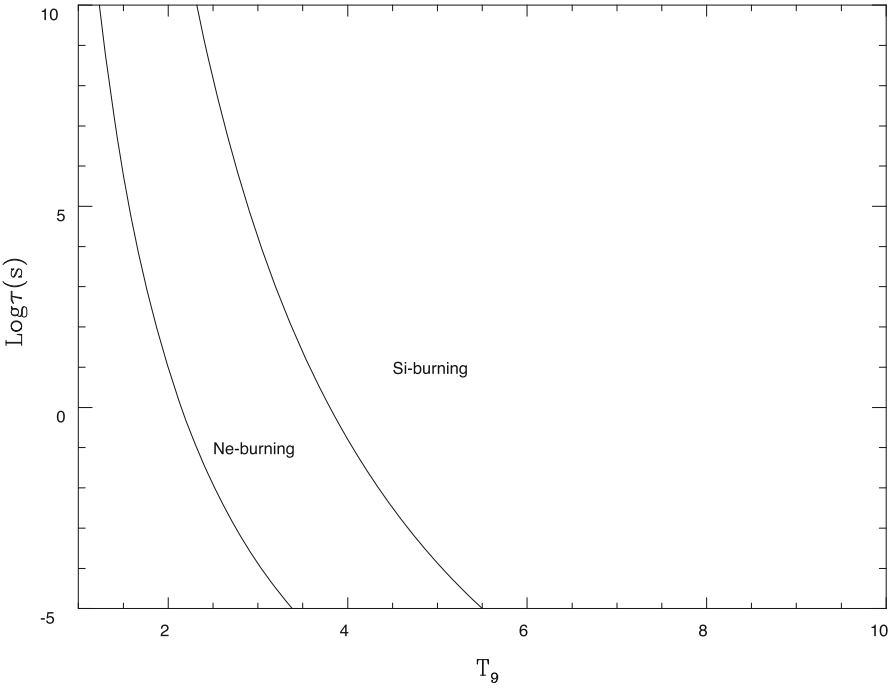
10
5
0
-5
2
4
6
8
10
Si-burning
Ne-burning
$\mathrm{Log}\tau(\mathrm{s})$
T_9

further extended discussions in (Hix and Thielemann 1996). An NSE abundance distribution is centred around Fe (with nuclei possessing the highest binding energies). These temperatures permit photodisintegrations with typical Q-values of 8–10 MeV as well as the penetration of Coulomb barriers in the capture reaction. In such an NSE, the abundance of each nucleus Y_i is only dependent on temperature T, density ρ, its nuclear binding energy B_i, and via charge conservation on $\sum_i Z_i Y_i = Y_e$ (see Eq. (8)). Y_e is altered by weak interactions on longer timescales. The above-mentioned quasi-equilibria can occur, if localized regions in the nuclear chart are in equilibrium with the background of free neutrons, protons and alphas, but offset from other regions of nuclei and thus their NSE values (Hix and Thielemann 1996, 1999a; Hix et al. 2007). Different quasi-equilibrium regions are usually separated from each other by slow reactions with typically small Q-values. Such boundaries between QSE groups, due to slow reactions, can be related to neutron or proton shell closures, like e.g. $Z = N = 20$, separating the Si- and Fe-groups in early phases of Si burning.

All the reactions presented above, occurring at different times in the sequence of burning stages, contribute to the three types of terms in the reaction network Eq. (16), determining the composition change of nuclear abundances Y_i. These stellar burning stages are essentially related to nuclei from H to the Fe-group, and not much beyond.

4.2 Explosive burning

4.2.1 Explosive He, C, Ne, O, and Si burning

Many of the hydrostatic nuclear burning processes occur also under explosive conditions at higher temperatures and on shorter timescales. One can define a timescale for a specific reaction destroying fuel Y_i in terms of $\dot{Y}_i = -1/\tau_i Y_i$. When considering Eq. (16), this leads to $-1/\tau_i$ for decays or photodisintegrations in a term $N_i^i \lambda_i$, in case of two-body reactions with a reaction partner Y_j to $N_{j,i}^i/(1+\delta_{ji})\rho N_A \langle \sigma v \rangle_{j,i} Y_j$ and in case of three-body reactions to a term $N_{j,k,i}^i/(1+\Delta_{j,k,i})\rho^2 N_A^2 \langle \sigma v \rangle_{j,k,i} Y_j Y_k$. Dependent on the burning process and the major destruction reaction, only one term out of either of the three sums in Eq. (16) defines the burning timescale, which is in case of photodisintegrations determined by $N_i^i \lambda_i(T)$ and not density dependent; for a dominant two-body reaction we find a linear ρ dependence, and for dominant three-body reactions (like in He burning) we find a quadratic ρ dependence. Keeping this in mind, Fig. 13 shows the corresponding behaviour, defining the timescales for (explosive) He, C, Ne, O, and Si burning as a function of temperature. With typical explosive timescales of 1s, i.e. $log(\tau) = 0$, many β-decay half-lives are longer than the explosive timescales, producing significant abundances of unstable isotopes, as burning proceeds. This requires in general the additional knowledge of nuclear reactions for unstable nuclei. The fuels for explosive nucleosynthesis consist mainly of $N = Z$ nuclei like ^{12}C, ^{16}O, ^{20}Ne, ^{24}Mg, or ^{28}Si (the ashes of prior stellar burning), resulting in heavier nuclei, again with $N \approx Z$. At high densities also substantial electron captures on nuclei

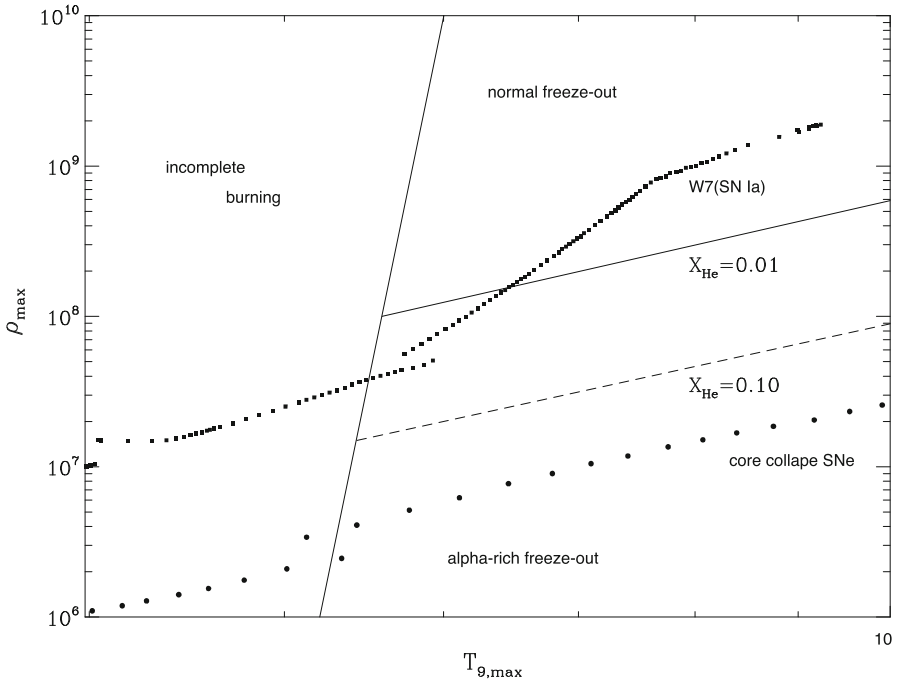

Fig. 14 Final results of explosive Si burning as a function of maximum temperatures and densities attained in explosions before adiabatic expansion. For temperatures in excess of 5×10^9 K, any fuel previously existing is photodisintegrated into nucleons and alpha particles before re-assembling in the expansion. For high densities, this is described by a full NSE with an Fe-group composition favoring nuclei with maximum binding energies and proton/nucleon ratios equal to Y_e. For lower densities, the NSE breaks into local equilibrium groups (quasi-equilibrium, QSE) with group boundaries determined by reactions with an insufficiently fast reaction stream. Alpha-rich freeze-out (insufficient conversion of alpha-particles into nuclei beyond carbon) is such a QSE-behaviour. Lines with 1% and 10% remaining alpha mass fraction are indicated, as well as typical conditions in type Ia and core collape supernovae that will be discussed in later sections. Image reproduced with permission from Thielemann et al. (2018a), copyright by Springer

$e^- +^A Z \rightarrow^A Z\text{-}1 + \nu$ can occur due to energetic, degenerate electrons when Fermi energies are high, as already discussed for late burning stages.

Explosive Si burning differs strongly from its counterpart during stellar burning phases and can be divided into three different regimes: (i) incomplete Si burning and complete Si burning with either (ii) a normal (high density, low entropy) or (iii) an alpha-rich (low density, high entropy) freeze-out of charged-particle reactions during cooling from NSE. At high temperatures or during a normal freeze-out, the abundances remain in a full NSE. The full NSE can break up into smaller equilibrium clusters (quasi-equilibrium, QSE), as already mentioned above, An example for such QSE-bevaviour is an alpha-rich freeze-out, caused by the inability of the triple-alpha reaction ^{4}He $(2\alpha, \gamma)^{12}$C, and the ^{4}He $(\alpha n,\gamma)^9$Be reaction to keep light nuclei like n, p, and ^{4}He, and nuclei beyond $A = 12$ in an NSE during declining temperatures, when the densities are small. This causes a large alpha abundance after freeze-out of

reactions. This effect is a function of entropy, being proportional to T^3/ρ in a radiation-dominated plasma (see Fig. 14).

4.2.2 The p-process or γ-process

In a range of temperatures related to explosive Ne/O burning, partial (but not complete) photodisintegration of pre-existing nuclei can occur, i.e. at $\approx 2-3\times10^9$K. This γ-process starts with the photodisintegration of stable seed nuclei that are present in the stellar plasma. During the photodisintegration period, neutron, proton, and alpha-emission channels compete with each other and with beta-decays further away from stability. In general, the process, acting like "spallation" of pre-existing nuclei, commences with a sequence of (γ,n)-reactions, moving the abundances to the proton-rich side of stability (see Fig. 4). At some point in a chain of isotopes, (γ,p) and/or (γ, α)-reactions become faster than neutron emissions, and the flow branches and feeds other isotopic chains. At late times, photodisintegrations become less effective, when decreasing temperatures shift the branching points and make beta-decays more important. Finally, the remaining unstable nuclei decay back to stability and can produce proton-rich stable isotopes as seen in Figs. 4 and 11. The branchings established by the dominance of proton and/or alpha-emission over neutron emission are crucial in determining the radioactive progenitors of the stable p-nuclei and depend on the ratios of the involved reaction rates. Numerous experimental and theoretical efforts have been undertaken to improve the reaction input, especially with respect to open questions in optical potentials for alpha particles and protons (Fülöp et al. 2005; Gyürky et al. 2006; Kiss et al. 2012; Gyürky et al. 2010; Güray et al. 2015; Korkulu et al. 2018; Mohr et al. 2020). Further details will be discussed together with the nucleosynthesis in explosive stellar events in Sects. 6 and 7.1.

4.2.3 The r-process in explosive burning

r-process nucleosynthesis (rapid neutron capture) was initially introduced shortly in Sect. 1.3, indicating that high neutron densities are required that lead to highly neutron-rich unstable isotopes off stability. This is accompanied by photodisintegrations via a sufficiently hot photon bath and results in a process path as shown in Fig. 4, where for each element the isotope with a maximum abundance is located. The beta-decay of these so-called "waiting point nuclei" determine the speed of of the build-up of heavy elements. Such sudden, high neutron densities result from explosive conditions that correspond to subsets of explosive Si burning, either with low or high entropies, experiencing a normal or alpha-rich freeze-out. The major requirement for a successful r-process is a neutron/heavy seed nuclei ratio of 10–150 after freeze-out of charged particle reactions (to produce all, including the heaviest, r-process nuclei via neutron capture from seed abundances). This translates for a normal freeze-out into $Y_e = 0.12-0.3$. Alternatively, for a moderate $Y_e > 0.40$, an extremely alpha-rich freeze-out is needed (see the discussion in later sections focusing on stellar r-process sites and, e.g. Cowan et al. 2021). Under these

conditions, the large mass fraction in ^{4}He (with $N = Z$) would permit ratios of remaining free neutrons to (small) abundances of heavier seed nuclei, which are sufficiently high to attain r-process conditions. In many cases QSE-groups of neutron captures and photodisintegrations are formed in the isotopic chains of heavy elements during the working of the r-process.

Such a so-called $(n,\gamma) - (\gamma,n)$ equilibrium leads to maxima in each isotopic chain at nuclei with essentially the same Q-value for neutron captures (also known in the inverse reaction as neutron separation energy S_n). It results from chemical equilibrium conditions for neutron capture reactions with $\mu_n + \mu(Z,A) = \mu(Z,A+1)$, and leads via utilizing the chemical potentials for a Boltzmann gas from Eq. (7) to the relation between neighboring abundances in an isotopic chain $Y(Z,A+1)/Y(Z,A)$

$$\frac{Y(Z,A+1)}{Y(Z,A)} = n_n \frac{G(Z,A+1)}{2G(Z,A)} \left[\frac{A+1}{A}\right]^{3/2} \times \left[\frac{2\pi\hbar^2}{m_u kT}\right]^{3/2} \exp\left(\frac{S_n(A+1)}{kT}\right). \tag{29}$$

This causes the existence of an r-process path (see Fig. 4), related to a specific neutron separation energy S_n (see Fig. 15), which is determined by the neutron density n_n and temperature T. Opposite to the s-process, where the beta-decay half-lives are fast in comparison to the slow neutron capture timescales, in an r-process, dominated by high neutron densities and sufficiently high photodisintegration rates to reach a fast abundance equilibrium in an isotopic chain, its speed of the buildup of heavy elements is controlled by the beta-decay half-lives. This is also the reason, why at the kinks in the path at closed neutron shells (where the path comes closest to stability and experiences the longest half lives) the corresponding A determines the position of the r-process peaks. This is an approximate behaviour, and in reality the calculations require a full network solution with all necessary nuclear input. However, such approximations give clues to a full understanding of the results.

This underlines that the final outcome is (besides of course the astrophysical environment, to be discussed in later sections) strongly dependent on the nuclear physics input, which enters decisively in producing the abundance pattern of the r-process. Major aspects are related to experimental progress in accessing unstable nuclei far from stability, combined with a growing theoretical understanding of their properties.

This includes novel detection technologies, employed at operational RIB facilities, to determine nuclear masses for nuclei far from stability with improved precision. This also leads to improve (empirical and microscopic) global mass models, which in r-process simulations determine the location of the r-process path in the nuclear chart. This has decisive consequences for the r-process mass flow across neutron-shell closures shaping the final r-process abundance distribution.

The measurement of β-decay half-lives for neutron-rich nuclei at and near the r-process path is of crucial importance for the speed with which the r-process moves matter to heavier nuclei and (in combination with the location of the r-process path)

for the height of peaks and the overall final abundance distribution. β-delayed neutron emission is important in the late phases during decay back to stability, in particular for nuclei close to the $N = 126$ shell closure. Such measurements will be of crucial relevance to determine the amount of matter that is transported beyond the third r-process peak into the fission region (see Fig. 16).

Fission plays a crucial role in current r-process models, in particular related to high neutron density environments. Here, fission terminates the flow to heavier nuclei beyond the actinides, causing fission cycling. This returns matter to lighter nuclei and is also a source of neutrons, which can shape the final abundance pattern. In these models, fission yields contribute strongly to the second r-process peak. Fission also affects the heaviest long-lived nuclei that are produced by the r-process. Heavy neutron-rich nuclei, in particular those at the $N = 184$ shell closure, are still experimentally out of reach. But experimental programs are envisioned to push the measurement of fission rates and yields to more neutron-rich nuclei than currently accessible. Such improvements are also required to address the question whether superheavy elements can be produced by the r-process.

Simulations identify α-decays, especially the decay chains originating from actinide nuclei, as important contributors to the emitted light curve expected from r-process events and do determine the r-process Pb abundance. Many of these decays are experimentally studied. It is an open question whether α-decays can compete with fission for heavy neutron-rich nuclei.

Neutron captures (and their inverse photodisintegration) affect the final abundance distribution during the r-process freeze-out period. (Fortunately, for a large variety of conditions during the r-process buildup, a chemical equilibrium between these two reactions can be maintained and the r-process path is determined solely by nuclear masses.) The nuclei involved can have very low neutron separation energies (with a low density of states) so that direct neutron captures might be favored over compound nucleus reactions. But direct measurements of neutron capture rates for r-process nuclei are experimentally still out of reach. If the direct capture is dominated by individual resonances, the rate can be constrained by indirect determination of the resonance parameters.

Without giving here a substantial number of related references, these issues are discussed in extended detail in a recent *Reviews of Modern Physics* article (Cowan et al. 2021). However, we want to point to a few studies which show the impact of mass models, beta decays, fission, and other decay properties (Mendoza-Temis et al. 2015; Eichler et al. 2015, 2019; Côté et al. 2019; Barnes et al. 2021; Zhu et al. 2021; Lund et al. 2022).

4.2.4 Neutrinos affecting explosive burning and the νp-process

Neutrinos, and in particular electron flavor neutrinos, can interact with the ejecta of explosive burning and reset the composition that is commonly determined by a balance between the following reactions:

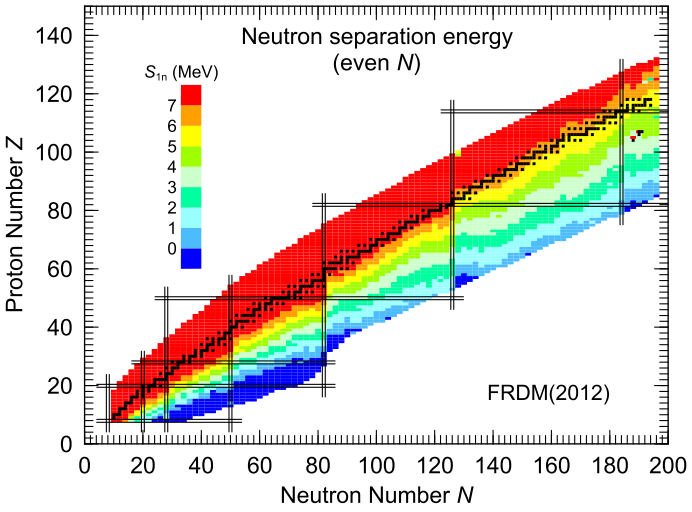

Fig. 15 Location of the valley of stability (black squares) and contour colouring of the value of the neutron separation energy S_n from Möller et al. (2016). The drip line is located at $S_n = 0$. The proton drip line is found closer to stability as the charge increase enhances the Coulomb repulsion. It is located close to the left limits of the contour shading shown in the plot. For images see https://t2.lanl.gov/nis/molleretal/

$$\nu_e + n \leftrightarrow p + e^- \tag{30}$$

$$\bar{\nu}_e + p \leftrightarrow n + e^+. \tag{31}$$

Therefore, neutrinos are responsible for dialing the local n/p ratio or Y_e. Due to the fact that the second reaction is energetically favored (because of the neutron–proton mass difference) when neutrino and anti-neutrino energies are of similar size, matter can become proton rich with $Y_e > 0.5$ under these conditions. If the material is sufficiently long subject to these processes, this tends to reach an equilibrium between neutrino and antineutrino captures (Qian and Woosley 1996; Martínez-Pinedo et al. 2017) and results in an electron fraction Y_e, which determines the ejecta composition

$$Y_e = Y_{e,\mathrm{eq}} = \left[1 + \frac{L_{\bar{\nu}_e} W_{\bar{\nu}_e}}{L_{\nu_e} W_{\nu_e}} \frac{\varepsilon_{\bar{\nu}_e} - 2\Delta + \Delta^2/\langle E_{\bar{\nu}_e}\rangle}{\varepsilon_{\nu_e} + 2\Delta + \Delta^2/\langle E_{\nu_e}\rangle}\right]^{-1}, \tag{32}$$

with L_{ν_e} and $L_{\bar{\nu}_e}$ being the neutrino and antineutrino luminosities, $\varepsilon_\nu = \langle E_\nu^2\rangle/\langle E_\nu\rangle$ (similarly for antineutrinos), $\Delta = 1.2933$ MeV the neutron–proton mass difference, and $W_\nu \approx 1 + 1.01\langle E_\nu\rangle/(m_u c^2)$, $W_{\bar{\nu}} \approx 1 - 7.22\langle E_{\bar{\nu}}\rangle/(m_u c^2)$ the weak-magnetism correction to the cross sections for neutrino and antineutrino absorption (Horowitz 2002) with m_u being the nucleon mass.

These reactions can turn matter neutron rich (of importance for the previous r-process subsection) or proton rich. The neutron-rich option is only given, provided the following condition is fulfilled, otherwise matter turns slightly proton rich with $Y_e > 0.5$,

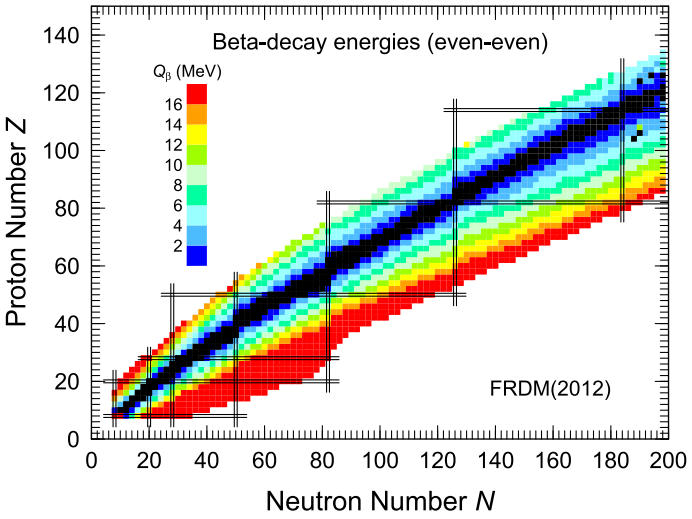

Fig. 16 Beta-decay Q-values as predicted by Möller et al. (2016), including β^- and β^+-decay on the neutron- as well as proton-rich side of stability. For images see https://t2.lanl.gov/nis/molleretal/

$$\varepsilon_{\bar{\nu}_e} - \varepsilon_{\nu_e} > 4\Delta - \left[\frac{L_{\bar{\nu}_e} W_{\bar{\nu}_e}}{L_{\nu_e} W_{\nu_e}} - 1\right](\varepsilon_{\bar{\nu}_e} - 2\Delta). \tag{33}$$

In case of a slightly proton-rich environment, the related ejecta can experience the so-called νp-process that produces nuclei beyond the Fe/Ni-group and possibly up to $A = 80 - 90$ (Fröhlich et al. 2006; Pruet et al. 2006; Wanajo 2006; Eichler et al. 2018), if matter is ejected under the influence of a strong neutrino flux. The result is that such conditions can overcome nucleosynthesis problems for the Fe-group (which will be discussed in the supernova section), but—depending on the entropy and the expansion of matter—only a fraction of those form the iron-group nuclei in the case of an alpha-rich freeze-out. In case of a proton-rich environment, there are also still free protons available at the time of the alpha freeze-out. Once the temperature drops to about 2×10^9 K, the composition of the ejecta consists mostly of ^{4}He, protons, and iron-group nuclei with N $\approx$ Z (mainly ^{56}Ni) of decreasing abundance. Without neutrinos, synthesis of nuclei beyond the iron peak becomes very inefficient due to bottleneck (mainly even–even $N = Z$) nuclei with long beta-decay half-lives and small proton-capture cross sections. Such a nucleus is ^{64}Ge. Thus, with the Y_e determined by neutrino interactions with free neutrons and protons in the early very hot phase of dissociated nuclei, nucleosynthesis leads to an alpha- and proton-rich freeze-out that does not stop at ^{56}Ni, but continues up to ^{64}Ge (which later decays to ^{64}Zn). This part of the story permits to produce Fe-group nuclei up to essentially ^{64}Zn.

However, if matter is subject to a large neutrino/antineutrino flux, antineutrinos are readily captured both on free protons and on heavy nuclei on a timescale of a few seconds. As protons are more abundant than heavy nuclei, antineutrino captures occur predominantly on protons, leading to residual neutron densities of

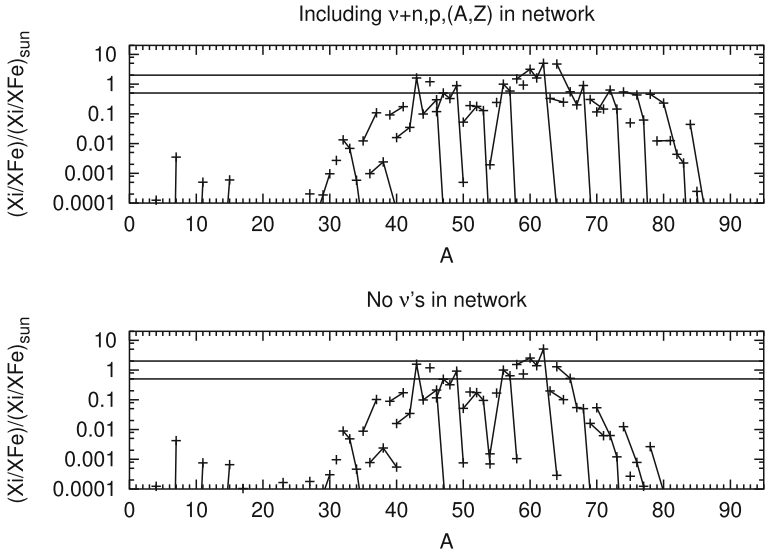

Fig. 17 Final abundances of explosive Si burning in matter that experienced neutrino irradiation, leading to proton-rich conditions ($Y_e > 0.5$). The lower part of the figure shows the neucleosynthesis results after alpha-rich and proton-rich freeze-out from Si burning, normalized to solar after decay. The top part of the figure also includes the interaction of anti-electron neutrinos with protons ($\bar{\nu}_e + p \rightarrow n + e^+$), produces neutrons, permitting the late change of ^{64}Ge via ^{64}Ge $(n,p)^{64}$Ga. This feature permits further proton captures to produce heavier nuclei (the so-called νp-process). Here, matter up to $A = 85$ is produced. Image reproduced with permission from Thielemann et al. (2018a), copyright by Springer

10^{14}–10^{15} cm^{-3} for several seconds. These neutrons are easily captured by heavy neutron-deficient nuclei, for example ^{64}Ge, inducing (n, p) reactions with timescales much shorter than the beta-decay half-life. This permits further proton captures and allows the nucleosynthesis flow to continue to heavier nuclei (see top part of Fig. 17). The νp-process (Fröhlich et al. 2006) is this sequence of (p, γ)-reactions, followed by (n, p)-reactions or beta-decays, where the neutrons are supplied by antineutrino captures on free protons. We will discuss direct applications to core-collapse supernova nucleosynthesis in the supernova section (Sect. 6).

5 Stellar evolution

In the last section, we have discussed nuclear burning processes in detail, including also individual reactions. In the present section, we will discuss the physics of stellar evolution and major observational features related to it, but leave a technical description of how mass, energy, and momentum conservation equations as well as energy transport (via radiation or convective motions) are treated to review articles or textbooks (see e.g. Kippenhahn et al. 2013).

The evolution of a star depends on its initial mass, metallicity, and rotation. Table 9 (note that the exact values may depend on many uncertainties in stellar modelling, such as the treatment of convection, overshooting, reaction cross sections,

Table 8 Neutrino reactions

$\nu_e + n \leftrightarrow p + e^-$ or n (ν_e, e^-)p
$\bar{\nu}_e + p \leftrightarrow n + e^+$ or p ($(\bar{\nu}_e, e^+)$n
$\nu_e + (Z,A) \leftrightarrow (Z+1,A) + e^-$ or ^{A}Z $(\nu_e, e^-)^A$Z + 1
$\bar{\nu}_e + (Z,A) \leftrightarrow (Z-1,A) + e^+$ or ^{A}Z $(\bar{\nu}_e, e^+)^A$Z-1
$(Z,A) + \nu \leftrightarrow \nu + (Z,A)^*$

Table 9 Stellar-evolution dependency on mass

	Central H burning	Central He burning	End stage
Low mass	pp chain	He flash	Degenerate CO core
	$0.8\,M_\odot < M < 1.2\,M_\odot$	$M < 2\,M_\odot$	
Intermediate mass	CNO cycle	Stable	Degenerate CO core
	$M > 1.2\,M_\odot$	$M > 2\,M_\odot$	$M < 8\,M_\odot$
Massive star	CNO cycle	Stable	Further stable burning
	$M > 1.2\,M_\odot$	$M > 2\,M_\odot$	Iron core ($M > 11\,M_\odot$)

etc.) shows a summary of the evolution dependency on the mass that we will shortly discuss here together with the metallicity dependency. The impact of rotation will be discussed at the end of this section.

5.1 Hydrogen burning

The first step of the evolution is H burning, while the star is on the so-called main sequence (MS) of the Hertzsprung–Russell (HR) diagram, relating the stellar luminosity to the surface temperature (colour). At the zero age main sequence (ZAMS), the position in the HR diagram depends on the mass and metallicity of the stars. Massive stars have higher luminosities and temperatures than low-mass stars. Stars on the ZAMS are in hydrostatic and thermal equilibrium. Metal-poor stars are hotter and have smaller radii. For low-mass stars, lower metallicity leads to lower bound-free and free–free opacity and thus to higher luminosities. For high-mass stars, the opacity is dominated by electron scattering that does not depend on metallicity; therefore, stars with different metallicities have the same luminosity. However, they have different central temperatures because hydrogen burning for high-mass stars proceeds via the CNO cycle, and depends on the metallicity, namely on the amount of C, N, and O. Therefore, a reduced metallicity requires a higher temperature to compensate for the reduced efficiency of the CNO cycle.

The evolution during the MS depends on the way hydrogen is burnt (Sect. 4): via the pp chain for stars with $0.08\,M_\odot < M < 1.2\,M_\odot$ and the CNO chain for

$M > 1.2\,M_{\odot}$. During the central hydrogen burning phase, stars remain in hydrostatic equilibrium. As discussed in Sect. 4, nuclear reactions are very sensitive to temperature. The CNO cycle energy generation goes with $\epsilon \propto T^{18}$ and, due to the fact that the highest temperatures are attained in the centre, a steep temperature gradient would result from radiation energy transport alone. This surpasses the steepness of the temperature gradient that would be caused by adiabatic mass movements and results, according to the Schwarzschild stability criterion, in the onset of convection. Therefore, stars with $M > 1.2\,M_{\odot}$, which experience H burning by the CNO cycle, have a convective core, while stars with $0.08\,M_{\odot} < M < 1.2\,M_{\odot}$, powered by the pp chain with a smaller temperature dependence $\propto T^4$, have a radiative core. Thus, the power of the central nuclear energy sources determines the structure of stars and changes with their masses. An additional aspect relates to energy transport through the stellar envelope outside the burning core. Low-mass stars tend to have a (relatively) compact structure (causing a relatively high density), also outside the core, combined with a low temperature, resulting in high radiation opacities $\propto \rho/T^{7/2}$ and a steep radiative gradient. This leads for stars with $M < 1.5\,M_{\odot}$ to a convective envelope. Therefore (see above), such lower mass stars are characterized by a radiative core and a convective envelope, while more massive stars have a convective core and a radiative envelope.

During core hydrogen burning, the luminosity is balanced by energy release from nuclear reactions in the central part and the star stays in hydrostatic and thermal equilibrium. Dependent on the type of energy transport in central burning (radiative or convective), hydrogen is continuously depleted, starting from the very centre in the first case, or alternatively throughout the whole convective core in the latter case. Therefore, the transition from central to shell H burning, starting in low-mass stars in the outer part of the core before moving to larger radii, is gradual, leading to an inert He core, surrounded by a then established H burning shell and a H-rich envelope. The shell burning occurs in a thick shell surrounding the isothermal He core that grows in mass. In case a limiting mass is reached (the Schönberg–Chandrasekhar SC limit, i.e. the isothermal core exceeds 8–10% of the total mass of the star), it will not be able to sustain the weight of the envelope and contracts while the envelope expands, cools, and turns convective. This follows—as a rule of thumb—what Pols calls the "mirror principle": if the core contracts, the envelope expands and vice versa[7]. In the HR diagram the star leaves the MS, moving onto the red giant branch (RGB). The core of low-mass stars is relatively dense and close to becoming degenerate when they leave the MS. This causes pressure support and a relatively "steady" evolution in the HR diagram. For all stars with $M < 2\,M_{\odot}$, the He core reaches electron degeneracy before the central temperature is high enough for He ignition. In the RGB, mass loss starts to be important as the envelope is loosely bound and the large photon flux can easily remove matter from the stellar surface.

The H-shell burning in intermediate-mass and massive stars starts relatively slow in a thin shell. The He core grows until reaching the SC limit, which leads to its contraction. At this point, the H shell burning accelerates and the star moves quite rapidly to the right in the HR diagram, combined with the expansion of the envelope.

[7] https://www.irya.unam.mx/gente/j.arthur/ESTELAR/.

As the temperature of the envelope decreases, the opacity rises, causing a convectively unstable red giant. In this phase, the base of the convective envelope reaches regions of the former H burning core and material that was processed by the CNO cycle is mixed throughout the envelope up to the surface. This is known as dredge-up. (This dredge-up occurs in low-mass stars as well, which develop a convective envelope.) The core of stars with $M > 2\,M_{\odot}$ remains non-degenerate during H-shell burning until it reaches $T_{\rm c} \simeq 10^8$ K and He is ignited in the core.

A good test for stars in the H burning stage is provided by the best observed star we have, our Sun. It can be constrained by (a) the surface abundance observations that have changed from 1D to 3D interpretations (Asplund et al. 2009, 2021) and should indicate also the initial central composition, the isotopic meteoric abundance composition (Lodders 2021), (b) helio-seismology, which permits determining the central structure, testing the sound speed and also the composition of the interior (Aerts 2021), and (c) solar neutrino observations that measure the neutrinos that are created in pp cycles, but also the CNO cycle (McDonald 2004) (in the Sun about 1% of the neutrino energy is escaping). In the standard solar model (Bahcall and Pinsonneault 2004; Bahcall et al. 2005, 2006), one of the major uncertainties is related to the metallicity of the core, i.e. the content of C, N, and O. The elemental abundances in the core, expected to be consistent with the spectroscopic analysis of the solar atmosphere, seem to disagree with the solar profiles of sound speed and density as well as the depth of the convective zone and the helium abundance obtained by helioseismology (Bahcall et al. 2005). Haxton and Serenelli (2008) noted that a direct study of the CN neutrinos, those from the beta-decay of ^{13}N and ^{15}O, can provide an independent measure of the solar metallicity. However, the CN neutrino flux depends not only on the CN abundance in the solar interior, but also on the associated CN reaction rates in the CNO cycle. The ^{14}N(p,γ)^{15}O reaction is the slowest one in the cycle, thus determining the energy release and neutrino production of the entire cycle. The CNO neutrinos are dominated by the beta-decay of ^{15}O. The recent Borexino results (Agostini et al. 2020) suggest an enhanced reaction rate for the ^{14}N(p,γ)^{15}O reaction at low energies, which is examined presently in underground laboratories (CASPAR) by research groups at Notre Dame and the South Dakota School of Mines (M. Wiescher, private communication). Thus, while our understanding of stellar evolution, even in the earliest burning stage, is quite advanced, there exist still open questions and uncertainties.

5.2 Helium burning

The H burning shell adds mass to the He core until temperatures are reached that allow for He fusion. The evolution depends on the stellar mass. For low-mass stars ($M < 2\,M_{\odot}$), the core is strongly (electron) degenerate, not only for vanishing temperatures but even for $T_{\rm c} \sim 10^8$ K, sufficient for He ignition. The energy generated by the 3α reaction (Sect. 4) increases the temperature. However, the degenerate pressure is at these temperatures only density dependent and the energy

release by fusion does not, yet, increase the pressure and expands the core. All nuclear energy goes into internal energy of the non-degenerate ions, leading to a further temperature increase and thermonuclear runaway. This thermonuclear runaway causes what is known as He flash and produces an enormous amount of energy in a few seconds. Due to energy loss by neutrino emission from the deep interior with the highest densities, and compressional heating released by the advancing H burning shell, this flash is initially ignited off-centre. Part of the core is still degenerate, leading to a series of smaller flashes that proceed towards the centre, accompanied by the formation of a convective core. All energy release is absorbed by expansion of the non-degenerate layers surrounding the core, without reaching up to the surface. Eventually, the degeneracy is lifted when $T \sim 3 \times 10^8$ K and the increasing temperature leads to an increase of the pressure and thus an expansion and cooling of the core. The energy generation decreases until balancing the energy loss rate and the core reaches a thermal equilibrium with stable burning.

For intermediate-mass and massive stars, the core is not degenerate and the He ignition proceeds quietly. Since He burning has an even higher temperature dependence than the CNO cycle ($\propto T^{41}$, Sect. 4), the energy production is concentrated towards the centre and a convective core develops. Once ^{12}C is produced by the 3α reaction, ^{12}C(α,γ) can become active and ^{16}O is produced at a rate that increases with time. The ^{12}C(α,γ) rate (deBoer et al. 2017) and local conditions in the star, affected also by the treatment of convection during the late stages of He burning, have a decisive influence on the C/O ratio at core He depletion (see e.g. Imbriani et al. 2001).

5.3 Late evolution for low- and intermediate-mass stars

After core He burning, a CO core forms with its further evolution determined by the stellar mass. For low- and intermediate-mass stars ($M < 8\,M_\odot$) the core becomes degenerate before the threshold temperature for C ignition is attained, therefore stabilizing the central core by degeneracy pressure and preventing to reach sufficient temperatures to continue through further burning stages or causing a CO flash. These stars evolve then through the asymptotic giant branch (AGB) with the following characteristic phases.

The early AGB phase starts after the He exhaustion, when the CO core contracts and He burning shifts to a surrounding shell. There are two active burning shells. Due to the energy produced in the He burning shell, the He-rich region above it expands and this causes the H burning shell to move to larger radii and thus lower temperatures, resulting in its extinction. The He burning shell adds mass to the growing CO core that becomes, however, degenerate for $M < 8\,M_\odot$ (see above). In stars with $M > 4\,M_\odot$, a second dredge-up takes place, as the convective envelope penetrates down into the He-rich shell layer, while for less massive stars the H burning shell stays active and prevents the mixing. Due to the double shell burning

the stars enter into a thermally pulsating phase where the He burning shell becomes unstable and undergoes periodic pulses TP-AGB. This is a critical phase for nucleosynthesis with many mixing episodes that lead to the s-process (Sects. 4 and 5.4).

Figure 18 shows the phase of thermal pulses and dredge-up. Most of the time the He burning shell is inactive and the H burning shell adds mass to the He-rich region. This brings the intershell mass to a critical value and to an unstable He ignition in a He-shell flash. The large energy flux causes the whole intershell to become convective and triggers efficient mixing. As the H burning shell expands and cools, nuclear reactions stop there and the convective layer can penetrate below it, mixing the envelope material with the intershell, known as third dredge-up. Later on the He burning shell expands and cools, leading to stable He burning. Following the third dredge-up, the H burning shell is active while the He burning shell stops producing energy. This type of thermal pulse cycle can act repeatedly.

5.4 s-process

The s-process is related to late stellar burning phases after core H burning, when stars have turned into giants (in most cases red giants with a large radius increase, but for stars with $M \geq 25\,M_{\odot}$ or rotating massive stars also into blue compact WR stars with mass loss, frequently experiencing rotational mixing). In the subsequent He burning phase (α,n)-reactions can release neutrons. One simple option is ^{22}Ne $(\alpha,n)^{25}$Mg, as already discussed in Sect. 4, due to ^{22}Ne created in He burning, acting on H burning product ^{14}N. The neutrons from this source lead in central He burning of massive stars to the so-called weak s-process with the formation of nuclei up to $A = 90$, via neutron captures and β^--decays. A reaction path was shown in Fig. 11, indicating neutron captures in horizontal steps within the isotopic chain of charge Z, and β^--decays to nucleus $(Z + 1, N - 1)$ with the same mass number A. For making elements as heavy as Pb and Bi more efficient neutron sources are required. The s-process (moving along stability) cannot go beyond these elements as it hits regions of alpha-decay. Neutron captures will populate nuclei above the alpha-emission threshold, and these (n,α) reactions go back to a reduced mass number $A - 3$. The s-process in low and intermediate-mass stars (the main s-process component) takes place due to the fact that the H- and He burning shells are located within a small distance. Both do not burn in a constant fashion. If the H burning zone is on, it creates He fuel. After sufficient He is produced, He is ignited in an unburnt He-rich zone (at sufficient densities and temperatures). The burning is not stable, the amount of energy created in a shallow zone is not sufficient to lift the overlaying H-shell, which could cause expansion and cooling, i.e. steady burning. Instead, He burning, being dependent on the density squared due to the ^{4}He $(2\alpha,\gamma)^{12}$C reaction, burns in a strong flash, causing then a stronger expansion, even stops H burning in the H-shell. This behaviour repeats in recurrent flashes, first introduced and extended by Sanders (1967); Ulrich and Scalo (1972); Iben and Truran (1978), and many further investigations (for reviews see Kappeler et al. 1989; Käppeler et al. 2011; Karakas and Lattanzio 2014; Bisterzo et al. 2017). H is mixed into the unburnt He fuel,

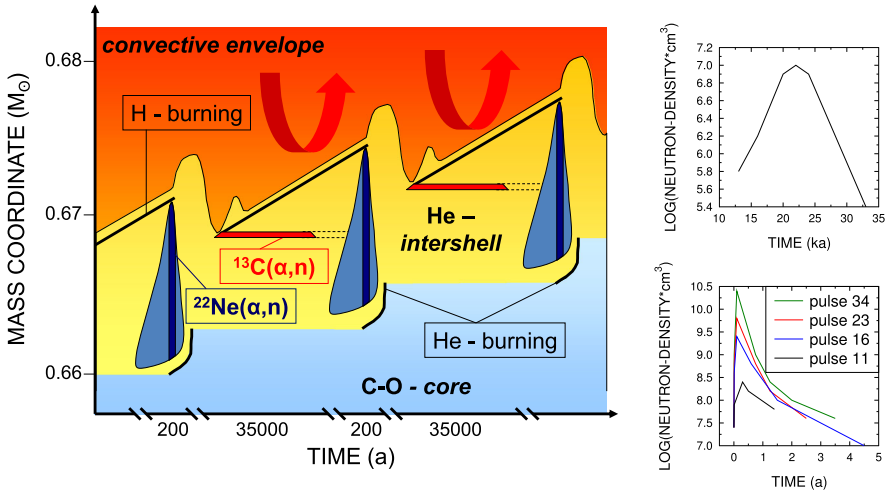

Fig. 18 Working of the s-process in low and intermediate-mass stars with an initial mass of less than $8\,M_{\odot}$. $^{13}C(\alpha,n)^{16}O$ is active in the interpulse period on timescales of more than 10^5 years, while $^{22}Ne\,(\alpha,n)^{25}Mg$ acts only during the He flash, on timescales of years. Image reproduced with permission from Reifarth et al. (2014), copyright by the authors

causing the $^{12}C(p,\gamma)^{13}N(\beta^+)^{13}C(\alpha,n)^{16}O$ reaction sequence (discovered as neutron source by Cameron in 1955) and the production of neutrons in a more efficient way than only via $^{22}Ne\,(\alpha,n)^{25}Mg$. This behaviour is shown in Fig. 18. Figure 19 shows how the strength of the s-process depends on the amount of hydrogen mixed into the He burning shell, which is again strongly dependent on the mass of the stellar model. It should be mentioned that there exists a large level of uncertainty in the production of the so-called ^{13}C pocket and a self-consistent treatment of the efficiency of mixing H into the He core is still missing (see e.g. the above reviews and detailed discussions in Denissenkov and Tout 2003; Buntain et al. 2017; Busso et al. 2021; Vescovi et al. 2021).

5.5 The final fate of low- and intermediate-mass stars

Low- and intermediate-mass stars with $M < 8\,M_{\odot}$ experience only central H- and He burning, leading to a core of C and O. H- and He burning shells move outwards in an unstable fashion with flashes and pulses (as discussed above), expelling the outer mass zones in a stellar wind (causing what is known as a planetary nebula), and leaving a central C + O white dwarf, an object being, even after cooling, stabilized by the degeneracy pressure of the electron gas for $M_{C+O} < 1.4\,M_{\odot}$ (the Chandrasekhar mass, Chandrasekhar 1984). More details can be found, e.g. in Karakas and Lugaro (2016); Kobayashi et al. (2020); Cseh et al. (2022). While we discuss the contribution of planetary nebulae in an integrated way to the inventory of the overall solar system abundances and the abundance evolution of galaxies in later sections, direct proofs for their ejecta composition can be found in the isotopic composition of meteorites, containing inclusions of dust condensates from their winds (Zinner and

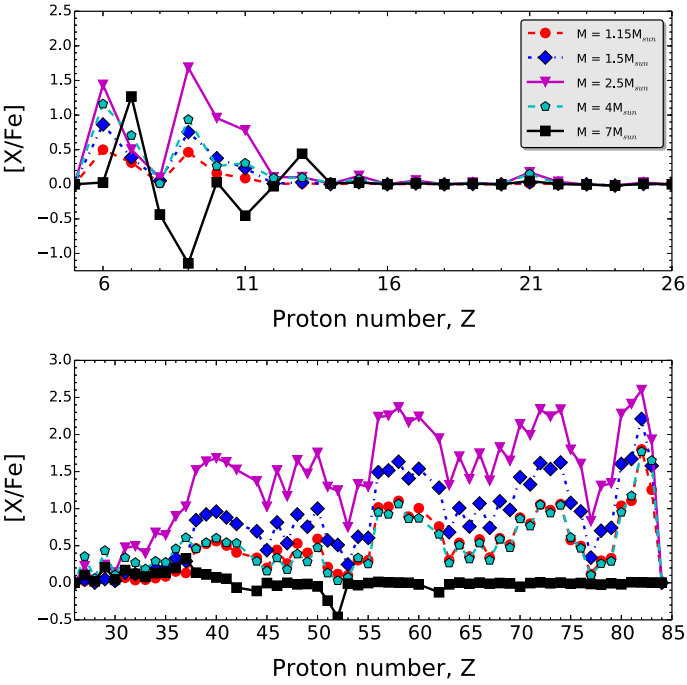

Fig. 19 The result of the s-process in He-shell flashes is dependent on the stellar mass. The process is most active for stars around 2.5 $M_{\odot}$, as can be noticed in this plot, showing the resulting abundance pattern at the end of the stellar life that is blown off in the planetary nebular phase. The overall solar s-process abundances are the result of a superposition of contributing stellar masses, and also of the initial stellar metallicities [Fe/H]. For a "secondary process", acting on pre-existing inherited seed abundances like Fe, the latter influence the n/seed ratios and determine the effectiveness of the process. Both aspects come close to an exponential superposition of neutron exposures τ_n. Image reproduced with permission from Karakas et al. (2018), copyright by the authors

Amari 1999; Lugaro and Gallino 2006; Lugaro and Chieffi 2011; Kobayashi et al. 2020; Busso et al. 2021), for a more general treatment of meteoritic dust inclusions, containing also the imprint from other sources see Nittler et al. (1996); Zinner (1998, 2008b, 2008a); Nittler and Ciesla (2016).

5.6 Massive stars: pre-supernova evolution

While low- and intermediate-mass stars develop a degenerate CO core with a mass smaller than the critical Chandrasekhar mass, avoiding contraction and therefore experiencing only temperatures below the C fusion/ignition temperature, massive stars ($M \gtrsim 8\,M_{\odot}$) can reach high enough temperatures ($T \sim 5 \times 10^8$ K) to undergo non-degenerate C burning. In the range 7–10 $M_{\odot}$ so-called super AGB stars (with properties between AGB stars and red supergiants) are close to the dividing line between becoming CO or NeOMg white dwarfs or permitting even further burning stages (Doherty et al. 2017; Gil-Pons et al. 2018; Leung and Nomoto 2018; Zha et al. 2019; Leung and Nomoto 2019; Leung et al. 2020). Due to (cool) degenerate cores in

that mass range the ignition of these burning stages starts off-centre before propagating to the centre, and the main question is whether this permits to reach core masses that also cause Ne and later O ignition. Stars close to the upper limit of that mass interval follow all nuclear burning stages until an Fe core is formed, that would lead to core-collapse supernova events, discussed in the next section. Characteristic of the late evolution of massive stars is also the mass loss by winds. The stellar wind mechanism is a combination of radiation pressure and pulsation but it is not yet fully understood. The effect of such winds is visible in Wolf–Rayet stars that are hot and have high luminosities combined with strong emission lines. Such winds lead to mass loss, which can prevent shell burning from causing sufficiently high core masses for the ignition of the next burning stage. This is the main reason why stars, which ignite C burning, do not automatically ignite also Ne and subsequently O and Si burning, but can rather lead to ONeMg dwarfs.

An important aspect for the late evolution beyond He burning is related to neutrinos. After the CO core forms, they are involved in the sequence of nuclear burning and core contraction cycles, becoming the main energy loss mechanism, while the earlier burning phases were dominated by radiation losses. Neutrino emission accelerates the evolution of the core while the outer envelope has no time to react and is disconnected from the core. Neutrinos are produced by nuclear reactions and also by weak interaction processes that become possible at high temperature: pair annihilation at $T > 10^9\,\mathrm{K}$ ($e^+ + e^- \rightarrow \nu + \bar{\nu}$), the photo-neutrino process ($\gamma + e^- \rightarrow e^- + \nu + \bar{\nu}$), the plasma-neutrino process, and via bremsstrahlung. Of these, the pair annihilation process is the most efficient in the evolution of massive stars due to their high central temperatures. At $T \sim 10^8\,\mathrm{K}$ neutrinos are the most important energy loss mechanism and balance the energy produced by nuclear reactions ($\dot{E}_{\mathrm{nuc}} \approx L_\nu$).

In Sect. 4, we have described the main reactions occurring beyond C burning, and here we will shortly describe the evolution and structure of the stars. When the temperature of the CO cores reaches $5 - 8 \times 10^8$ K, carbon burning proceeds and $^{12}\mathrm{C} + {}^{12}\mathrm{C}$ produces mainly $^{20}\mathrm{Ne}$ and $^{24}\mathrm{Mg}$. This is affected by the initial C/O ratio, depending on the uncertain $^{12}\mathrm{C}(\alpha,\gamma)^{16}\mathrm{O}$ rate and the treatment of mixing in core He burning (see the earlier discussion and Imbriani et al. 2001; deBoer et al. 2017). After all C has been burnt in the centre, the core contracts and C burning continues in a convective shell surrounding the core, taking place in a number of subsequent convective episodes that depend on the initial stellar mass.

As mentioned above, in the lower part of the mass interval of super AGB stars the CO core is partially degenerate and turns after C burning into a degenerate ONeMg core without further nuclear burning taking place. The following evolution depends on whether the Chandrasekhar mass limit is reached for the core after shell burning or whether mass loss is high enough and an ONeMg white dwarf is left behind. For larger stellar masses the ONe core reaches $\approx 1.5 \times 10^9\,\mathrm{K}$ and Ne burning produces O and Mg in a convective core with accelerated evolution due to neutrino losses. After this phase, the Ne burning shifts to a shell, and when the core reaches $\approx 2 \times 10^9\,\mathrm{K}$, $^{16}\mathrm{O} + {}^{16}\mathrm{O}$ produces mainly $^{28}\mathrm{Si}$ and $^{32}\mathrm{S}$ in a convective core. The silicon burning starts when the central temperature is rather high $\approx 3 \times 10^9\,\mathrm{K}$ and

combination of photo-disintegration and alpha-capture reactions occur. As the temperature further increases, NSE is reached and iron group nuclei are favored. These central and shell burning phases lead to an onion-shell like structure as schematically shown in Fig. 20. Table 10 lists these burning stages with typical central densities and temperatures, the duration of such burning stages and the typical luminosity in photons (Woosley and Weaver 1995). Table 11 lists properties of the same burning stages from more recent results (Limongi and Chieffi 2018), a 13 $M_{\odot}$ star burns at slightly lower temperatures and slightly higher densities, resulting in more extended timescales of individual burning stages.

The discussion in this subsection centred around the question if and how stars can enter stages beyond core He burning, not ending as CO white dwarfs in their final evolution. The super AGB stars in the mass interval 7–10 $M_{\odot}$ played a central role bridging the fate of becoming a CO white dwarf and passing through all burning stages until Si burning, resulting in an Fe core. An intermediate role is played by stars that initiate C burning, but result then in an ONeMg white dwarf. It has long been emphasized that the C burning products ^{20}Ne and ^{24}Mg can experience electron capture by electrons with high Fermi energies in the quite degenerate cores. This causes pressure reduction of the degenerate electron gas and can lead to a sudden contraction. It can turn into a collapse and fast compression, causing high temperatures, immediately leading to an NSE abundance composition dominated by Fe-group nuclei. In such a case an Fe core would emerge already after C burning without going through all later stellar burning stages. Such an Fe core would be prone to a core-collapse supernova explosion, as will be discussed in the following section, in this case a so-called electron capture or EC supernova (see e.g. Leung et al. 2020, and references therein). There have been speculations that this does actually not take place under certain circumstances, because of a highly enhanced electron capture rate on ^{20}Ne (Kirsebom et al. 2019a, b), coming to the conclusion that for ignition of the ONeMg core after C burning at densities below 10^{10} g cm^{-3} an O-deflagration (see Sect. 7.1) destroys the whole star in an explosion similar to type Ia supernovae. However, Zha et al. (2019) and Leung et al. (2020) find that in more realistic stellar evolution modeling the ignition takes place for densities above 10^{10} g cm^{-3} and the collapse continues towards an Fe core, leading to an EC supernova explosion.

Detailed stellar evolution models, including all relevant nuclear physics for all the burning stages of the tables shown here, as well as dynamics, radiation transport, mixing via convective instabilities or induced by rotation, and mass loss via stellar winds have evolved from first investigations (Arnett 1977; Weaver et al. 1978) to the present-day stellar evolution codes FRANEC, KEPLER, GENEC and MESA, including also rotation (see e.g. Maeder and Meynet 2012; Limongi and Chieffi 2018; Eggenberger et al. 2021). Overviews can be found at many places (e.g. Heger et al. 2003; Heger and Woosley 2010; Thielemann et al. 2018a). The most recent developments, attacking 3D hydrodynamic instabilities in late stages of stellar evolution, are outlined in Arnett et al. (2019); Kaiser et al. (2020).

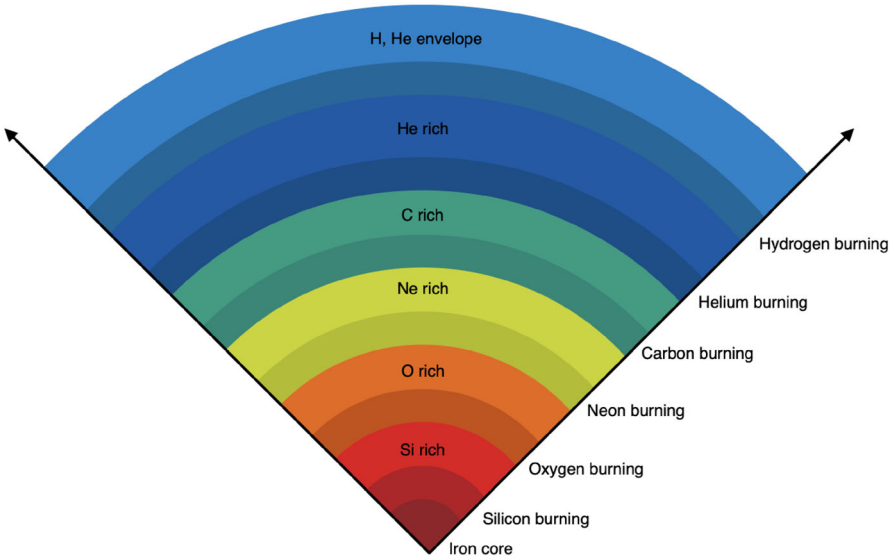

Fig. 20 Schematic structure of a massive star at the end of its life before core-collapse supernova

Table 10 Burning stages of a $20\,M_{\odot}$ star

Fuel	ρ_c (g cm^{-3})	T_c (10^9 K)	τ (year)	L_{phot} (erg s^{-1})
Hydrogen	5.6 (0)	0.04	1.0 (7)	2.7 (38)
Helium	9.4 (2)	0.19	9.5 (5)	5.3 (38)
Carbon	2.7 (5)	0.81	3.0 (2)	4.3 (38)
Neon	4.0 (6)	1.70	3.8 (-1)	4.4 (38)
Oxygen	6.0 (6)	2.10	5.0 (-1)	4.4 (38)
Silicon	4.9 (7)	3.70	2 days	4.4 (38)

Table 11 Burning stages of a $13\,M_{\odot}$ star

Fuel	τ (year)	L_{phot} ($L/L_{\odot}$)
Hydrogen	1.61 (7)	4.53
Helium	1.09 (6)	4.70
Carbon	9.09 (3)	4.82
Neon	5.68 (0)	4.82
Oxygen	4.17 (0)	4.82
Silicon	3.50 (−1)	4.82

6 Core collapse of massive stars

Core collapse marks the end of the life of stars with at least eight times the mass of our Sun, leading to the birth of neutron stars and/or stellar-mass black holes (Fig. 21). In observations, one notices a variation in explosion energies, dividing them into two categories: low- and high-energy explosion (often also utilizing the terms core-collapse supernovae and hypernovae). The low-energy explosions ($E_{\rm exp} \sim 1\,{\rm B} = 10^{51}\,{\rm erg}$) are probably triggered by neutrinos that can transport the energy from the hot proto-neutron star (emerging from core collapse) to the stalled shock with the help of convection and instabilities (Burrows 2013; Kotake et al. 2012; Janka et al. 2016; Müller 2016; Burrows and Vartanyan 2021; Radice et al. 2018; Müller 2020; Vartanyan et al. 2022; Varma et al. 2022). More energetic explosions may be driven by strong magnetic fields (LeBlanc and Wilson 1970a; Nomoto et al. 2006; Varma et al. 2022). Here we summarise briefly the explosion mechanism before discussing the rich nucleosynthesis occurring in core-collapse supernovae.

At the end of their lives, massive stars have an iron core surrounded by shells of lighter elements produced in the sequence of hydrostatic burning stages. This is known as onion-shell-like structure and shown in Fig. 20. The core is initially stable due to the pressure of degenerate electrons and contracts slowly approaching the Chandrasekhar mass. This critical limit determines the maximum mass that can be sustained by degeneracy pressure and is proportional to the fraction of electrons (Y_e): $M_{\rm Ch} \approx 1.45(2Y_e)^2\,M_\odot$, but for more massive stars, with not completely degenerate cores, it contains also a temperature correction $1 + (S_e/\pi Y_e)^2$, with S_e being the electron entropy per baryon. Electron captures on heavy nuclei and photodissociations lead to a collapse on dynamical time scales. Initially neutrinos, produced mainly by electron captures, leave the core releasing energy. However, when densities reach values around $\sim 10^{11}\,{\rm g\,cm^{-3}}$, the neutrino mean free path is comparable to the size of the core and neutrinos are trapped. The collapse only stops when the inner core reaches nuclear saturation density and the repulsive part of the nuclear force dominates. The sudden stop of the collapse produces a bounce, and a shock wave is launched at the edge of the inner core.

The shock wave loses energy by photodisintegration of the heavy nuclei from the in-falling iron core into free nucleons and by neutrino emission. This is critical during and after the neutrino burst that occurs when the shock leaves the region of neutrino trapping ($\rho \sim 10^{11}\,{\rm g\,cm^{-3}}$). Due to the energy loss, the shock becomes a stalled accretion shock, how it is revived is still being investigated (see references given above). The most promising mechanism is based on neutrinos that can transport the energy from the hot proto-neutron star to the region below the shock, increasing the thermal pressure and pushing the shock outwards. This neutrino-driven mechanism works in spherically symmetric simulations only for low-mass progenitors with an ONeMg core (e.g. Leung et al. 2020), also known as electron capture EC supernovae ($M \sim 8$–$10\,M_\odot$). For massive progenitors, the neutrino energy deposition needs to be supported by multi-dimensional fluid instabilities such as convection or SASI (standing accretion shock instability).

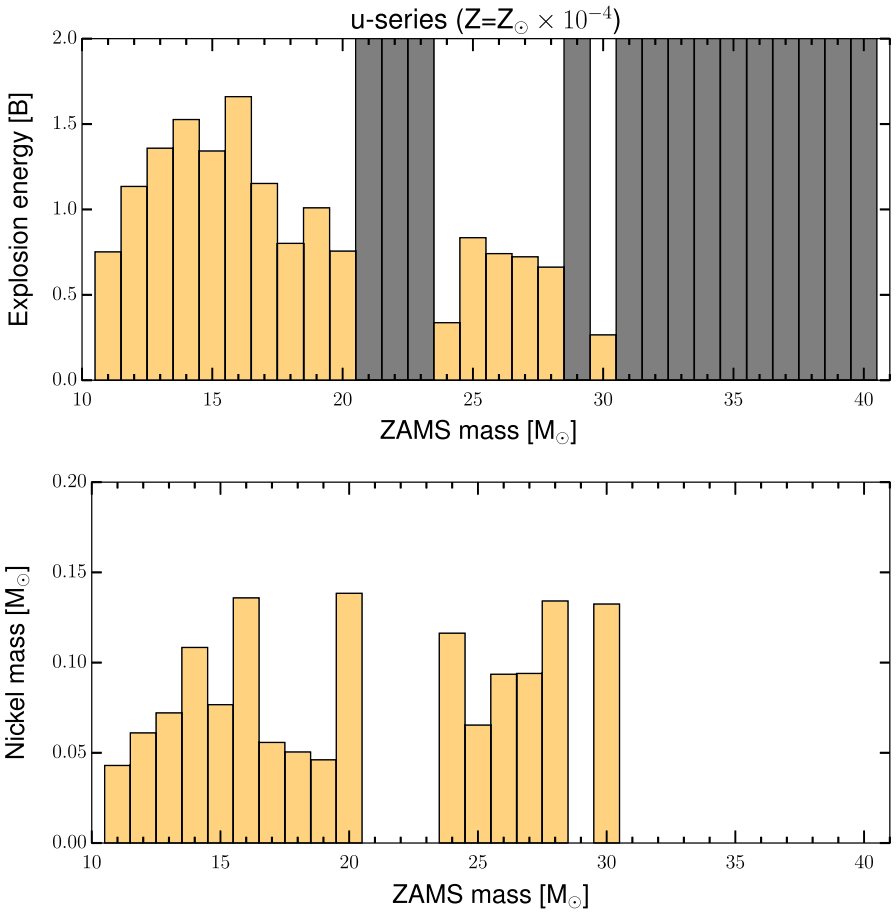

Fig. 21 Results of core-collapse supernova simulations for stars with a low metallicity ([Fe/H]= −4) as a function of progenitor mass. Typical explosion energies of 1 Bethe (= 10^{51} erg) are found up to about $30\,M_{\odot}$. For higher masses, the collapse leads to black hole formation. There exists also a narrow mass range between 20 and $30\,M_{\odot}$ where black hole formation takes place, due to the structure/compactness of these specific stellar models. Explosions occur typically 300 to 700 ms after collapse. The amount of ^{56}Ni ejecta ranges from about 0.04 to $0.12\,M_{\odot}$ (for SN1987A $0.07\,M_{\odot}$ was determined observationaly). Similar results are found in Ertl et al. (2016). Image reproduced with permission from Ebinger et al. (2020), copyright by AAS

An exciting alternative to trigger explosions is the magneto-rotational mechanism that may explain a fraction of highly energetic explosions, hypernovae with $E_{\rm exp} \sim 10^{52}$ ergs (Nomoto et al. 2006). This mechanism requires fast rotation that supports the amplification of the magnetic field during collapse. It would either leave a highly magnetized neutron star (magnetar) or a central black hole (collapsars). Observational indications of such explosions are not only hypernovae, but also highly magnetized pulsars (magnetars) and long gamma-ray bursts, lGRB's, associated with such highly energetic supernovae. Another suggested exotic mechanism, based on a first-order QCD phase transition, leads to a second collapse

of the neutron star until being supported by quark matter and a successful additional shock (Fischer et al. 2011, 2020b). However, the densities when the transition occurs, which depend strongly on details of the equation of state, need to be followed in a perfect timing with the dynamics of the collapse.

All classes of core-collapse events including regular core-collapse supernovae, ending in central neutron stars, black hole formation events, i.e. collapsars and hypernovae, pair creation supernovae, up to events producing very massive stellar-mass black holes (Heger et al. 2003) are critical for the chemical history of the universe. They eject elements into the interstellar medium, synthesised during the lives of stars in hydrostatic burning, dependent on the initial progenitor composition, and—in addition—also those ones that are newly produced during the explosion. In the nucleosynthesis, one can distinguish different components that we discuss below.

6.1 Core-collapse supernovae

After a short overview over the possible fates of massive stars and their explosive final stages, given in the introduction of this section, we want to focus in this subsection on those cases that end as a "regular" neutrino-driven supernova explosion. These are the ones leading to a central neutron star remnant and explosively ejected outer layers, where the outermost layers have a composition essentially identical with the pre-collapse composition from stellar evolution, and the inner ejecta, being processed explosively, lead to explosive Si, O, Ne, and also C burning, while the innermost ones have also experienced interactions with neutrinos during the central supernova explosion, affecting the Y_e of the ejected matter. Below we will pass through several aspects leaving their imprint on the composition, which might to some extent are also of importance for the following two subsections on magneto-rotational supernovae and collapsars.

6.1.1 Shock nucleosynthesis

When the shock moves out through the stellar layers it changes the composition of the accreted matter. These changes depend on the shock temperature and go from photodissociating iron group nuclei into nucleons to only modifying slightly the composition of existing nuclei and producing small amounts of some isotopes. In the early explosion, the shock is very energetic and still inside the iron core. The shock temperature can reach 10–20 GK and thus bring the accreted matter into NSE. The exact evolution, when this accreted matter further expands and cools, depends strongly on the neutrinos and will be discussed below. When the shock reaches intermediate layers, its temperature is too low to reach NSE but is still high enough to have explosive burning of Si, O, Ne, and C that produces additional ^{56}Ni, Si, Mg, O, and Ne. The main reactions and products of the explosive nucleosynthesis have been discussed in Sect. 4, an application for a $16\,M_\odot$ star is shown in Fig. 22.

The shock nucleosynthesis can be studied with methods that deposit a given amount of energy in the pre-explosion progenitor model. However, these methods are not suitable to investigate the innermost ejecta that are exposed to neutrinos and

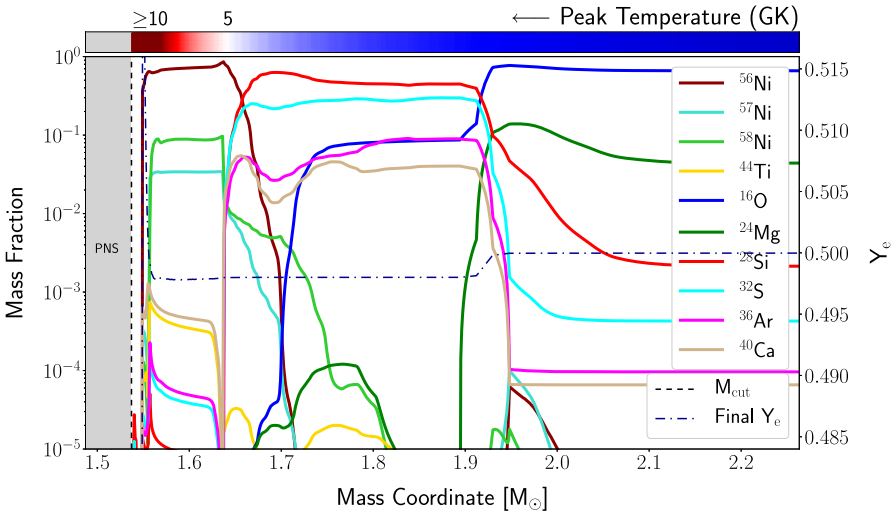

Fig. 22 Results of explosive nucleosynthesis processing in a 16 $M_\odot$ progenitor star after a shock wave ran through the matter outside the (initially hot) proto-neutron star. All matter outside the mass cut will be ejected. The composition outside of $\approx 2.1\,M_\odot$ remains unchanged, inherited from prior stellar evolution of this massive star, which experienced all burning stages from H- to Si burning, here dominated by Ne burning products, i.e. ^{16}O, ^{24}Mg, and admixtures of ^{28}Si, ^{32}S and ^{36}Ar. The layers further in are characterized by explosive O burning, changing the initial composition within seconds into ^{28}Si, ^{32}S, ^{36}Ar, and ^{40}Ca. Matter inside 1.7 $M_\odot$ experienced explosive Si burning, resulting mainly in ^{56}Ni, ^{58}Ni (stable), ^{57}Ni and admixtures of ^{40}Ca (stable) and ^{44}Ti. Y_e, the proton/nucleon ratio, being 0.5 for nuclei symmetric in neutrons and protons, is close to 0.5 in the outer layers, turned slightly neutron-rich (<0.5) during late burning stages due to β^+-decays and electron captures on nuclei, and is turned proton rich in the innermost ejecta due to weak interactions with the neutrino wind escaping the hot proto-neutron star. It becomes very small ($\ll$0.5) inside the proto-neutron star due to capture of electrons with high Fermi energies of the degenerate electron gas on protons. Image reproduced with permission from Curtis et al. (2019), copyright by AAS

strongly affected by details of the neutrino-driven explosion and multi-dimensional effects. There are three main ways of artificially triggering explosions: piston (Woosley and Weaver 1995), thermal energy bombs (Thielemann et al. 1986) or kinetic energy bombs (Limongi and Chieffi 2006). In all these models the explosion energy and mass cut between the proto-neutron star and ejecta are free parameters. The piston method assumes a mass shell and prescribes its outward movement to reach the typical explosions energies $E_{\rm exp} \approx 10^{51}$ erg. Below the selected mass shell there is a mass that does not enter into the simulations. This mass cut between the neutron star and the ejecta is specified by the chosen position of the piston and an entropy value. In the thermal and kinetic energy bomb methods, energy is artificially deposited in an inner layer of the progenitor model to trigger the explosion. The mass cut is obtained by integrating the nucleosynthesis and constraining the amount of ^{56}Ni to typical observed values of around 0.1 $M_\odot$. These approaches allow for a broad study of many progenitors and can provide reliable information for nucleosynthesis that is not strongly affected by the details of the explosions including the neutrinos. However, the nucleosynthesis of the iron group and beyond

requires methods that include the physics of the explosion phase with self-consistent explosion energies.

6.1.2 p-process

After having discussed the basic working of the p- or γ-process in Sect. 4, here we focus on the astrophysical side. In the (outer) layers of explosive Ne burning the shock has lost most of its energy and encounters temperatures barely sufficient for extensive fusion reactions but still high enough to trigger some photo-dissociations on existing nuclei, which lead to the classical p-process or γ-process. A number of proton-rich (p-)isotopes of naturally occurring stable heavy nuclei cannot be produced by neutron captures along the line of stability. The most favored production mechanism for those 35 p-isotopes between Se and Hg is therefore photodisintegration of intermediate and heavy pre-existing elements during the shock-wave passage of massive stars (Woosley and Howard 1978; Rayet et al. 1990, 1995). However, not all p-nuclides can be produced satisfactorily, yet. A well-known deficiency in the model is the under-production of the Mo–Ru region, but the region $151 < A < 167$ is also underproduced, even in recent calculations (Rauscher et al. 2002; Arnould and Goriely 2003; Rapp et al. 2006; Dillmann et al. 2008; Rauscher et al. 2013; Pignatari et al. 2016; Rauscher et al. 2016; Travaglio et al. 2018). There exist deficiencies in astrophysical modelling and the employed nuclear physics. Recent investigations have shown that there are still considerable uncertainties in the description of nuclear properties governing the relevant photodisintegration rates. This has triggered a number of experimental efforts to directly or indirectly determine reaction rates and nuclear properties for the p/γ-process (Rauscher 2006; Rauscher et al. 2016). Here it is important to investigate the sensitivity of the location of the γ-process path with respect to reaction rate uncertainties.

The problems encountered, especially in reproducing the light p-nuclei, led also to the suggestion of alternative sites. One option is related to type Ia supernovae (Howard et al. 1991; Goriely et al. 2002; Travaglio et al. 2011, 2015; Nishimura et al. 2018; Battino et al. 2020), discussed in more detail in Sect. 7. Another option is related to the νp-process in core-collapse supernovae, which will follow in one of the upcoming subsections.

6.1.3 ^{26}Al, ^{60}Fe

Two long-lived isotopes ^{26}Al (with a half-life of 7.17×10^5 year) and ^{60}Fe (with a half-life of 1.5×10^6 year) can be either observed by their decay gamma-ray emission indirectly or directly in deep-sea sediments and serve as a witness for recent stellar contributions to the interstellar medium or even in near earth events. Here, we investigate their possible production in massive stars.

The radioactive ^{26}Al is produced hydrostatically during stellar evolution and explosively by the supernova shock. It occurs in the regions of explosive Ne/C burning. Under these conditions ^{25}Mg is produced via ^{24}Mg $(n,\gamma)^{25}$Mg and the protons arise from ^{23}Na $(\alpha,p)^{26}$Mg, similar to the reaction pattern shown in Table 6

for hydrostatic Ne burning (and partially also C burning). Under explosive conditions at temperature of the order 2.3×10^9 K, these burning stages act explosively in a combined way and the temperatures are also sufficiently high to utilize the released protons for the ^{25}Mg $(p,\gamma)^{26}$Al reaction. However, neutrons are produced abundantly. They, in fact, act as the main destructive species via (n, p) and (n,α) reactions. The mass involved in explosive Ne/C burning is strongly dependent on the progenitor mass. Thus, we expect a dramatic increase with increasing initial stellar masses. The detailed analysis in Woosley and Weaver (1995); Limongi and Chieffi (2006, 2018) has found the contributions from (i) wind ejecta during stellar evolution, (ii) hydrostatic burning products ejected during the explosion, and (iii) explosive Ne/C burning. The latter dominates up to about $60\,M_\odot$ and increases from initially about $2 \times 10^{-5}\,M_\odot$ per event to $2 - 3 \times 10^{-4}\,M_\odot$. Then wind ejecta start to take over and flatten out close to $10^{-3}\,M_\odot$ at initial stellar masses of 120–140 $M_\odot$. The latter are subject to rotational effects (Langer et al. 1995; Meynet et al. 1997; Palacios et al. 2005) and increase with higher rotation rates. Tur et al. (2009) have reanalyzed this behaviour in the lower mass range from 15–25 $M_\odot$ and confirmed this trend. They also did not find a strong dependence of the result on the He burning reactions triple-alpha and ^{12}C$(\alpha,\gamma)^{16}$O. They show nicely how ^{26}Al is produced starting in H burning, but the final explosion produces close to a factor of 10 more of it.

^{60}Fe should only be mentioned here because of completeness. It is entirely produced in the s-process during shell He burning and thus a pure product of stellar evolution rather than explosive nucleosynthesis. The explosion only acts in terms of ejecting the corresponding layers. As ^{60}Fe is produced via neutron capture of beta-unstable ^{59}Fe, a relatively high neutron density of about 3×10^{10}cm^{-3} is required in order for its efficient production. This is only attained in shell He burning during late evolution stages after core C burning. The production ranges from 2×10^{-6} to $8 \times 10^{-5}\,M_\odot$ for initial stellar masses between 10 and $40\,M_\odot$. This result is dependent on the He burning reactions triple-alpha and ^{12}C$(\alpha,\gamma)^{16}$O, as they compete with the neutron producing reaction ^{22}Ne $(\alpha, n)^{25}$Mg. There exist also uncertainties in ^{59}Fe $(n,\gamma)^{60}$Fe and ^{60}Fe $(n,\gamma)^{61}$Fe, which cause yield variabilities by a factor of up to 5. If the star experiences strong mass loss, the He burning shell does not encounter the higher density conditions required for the high neutron density of 3×10^{10} cm^{-3}. Thus, for initial stellar masses in excess of $40\,M_\odot$ the mass loss treatment can also lead to variations of more than a factor of 10. Apparently a strong mass loss rate is required to not overproduce ^{60}Fe in high-mass stars $M > 40\,M_\odot$ (Limongi and Chieffi 2006, 2018).

6.1.4 Neutrino-driven nucleosynthesis

Neutrinos play a central role determining the conditions of the innermost ejecta and their nucleosynthesis. Even if matter can be ejected in different ways, the neutrino-driven nucleosynthesis acts similarly and depends on three parameters: electron fraction, entropy, and expansion time scale. Mass accreted through the shock during

the early explosion gets dissociated into nucleons and alpha particles, depending on the temperature of the shock. This material can be then accreted down to the proto-neutron star or stay in the gain region and expands. In spherically symmetric simulations, the accretion takes place only in the first second after bounce while in multidimensional simulations downflows stays active during several seconds, providing a continuous nucleosynthesis source. In general, the matter ejected comes from two regions: surface of the proto-neutron star and the layers behind the shock. The outer layers of the proto-neutron star and the matter that has been accreted on its surface can be ejected by neutrinos. If this ejection occurs when there is no matter being accreted any more and the outflow becomes supersonic, it is known as neutrino-driven wind. This was suggested as the r-process site (see Qian and Woosley 1996; Arcones and Thielemann 2013 for review and references). However, the neutrinos not only deposit the necessary energy to unbind and eject material, they also change neutrons into protons preventing an r-process to occur.

The nucleosynthesis of the neutrino-driven wind follows similar burning features as that of the matter that is not accreted down to the proto-neutron star, but it is exposed to neutrinos. Here we summarize the main possibilities to produce elements around and beyond iron in core-collapse supernovae in the neutrino-driven ejecta (Fig. 23). The temperature is sufficient to reach NSE and follows photodissociation, resulting in an initial composition dominated by neutrons and protons. As matter expands, its temperature and density drop, allowing nuclear reactions to start building alpha particles and seed nuclei. The composition of the seed distribution and the final abundances depend on three quantities: entropy, expansion time scale, and electron fraction (Qian and Woosley 1996). These parameters determine the ratio between nucleons and seed nuclei: neutron-to-seed ($Y_n/Y_{\rm seed}$) and proton-to-seed ($Y_p/Y_{\rm seed}$) ratios. Depending on the value of these ratios at temperatures around 3 GK, three processes are possible:

– r-process (Hoffman et al. 1997; Freiburghaus et al. 1999a; Thompson et al. 2001; Farouqi et al. 2010) if $Y_n/Y_{\rm seed} > 100$, however, this does not occur in neutrino-driven supernova in general (as expected initially by Woosley et al. 1994; Takahashi et al. 1994, see discussion below about magneto-rotational supernovae),

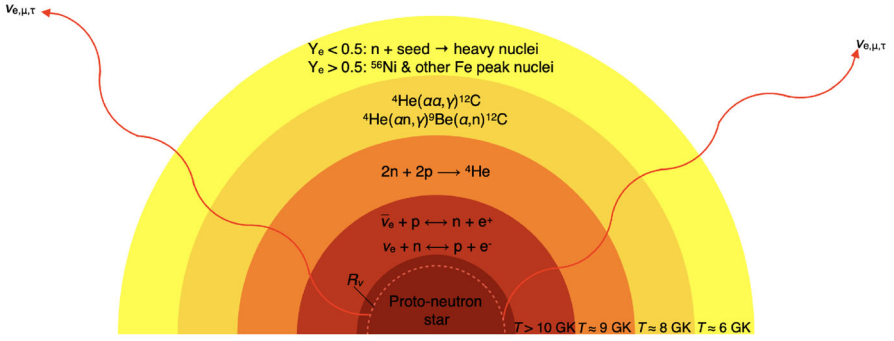

Fig. 23 Neutrino-driven nucleosynthesis

- weak r-process (Arcones and Bliss 2014; Bliss et al. 2018; Ghosh et al. 2022), if $Y_n/Y_{\rm seed} \sim 1$,
- νp-process (Fröhlich et al. 2006; Pruet et al. 2006; Wanajo 2006), if $Y_n/Y_{\rm seed}$ is very small and $Y_p > Y_n$, i.e. for proton-rich conditions (see Sect. 4.2.4).

How the wind parameters affect the neutron-to-seed ratio has been extensively studied in the context of the r-process (see e.g. Otsuki et al. 2000; Thompson et al. 2001; Qian and Woosley 1996). The entropy in radiation-dominated environments depends on temperature and density: $S \propto T^3/\rho$. As discussed before, high entropies favor an extremely alpha-rich freeze-out from NSE (see Fig. 14) and the accompanying low densities cause a small production of seed abundances $Y_{\rm seed}$ via three body reactions: $3\alpha \rightarrow {}^{12}$C and ^{4}He ($\alpha$n,$\gamma$)^{9}Be ($\alpha$,n)^{12}C. Dependent on Y_e, with a dominant abundance of $N = Z$ ^{4}He, additional neutrons or protons remain after freeze-out, leading to a resulting neutron-to-seed or proton-to-seed ratio. This effect depends on the entropy, Y_e, and the expansion time scale of matter, affecting the time over which ^{4}He can be transferred to C and beyond. The electron fraction determines whether the ejecta are neutron rich ($Y_e < 0.5$) or proton rich ($Y_e > 0.5$).

If the electron fraction is very low $Y_e < 0.2 - 0.3$, the neutron-to-seed ratio will be high enough for the r-process to occur. Such low electron fractions are not found in state-of-the-art neutrino-driven supernova simulations, because the neutrinos change neutrons into protons, leading to a higher Y_e. However, neutron-rich matter can be ejected in supernovae with strong magnetic fields and rotation as we will discuss below.

If $0.4 < Y_e < 0.5$, a weak r-process is possible but not a strong r-process up to the third peak, unless the entropy is very high and/or the expansion time scale very short. However, such extreme cases are not found in current neutrino-driven explosion models. Slightly neutron-rich neutrino-driven ejecta are characterized by a nucleosynthesis path not far from stability or along stability, depending on the conditions (Bliss et al. 2018). Already in NSE, nuclei up to $Z \sim 40$ may be produced, and in some cases additional charge-particle reactions after NSE lead to the production of heavier elements (Bliss et al. 2018). In the weak r-process, beta decays are much slower than the ejecta expansion timescale. After the initial NSE phase, several reactions, that are faster than beta decays, keep moving matter from light to heavy nuclei. These reactions include (α, n), (p, n), (α, γ), (p, γ) on stable or close to stability nuclei. This process has been studied recently and key (α, n) reactions have been identified (Bliss et al. 2020).

In proton-rich conditions ($Y_e > 0.5$), heavy elements are synthesized from seed nuclei via charged-particle reactions, i.e. (p, γ), (α, γ), (α, p), and beta decays. These reactions allow the flow of matter to move on the proton-rich side of stability up to ^{56}Ni and ^{64}Ge. This nucleus has a beta half-life much longer than the expansion time scale of the ejecta. However, a high electron antineutrino flux produces neutrons that facilitate to pass these bottlenecks by (n,p) reactions (Fröhlich et al. 2006; Pruet et al. 2006; Wanajo 2006). The νp-process may be responsible for the production of light heavy p-nuclei (see Sect. 4.2.4 and Fig. 24 from Ghosh et al. 2022).

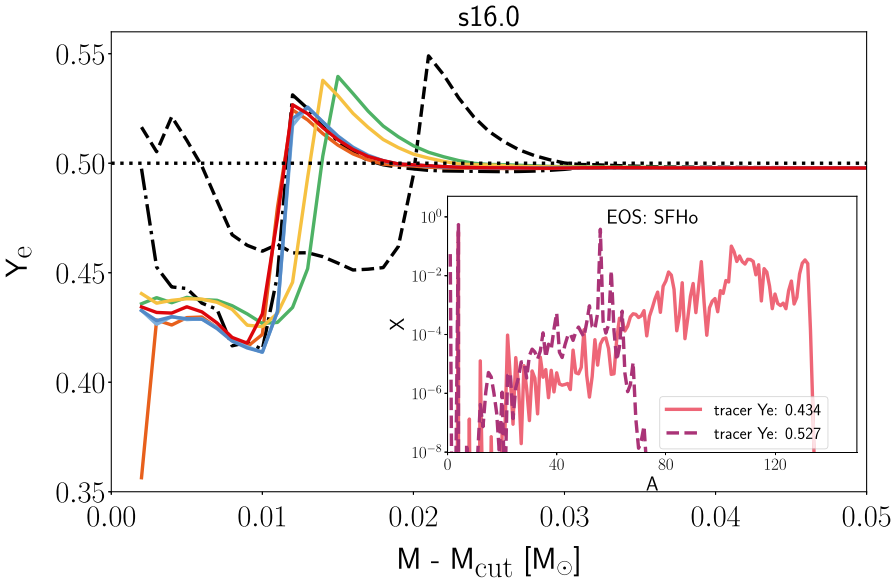

Fig. 24 Innermost ejecta composition determined by moderately low Y_e-matter from collapse and moderately proton-rich conditions due to neutrino interactions during the explosion, leading to a *νp*-process and a very weak r-process (collapse calculations performed with different equations of state). Image reproduced with permission from Ghosh et al. (2022), copyright by the authors

Observations indicate that there is an additional process that contributes to the production of elements between Sr and Ag (Sneden et al. 2008). This can be the lighter element primary process (LEPP) (Travaglio et al. 2004; Montes et al. 2007), a low metallicity s-process (Frischknecht et al. 2016) or charged particle reactions (Qian and Wasserburg 2007) combined with a weak r-process and/or the *νp*-process (Arcones and Martínez-Pinedo 2011; Arcones and Bliss 2014; Eichler et al. 2018; Ghosh et al. 2022). Fig. 24 (Ghosh et al. 2022) shows the electron fraction as a function of mass, including slightly neutron-rich conditions and proton-rich conditions, and the nucleosynthesis outcome when combining weak r-process and *νp*-process conditions (see also Arcones and Martínez-Pinedo 2011; Hansen et al. 2014 for previous studies).

The supernova ejecta vary for different progenitors, with explosion energies, anisotropies in the evolution of the explosion, and the timing of the explosion after bounce. Therefore, a complete picture of the nucleosynthesis from neutrino-driven ejecta requires a large number of three-dimensional simulations, following the explosion during few seconds and for different progenitors. This is far from being possible because of the huge computational time necessary and also due to the still uncertain details of the explosion, neutrino matter interactions on the surface of the neutron star (Martínez-Pinedo et al. 2012; Roberts et al. 2012), neutrino oscillations (Mirizzi et al. 2016), rotation and magnetic fields (see Sect. 6.2). On the other hand, traditional methods (see above) are not suitable for the nucleosynthesis of the innermost zones that depends on the Y_e and thus on detailed neutrino transport. There

are few nucleosynthesis predictions from multi-dimensional simulations (see e.g. Harris et al. 2017; Wanajo et al. 2018; Eichler et al. 2018 for nucleosynthesis based on 2D simulations and Wongwathanarat et al. 2017 for nucleosynthesis based on parametric 3D models). There exist also approximate methods to obtain neutrino-driven explosions in spherically symmetric models, based on a modified neutrino heating deduced from full multi-D models. Light-bulb methods parameterize the neutrino luminosities at an inner boundary and get explosion when increasing it above some limiting value (Ugliano et al. 2012; Ertl et al. 2016; Sukhbold et al. 2016). Other methods include the neutron star and calculate the neutrino transport from the centre to the shock, but they include a neutrino heating enhancement or extra neutrino absorption that increases the energy deposited by neutrinos in the gain layer that is tuned to the results from multi-D models (see Curtis et al. 2019; Ebinger et al. 2020; Ghosh et al. 2022 for nucleosynthesis within the PUSH method or alternatively Witt et al. 2021; O'Connor and Ott 2011).

6.1.5 *ν*-process

The neutrinos emitted during the protoneutron star cooling also produce nuclear transmutations that can contribute to the nucleosynthesis of some isotopes by the so-called neutrino process (Woosley et al. 1990; Heger et al. 2005). Due to their relatively large energies, neutrinos excite the nucleus, by both the charged and neutral weak current, to states above particle emission thresholds that decay by emission of one or several protons, neutrons and/or alpha particles. As this process occurs while the supernova shock wave travels through the stellar mantle, neutrinos can modify the composition of the stellar progenitor and of the isotopes freshly produced during explosive nucleosynthesis. This process is mostly responsible for explaining very small abundances of specific isotopes that can be produced essentially by this type of "neutrino spallation" reaction from nearby nuclei in the nuclear chart with large abundances (for latest results see e.g. Sieverding et al. 2019).

6.2 Magneto-rotational supernovae

In addition to neutrino-driven explosions, observations of very energetic supernovae (Nomoto et al. 2010), long gamma-ray bursts (GRB) (Woosley and Bloom 2006), and pulsars with extremely high magnetic fields (magnetars, Kramer 2009; Greiner et al. 2015) indicate the key role of magnetic fields in some explosions, here summarized under the name of so-called magneto-rotational supernovae (MR-SN). There are very energetic explosion known as hypernovae (HN) (Iwamoto et al. 1998) with nucleosynthesis features different from regular core-collapse supernovae (Nakamura et al. 2001) that reach energies of about ~ 10 B, which cannot be explained by the neutrino-driven mechanism. These HNe are associated to the collapse of massive stars with > 30–$40\,M_{\odot}$. In all these cases magnetic fields and rotation play a dominant role in the explosion mechanism, which can end either with a central highly magnetized neutron star (magnetar) or alternatively a central stellar-mass black hole. In this subsection, we will mostly concentrate on the first subclass of magneto-rotational supernovae, while in the following subsection we will focus on

the second case with black hole formation (collapsars), often in the literature identified with hypernovae.

The magneto-rotational mechanism proposed in the 1970s (LeBlanc and Wilson 1970b) relies on the extraction of rotational energy from the core via the magnetic field. Therefore, rapid rotation of the iron core is necessary, as well as an amplification of the magnetic field by rotational winding and/or the magneto-rotational instability (MRI) (Obergaulinger et al. 2009). After bounce, the strong magnetic pressure launches jets along the rotational axis (Burrows et al. 2007; Takiwaki et al. 2009; Winteler et al. 2012; Mösta et al. 2014; Obergaulinger et al. 2014). However, some 3D models lead to kink instabilities and the formation of less collimated bipolar jets (Mösta et al. 2014, 2018; Kuroda et al. 2020).

Even if MR-SNe may be rare compared with regular CC-SNe, they were probably important contributors to the enrichment of galaxies with heavy elements in the early universe as progenitors with rapid rotation are more frequently observed at low metallicities. The existence of fast rotating massive stars at early times is also supported by detection of Ba and La in metal-poor stars (Chiappini et al. 2011), which is explained by the enhanced s-process via strong rotational-induced mixing (Frischknecht et al. 2016; Nishimura et al. 2017). Even if MR-SNe are only active in early galaxies, they can be responsible for the production of r-process elements (Côté et al. 2019).

LeBlanc and Wilson (1970b) and later Cameron (2003) proposed MR-SNe as an r-process site. First simulations, although ignoring or simplifying the neutrino treatment, found a successful r-process in 2D (Nishimura et al. 2006) and 3D (Winteler et al. 2012). There are still large uncertainties of progenitor rotation and magnetic field, therefore recent investigations have varied both to explore their influence on the r-process. Based on a simple neutrino treatment, Nishimura et al. (2015, 2017) have explored the impact on the nucleosynthesis of different magnetic field strengths and rotation rates, also varying neutrino luminosities. The strength of the magnetic field required to produce r-process may depend also on a 2D vs. 3D treatment. Mösta et al. (2018) assumed that the neutron-rich material and thus the r-process occurs in the collimated ejecta and argue that this jet-like structure is not a robust 3D feature due to the kink instabilities (Kuroda et al. 2020). Also, a misalignment of the magnetic field with respect to the rotational axis can have an influence on the neutron-richness of the ejecta (reducing it), so that the r-process becomes weaker (Halevi and Mösta 2018). For the neutrinos, there are less uncertainties than for the magnetic field, but only recently it has been possible to perform MHD simulations with accurate neutrino transport, first in 2D (Obergaulinger and Aloy 2017) and recently in 3D (Obergaulinger and Aloy 2021; Kuroda et al. 2020). There are many advances exploring the different aspects of these energetic and rare explosions including the nucleosynthesis.

MR-SN have a very rich nucleosynthesis as they have several components: neutrino-driven and shock nucleosynthesis as standard supernovae (see above) and, in addition, elements formed in the ejecta triggered by magnetic fields. These explosions have an early and fast ejection of matter where the r-process can efficiently produce heavy elements, similar to the prompt explosions found in the 1970s (Hillebrandt et al. 1976). This matter gets collimated around the jets (Reichert

et al. 2021). In addition to this prompt neutron-rich ejection, long-time simulations that follow the evolution seconds after collapse show that rotation and magnetic field impact the proto-neutron star shape making it very deformed (Reichert et al. 2021; Aloy and Obergaulinger 2021). At late times, due to angular momentum redistribution by the magnetic field, a sudden deformation of the neutron star can occur. The change in the neutron star may allow some neutron-rich material to enter outflow regions, leading to a late ejection of neutron-rich material. This enables the weak r-process to produce elements up to the second peak. Further possibilities to eject matter with favorable r-process conditions may be found in coming years as more MR-SN simulations become possible (Reichert et al. 2022). To summarize the nucleosynthesis aspects of ejected matter from this subset of magneto-rotational supernovae, leading to highly magnetized central neutron stars, one should point out that the initial hopes to have a full-fledged strong r-process (Winteler et al. 2012) are only partially confirmed in more realistic simulations and more work is needed to get the complete picture. The strong r-process depends on a very high magnetic field of the rotating core before collapse. This would permit to have a fast ejection of neutron-rich matter. If the magnetic fields are weaker and get enhanced by magneto-rotational instabilities (MRI) only during the onset of the explosion, this permits neutrinos streaming out from the proto-neutron star to enhance the Y_e of the ejecta and consequently reduces the strength of an r-process. The dependence of the abundances on the magnetic field can be seen in the Table 12 for the models of Reichert et al. (2021).

6.3 Collapsars

Other potential r-process sites associated with MR-SNe (not related to the jet ejecta) are the accretion discs that form surrounding a massive neutron star (magnetars) or a black hole (collapsars). In this subsection we want to focus on black hole accretion disks, i.e. collapsars. Pioneering nucleosynthesis studies (Surman and McLaughlin 2004; McLaughlin and Surman 2005; Surman et al. 2006) have demonstrated that also here neutrinos can play a critical role, reducing the neutron-richness of the ejecta and thus the possibilities for the r-process in recent studies are not conclusive, yet. Nevertheless, we will explore this line of investigations for the moment.

An interesting question is related to whether some environments can actually lead to an actinide boost while others produce a normal solar-type r-process distribution. Recent studies (Holmbeck et al. 2019b) based on one hydrodynamic trajectory from tidal dynamical ejecta conclude that actinides are substantially overproduced relative to lanthanides for Y_e-values in the range 0.1–0.15, due to the influence of fission cycling. This is consistent with Wu et al. (2017) and a recent study of Eichler et al. (2019), which finds, with a variety of nuclear mass models, that slightly larger electron fractions in the range of ~ 0.15 are most favorable to explain "actinide boost" matter. Given that "actinide boost" compositions require a dominant fraction of the ejecta to originate from a very narrow Y_e- range in order to reproduce their observed abundance pattern, indicates that nature robustly produces a restricted range of conditions where such Y_e-values occur. The question is how? To date this question is not settled and we want to discuss here a new possibility, recently

suggested in Farouqi et al. (2022). The equilibrium electron fractions for neutrino-driven winds read (Qian and Woosley 1996; Martínez-Pinedo et al. 2017, with the same expressions as in Eq. (32))

$$Y_e^{\rm eq} \approx \left[1+\frac{L_{\bar{\nu}_e}\left(\epsilon_{\bar{\nu}_e}-2\Delta+1.2\Delta^2/\epsilon_{\bar{\nu}_e}\right)}{L_{\nu_e}\left(\epsilon_{\nu_e}+2\Delta+1.2\Delta^2/\epsilon_{\nu_e}\right)}\right]^{-1} \approx \left[1+\left(\frac{\epsilon_{\bar{\nu}_e}}{\epsilon_{\nu_e}}\right)\left(\frac{L_{\bar{\nu}_e}}{L_{\nu_e}}\right)\right]^{-1}. \quad (34)$$

In the approximation on the right, we have assumed that neutrino energies are large enough so that, for acceptable accuracy, the terms containing Δ can be neglected. If a black hole is present or forms, the neutrino irradiation is dramatically quenched and the gas flow around the BH robustly regulates itself into a state of mild electron degeneracy. Due to negative feedback between electron degeneracy and neutrino cooling (higher degeneracy leads to fewer electrons and positrons, therefore reducing the neutrino emission, which leads to a higher temperature and thus to a lowering of the degeneracy), the disk midplane settles inside of the inner $\sim 10\,{\rm GM_{BH}}/c^2$ to electron fractions of $Y_e \approx 0.1$ (Beloborodov 2003). Interestingly, this occurs once the accretion rates exceed an "ignition value" that depends on the BH spin (Chen and Beloborodov 2007) and the corresponding accretion rates are those that are needed to

Table 12 Explosion energy and yields of selected isotopes and elements for various models of Reichert et al. (2021) with various magnetic fields and rotation: 35OC-RO has the original rotation and magnetic field of the progenitor (Woosley and Heger 2006), the model 35OC-Rw has weaker magnetic field, 35OC-Rs has stronger magnetic field, 35OC-RRw has faster rotation and weaker magnetic field

	35OC-RO	35OC-Rw	35OC-Rs	35OC-RRw
$E_{\rm exp}[B]$	1.78	2.8	4.16	0.21
^{26}Al	2.26 (−7)	1.94 (−6)	3.62 (−7)	4.33 (−7)
^{44}Ti	6.60 (−5)	1.34 (−4)	2.06 (−5)	1.16 (−5)
^{60}Fe	4.94 (−4)	1.55 (−4)	3.62 (−3)	1.69 (−7)
^{56}Ni	4.73 (−2)	1.21 (−1)	2.54 (−2)	7.32 (−3)
^{129}I	–	1.75 (−6)	6.93 (−4)	–
^{137}Cs	–	–	3.18 (−6)	–
^{247}Cm	–	–	2.30 (−12)	–
Mn	1.53 (−4)	6.23 (−4)	2.74 (−4)	6.87 (−4)
Zn	9.77 (−3)	4.23 (−3)	2.74 (−2)	2.81 (−3)
Sr	2.20 (−4)	2.56 (−4)	1.03 (−3)	1.65 (−6)
Y	2.22 (−5)	4.05 (−5)	2.23 (−4)	8.42 (−8)
Zr	2.01 (−4)	2.84 (−4)	3.45 (−4)	1.29 (−7)
Ba	–	2.84 (−10)	2.07 (−5)	–
Pr	–	–	7.94 (−7)	–
Nd	–	–	1.07 (−5)	–
Eu	–	–	5.19 (−6)	–
Dy	–	–	5.29 (−5)	–
Pt	–	–	6.39 (−5)	–
Au	–	–	1.06 (−5)	–

Yields in $M_\odot$ using the notation $A(B)$ for $A \times 10^B$. Radioactive isotope yields are given as maximum synthesized value. Note that ^{26}Al and ^{60}Fe are also synthesized during stellar evolution

power (long or short) GRBs (Lee and Ramirez-Ruiz 2007). While discovered in semi-analytic models, this self-regularization to low Y_e-values in the disk midplane is also found in full-fledged numerical (magneto-) hydrodynamic simulations, see e.g. Siegel and Metzger (2018) and Fernández et al. (2019).

The simulation of such neutrino-cooled accretion flows is a major challenge since models should include the (potentially self-gravitating) MHD flow around a rapidly spinning black hole, (semi-transparent) neutrino transport and effects of composition, degeneracy and nuclear recombination. To make things even harder, one needs to resolve the small length scales of the magneto-rotational instability (Chandrasekhar 1960; Balbus and Hawley 1998) and to evolve the black hole torus system for a very large number of dynamical time scales (up to several seconds, while the dynamical time scales are $\sim$ ms). Therefore, it is not entirely surprising that the exploration of this topic is still in initial stages, that large parts of the relevant parameter space are not explored yet and, where parameters are comparable, the results do not yet agree (at least not concerning the ejecta composition). The currently existing GRMHD explorations (Siegel and Metzger 2017, 2018; Miller et al. 2020; Fernández et al. 2019) agree that a large fraction ($\sim 40\%$) of the initial torus mass becomes unbound, but to date there is no agreement about the resulting Y_e and composition of the ejecta. For example, Fernández et al. (2019) find Y_e values around 0.12, those of Siegel and Metzger (2018) peak around ~ 0.14, while Miller et al. (2020) find a broad distribution between 0.2 and 0.4. Despite the current lack of consensus about the ejecta properties, we find the black hole torus idea for the source of "actinide boost" material compelling.

The progenitor systems of actinide boost material could then come from massive accretion disks around black holes, forming substantial tori (either from low-mass black holes or large BH spins) and, potentially, also collapsar accretion disks. There are good reasons to believe that the relativistic jets needed for GRBs are triggered when a black hole forms (McKinney et al. 2013, 2014; Ruiz et al. 2016; Murguia-Berthier et al. 2017; Ruiz et al. 2019) (but see e.g. Mösta et al. 2020 for a possible alternative.). If black hole torus systems indeed manage to eject matter with properties similar to what they produce robustly in their inner torus regions, and a black hole is needed to launch an (either long or short) GRB (rather than, say, a magnetized neutron star), then it would be the GRB engines that produce the "actinide boost" matter.

7 Binary systems and their explosive end points

Binary stellar systems can have explosive endpoints. The majority of stars are born in binary and multiple stellar systems. The gravitational interaction among them can lead to mass exchange and mergers, affecting their final fate. This can take place (a) via mass overflow, when one of the binary members fills the so-called Roche Lobe[8] and the attraction for mass elements of one binary towards the other binary member can supersede its own gravity. The other option (b) is that the emission of

[8] The critical equipotential surface of the joint system for which the individual equipotential surfaces of both binary members touch in one point.

gravitational waves causes rotational energy loss and a reduction of the distance of the two members, resulting in an inspiral and a merger of both objects. (a) can be important when one of the members experiences tremendous radius changes by a factor of 100 or more, e.g. during the transition from an H burning main sequence star to a red giant after the central H core is exhausted. This can lead to the expansion beyond the Roche lobe and therefore mass overflow. (b) involves often binary systems with both members being already in their final stage of stellar evolution, i.e. compact objects like white dwarfs (after a planetary nebular event), neutrons stars or black holes (after a supernova explosion).

Compact objects like white dwarfs and neutron stars are typically in thermodynamic conditions of a cold (degenerate) Fermi gas (electrons in white dwarfs, nucleons and electrons in neutron stars), where the pressure (being in general temperature and density dependent) $P(\rho, T, \text{composition})$ lost its temperature dependence and is determined only by the density. Mass transfer of unburnt hydrogen from the outer layers of the companion (accretion) onto the surface of compact objects can lead to ignition and an energy release by nuclear reactions, which enhances the exponentially temperature-dependent thermonuclear reaction rates. Up to a critical point the pressure (initially lacking all temperature dependence) is not increasing. A temperature dependence could otherwise control and stabilize the situation via expansion of matter leading to a pressure reduction. The fast transition from a degenerate, only density-dependent, pressure to a highly temperature-dependent behaviour after extensive energy release, leads to thermonuclear runaways, causing an exploding behaviour. This ignites explosive hydrogen burning, causing nova events on the surface of white dwarfs and X-ray bursts on the surface of neutron stars.

If the accreting mass overflow is larger, it leads to a temperature increase already during the accretion stage, i.e. before a runaway and avoiding ignition under degenerate conditions. This permits subsequent quiescent H- and He burning on the surface of an accreting white dwarf. This way the mass of the initially existing CO white dwarf can grow towards the critical Chandrasekhar mass. It follows a progressive and significant central density increase and C is ignited under degenerate conditions before the Chandrasekhar mass is reached. [Otherwise a core collapse and core-collapse SN type of event would take place, termed accretion-induced collapse (Nomoto and Kondo 1991; Dessart et al. 2006; Ruiter et al. 2019).] Two options of central degenerate ignition of C burning can occur: (i) directly, close to reaching the Chandrasekhar mass, or (ii) it is also possible that a thermonuclear runaway He ignition sets in at the base of the He zone for lower CO core masses, causing a shock wave propagating to the centre where C is then ignited explosively. Both cases lead to a complete explosive disruption of the white dwarf, known as type Ia (Chandrasekhar mass or sub-Chandrasekhar) supernova. Both of these explosive ignitions (i) and (ii) are of the type (a), i.e. driven by mass overflow. On the other hand, the gravitational inspiral (b) of binary white dwarfs can also lead to type Ia supernovae. The inspiral of a binary neutron star system leads to neutron star mergers.

We will not discuss here in detail novae and X-ray bursts, as their nucleosynthesis contribution to our known abundance pattern is close to negligible. Novae, due to

high temperatures attained in H burning, burn H in the accreted material not via the well-known CNO cycle, but in the so-called hot CNO cycle. It is characterized by the fact that in the branching between the slow beta-decay of ^{13}N and a further proton capture to ^{14}O, the proton capture wins because of a highly enhanced reaction rate for such conditions. In a similar way hot CNO-type cycles for elements beyond Ne rearrange nuclei up to Mg and Si. When including ejecta of such nova explosions, a few not highly abundant isotopes up to Mg and Si can be considered to have a non-negligible contribution from novae (José et al. 2004; José and Coc 2005). There exist also indications that novae can play an important role in the production of ^{7}Li (D'Antona and Matteucci 1991; Romano et al. 2001; Izzo et al. 2015) and ^{26}Al (Vasini et al. 2022).

In type I X-ray bursts, due to the explosive ignition of H- and subsequent He burning reactions, matter from the hot CNO cycle can even be transferred to heavier nuclei up to ^{100}Sn (Rembges et al. 1997; Schatz et al. 1998). This is an important stellar explosion, observed in X-rays, but the explosion energy is likely not sufficient to eject matter out of the high gravitational binding of the neutron star. While some elements can be identified in the observed X-ray spectra, such events do very likely not contribute to our universal abundance pattern. For the reasons discussed above, we will concentrate here on type Ia supernovae and neutron star, as well as neutron star–black hole mergers. A detailed discussion of novae and X-ray bursts can be found in Jose (2016), the evolution of knowledge on the nuclear reactions evolved over many years from Wiescher et al. (1986) over Cyburt et al. (2010) to Meisel et al. (2020).

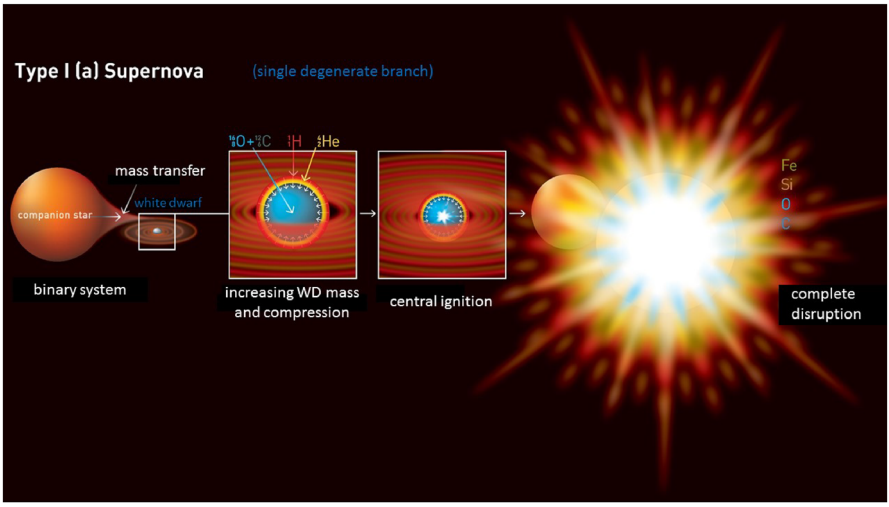

Fig. 25 Evolution of a binary system with one star in an advanced burning stage (a red giant that increased its radius by a factor of 100 or more after central H burning), permitting under these conditions the mass transfer to the companion white dwarf. For sufficiently high accretion rates H (and subsequently He) burns quiescently, increasing the mass of the original C/O white dwarf towards the critical Chandrasekhar limit, causing compression and central C-ignition, which ends in a complete explosive disruption of the object

7.1 Type Ia supernovae

Figure 25 shows case (a) of a binary system containing an advanced star and a white dwarf (the "single degenerate" option), leading here to a Chandekhar-mass type Ia supernova event. The early understanding of type Ia supernovae goes back to Hoyle and Fowler (1960). First carbon-detonation models of a Chandrasekhar-mass white dwarf were developed starting in the late 1960s and early 1970s (Arnett 1969; Arnett et al. 1971; Woosley et al. 1986). A detonation involves a burning front that ignites matter via a compression wave, resulting in a propagation velocity in excess of the sound speed for matter ahead of the front. This does not permit pre-expansion of the material and burns (if ignited with a strong artificial flame for high densities with $\rho > 10^7$ g cm^{-3}, as experienced in the centre of Chandrasekhar-mass white dwarfs) essentially the whole white dwarf to nuclei with the highest binding energies in the Fe-group. Such early predictions were not consistent with observational spectra. The theoretical groundwork for the so-called single and double degenerate (white dwarf merger) systems were laid out by Iben and Tutukov (1984); Webbink (1984). First 1D carbon-deflagration models with subsonically propagating burning fronts were developed in the 1980s (Nomoto 1982; Nomoto et al. 1984; Woosley and Weaver 1986). Here the burning front starts in the centre only with the speed permitted by heat conduction (due to the mean free path of electrons), which is smaller than sound speed, resulting in explosions where in the outer layers unburnt matter survives. General combustion approaches, including so-called delayed detonations, were undertaken by Mueller and Arnett (1986); Khokhlov et al. (1993), where a transition from an initial deflagration to a detonation takes place. Presently, in addition to single-degenerate Chandraskhar-mass systems, starting with a central or off-centre carbon ignition, also single degenerate systems with He ignition in accreted matter, before the Chandrasekhar mass is attained, are considered. Such sub-Chandrasekhar models are triggered by double detonations, where a detonation is ignited in outer layers at the bottom of the accreted He zone, resulting also in an inward moving compression wave that causes finally a central detonation ignition, but in a pre-expanded medium with a density $\rho < 10^7$ g cm^{-3}, avoiding unwanted abundance features from central detonations as initially considered in Chandrasekhar-mass white dwarfs.

The major problem for all these approaches is that a fully self-consistent simulation, resulting in a thermonuclear ignition at high densities but initially low temperatures, is problematic in grid-based codes, because they are limited in their time steps by the sound speed between grid points, causing excessive computing demands (Zingale et al. 2018). Instead, in most cases artificially ignited flames (and their distributions) have been utilized. This problem can be avoided in dynamical events like double degenerate mergers.

A number of general reviews discuss all of the aboved mentioned scenarios (Höflich et al. 1998; Röpke et al. 2012; Hillebrandt et al. 2013; Pakmor et al. 2013; Dan et al. 2015; Maeda and Terada 2016; García-Senz et al. 2016; Jiang et al. 2017; Röpke and Sim 2018; Thielemann et al. 2018b; Shen et al. 2018; Leung and Nomoto 2018; Gronow et al. 2021; Lach et al. 2022), leaving also room for pure deflagration

models as a best explanation for the subclass of SNeIax. There exist also suggestions that a rare and small fraction of type Ia supernovae goes back to white dwarf collisions (Raskin et al. 2009; Rosswog et al. 2009; Garcia-Senz et al. 2013). At present the major aid is coming from observational features, disentangling the possible scenarios that lead to the full sample of observations (Maoz et al. 2014; Noebauer et al. 2017; Goldstein and Kasen 2018; Seitenzahl et al. 2019), which via light curve and spectral modelling permit an optical tomography of the exploding object and provide support for the existence of both Chandrasekhar as well as sub-Chandrasekhar models (Seitenzahl et al. 2019). In a later section, this will be combined with galactic evolution tests.

An important feature is the contribution of type Ia supernovae to Mn (^{55}Mn from ^{55}Co-decay), shown in an early (spherically symmetric) simulation of the carbon-

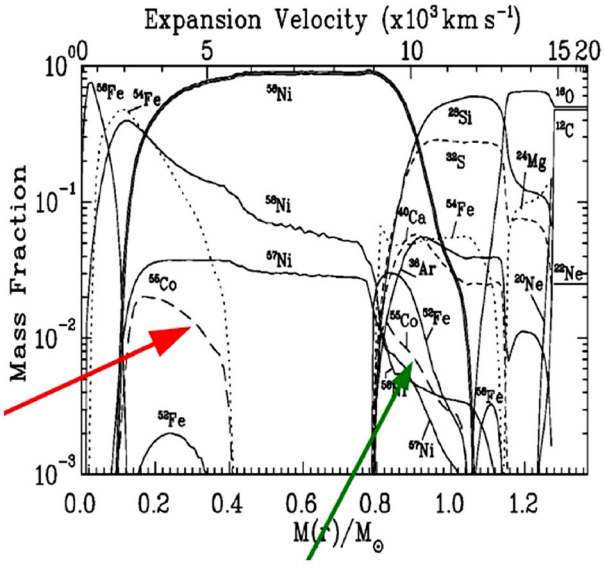

Fig. 26 Nucleosynthetic composition of the first W7 carbon-deflagration model after the explosion (Nomoto et al. 1984; Thielemann et al. 1986). The bottom *x*-axis indicates the position in terms of radial mass zones from the centre to the surface of the exploding white dwarf (close to a Chandrasekhar mass of $1.4\,M_\odot$), the top *x*-axis shows the respective expansion speed of that matter after the explosion. The y-axis indicates the mass fractions of (a few) important species produced. One notices about $0.6\,M_\odot$ of ^{56}Ni (decaying later to ^{56}Fe) and in the outer layers the results of incomplete Si as well as explosive O, Ne, and C burning, leaving even unburnt fractions of C and O at the surface. An interesting aspect is that in the central regions stable ^{56}Fe and ^{54}Fe are produced directly, being more neutron rich than ^{56}Ni, due to the high Fermi energies of electrons in degenerate matter and electron capture on protons and nuclei. This effect is measured by Y_e. This process is also responsible for producing ^{55}Co (decaying later to ^{55}Mn) in the inner layers between 0.1 and $0.4\,M_\odot$ (red arrow) and responsible for the increase of [Mn/Fe] in Fig. 2 at [Fe/H]$= -1$. The green arrow points to a region where no electron capture occurred and Y_e is determined by the initial metallicity of the white dwarf or the accreted matter. In H burning via the CNO cycle all CNO nuclei are turned to ^{14}N (with the slowest proton-capture reaction) and in subsequent He burning this is turned into ^{22}Ne via $^{14}\mathrm{N}(\alpha,\gamma)^{18}\mathrm{F}(\beta^+)^{18}\mathrm{O}(\alpha,\gamma)^{22}\mathrm{Ne}$, a nucleus that is with $N = Z + 2$ slightly neutron-rich. Thus, the fraction of ^{55}Co in the outer zones is dependent on pre-existing CNO, but the more central part is a unique feature of the single-degenerate Chandrasekhar-mass branch of type Ia supernovae

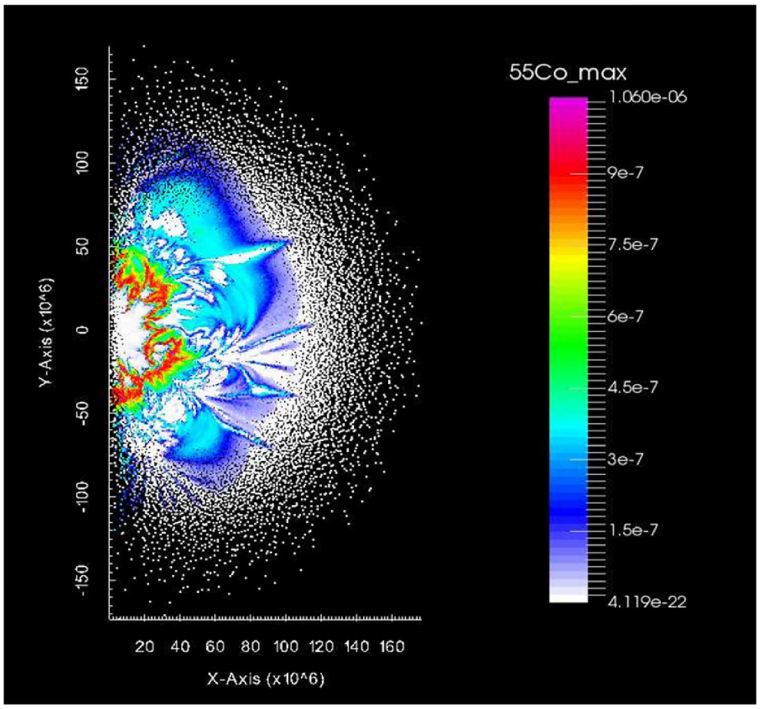

Fig. 27 Results of a 2D simulation, where the ^{55}Co enhancement can be seen in the inner layers, resulting from a more general, non-spherically symmetric, topology. Image courtesy C. Travaglio

deflagration model W7 (Nomoto et al. 1984; Thielemann et al. 1986) in Fig. 26 and more recent 2D and 3D simulations (Maeda et al. 2010; Travaglio et al. 2011) in Fig. 27. In Chandrasekhar-mass deflagration models ^{55}Co is produced in the inner regions of explosive Si burning due to Y_e-values that result from electron capture at high densities and consequently high electron Fermi energies (see Sect. 2). In the outer regions incomplete Si burning and a Y_e due to the metallicity of the object leads to similar results (see Sect. 4 with respect to the build-up of ^{22}Ne after He burning). Sub-Chandrasekhar mass single-degenerate models do not experience the high density conditions in the central parts, but they find similar conditions as shown in Fig. 26 for the outer parts, due to a Y_e inherited from the metallicity of the objects.

As can be seen from the discussion above, the dominant scenario for type Ia supernovae is not fully determined, yet, but observations indicate that apparently all of the mentioned scenarios can contribute. This will be analyzed further in the chemical evolution section. Nevertheless, a defining feature is that type Ia supernova models produce on average about $0.6\,M_\odot$ of ^{56}Ni, decaying to ^{56}Fe in comparison to about $0.1\,M_\odot$ from core-collapse supernovae (see previous section). Therefore type Ia supernovae are a major or the dominant producer of Fe in galaxies (the higher frequency of core-collapse events makes up about a factor of 4–5), indicating that SNeIa produce 55–50% of the Fe in the solar system, leaving the remaining fraction for core-collapse supernovae. When having a look at Figs.22 and 26, we come to the

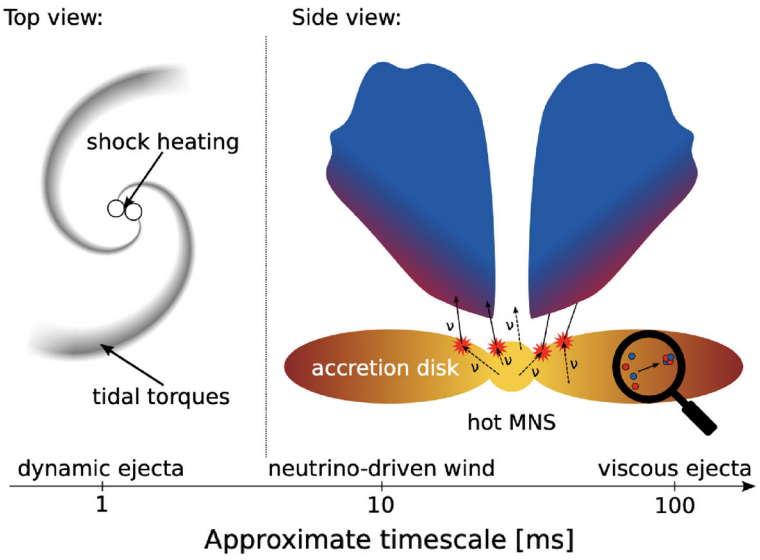

Fig. 28 Schematic representation of a neutron star merger and its ejecta

conclusion that for the alpha elements core-collapse supernovae dominate, while type Ia supernovae can essentially only contribute from Si to Ca, possibly of the order 33%.

In addition, light curve observations of the whole class lead to an empirical relation between their maximum luminosity (related to the ^{56}Ni mass) and the luminosity decline as a function of time. This way they can act as standardizable candles to determine their intrinsic brightness and can therefore be utilized as distance indicators, which permitted to understand the accelerated expansion of the Universe (leading to Nobel Prizes for Perlmutter, Riess, and Schmidt in 2011 "for the discovery of the accelerating expansion of the Universe through observations of distant supernovae").

7.2 Neutron star and neutron star–black hole mergers

A number of proposals for producing the heaviest (r-process) nuclei in Nature have come forward over the years. These include especially neutron star mergers, going back to early suggestions (Lattimer and Schramm 1974, 1976; Eichler et al. 1989), and concrete predictions for resulting abundance features (Freiburghaus et al. 1999b; Rosswog et al. 1999; Korobkin et al. 2012; Wanajo et al. 2014; Just et al. 2015; Eichler et al. 2015; Goriely 2015; Mendoza-Temis et al. 2015; Shibagaki et al. 2016; Radice et al. 2016; Wu et al. 2016; Rosswog et al. 2017; Lippuner et al. 2017; Siegel and Metzger 2017; Bovard et al. 2017; Baiotti and Rezzolla 2017; Thielemann et al. 2017) before the observation of GW170817. The follow-up of the gravitational-wave event GW170817 (Abbott et al. 2017) revealed strong electromagnetic emission in the aftermath of the merger (Kasliwal et al. 2017; Evans et al. 2017; Villar et al.

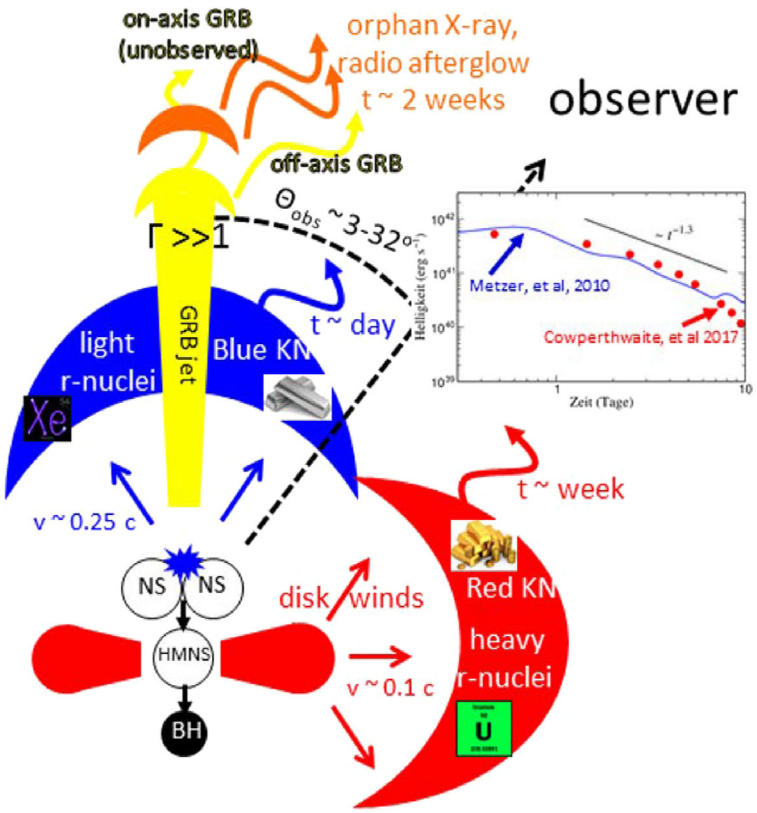

Fig. 29 The central merged object is (although beyond the stable neutron star mass limit) initially supported by thermal and rotational energy and forms a hypermassive neutron star that blows off a neutrino powered wind, as in core-collapse supernovae, preferentially in axis direction. After the formation of the black hole an accretion disks forms that leads to axial jets (causing a gamma-ray burst with very large Lorentz factors Γ) and horizontal accretion disk outflows. The tidal (almost pristine) very neutron-rich ejecta and the accretion disk outflows form the heaviest elements. The neutrino-powered wind increases the (initially very low) Ye from values <0.1 up to possibly 0.3 via neutrino captures on neutrons ($\nu + n \rightarrow p + e^-$), causes only a weak r-process and less massive nuclei. Due to the higher density of electronic states in the heaviest elements (lanthanides and actinide) photonic radiation transport leads to a red appearance of the hot object, while the intermediate to light heavy elements cause an appearance in blue light. Image courtesy of B. Metzger

2018; Drout et al. 2017) and showed in particular the expected signatures of an r-process powered kilonova. The decay of its bolometric lightcurve agreed well with the expectations for radioactive heating rates from a broad range of r-process elements (Metzger et al. 2010; Rosswog et al. 2018; Zhu et al. 2018; Metzger 2019). The kilonova duration, brightness, and colour provide critical information about the composition, amount, and velocity of the matter ejected. Observations of the 2017 kilonova (AT2017gfo) showed that it was initially blue indicating the synthesis of elements lighter than barium ($Z = 56$) (Kasen et al. 2017). These elements have low density of atomic levels and make the medium less opaque, allowing light to escape

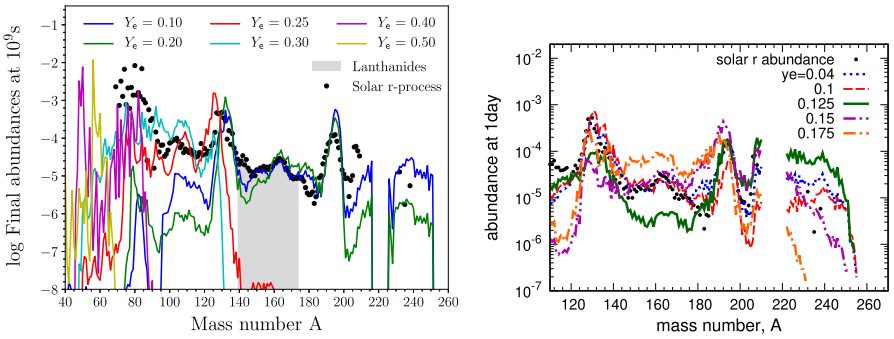

Fig. 30 (Left panel) Abundances as a function of the mass number (A) at 10^9 seconds after merger for trajectories characterized by $s \approx 11 k_B$baryon^{-1} and $\tau \approx 11$ ms, but for different initial Y_e's, computed using the SkyNet nuclear network (Lippuner and Roberts 2017; Perego et al. 2021). Black dots represent the Solar r-process residual, as reported by Prantzos et al. (2020). (Right panel) Abundances again as a function of A (Wu et al. 2017; Thielemann et al. 2020), focusing on low Y_e values and the abundances of actinides. Images reproduced with permission from [left] Perego et al. (2021), copyright by Springer Nature; and from [right] Thielemann et al. (2020), copyright by the authors

(decouple from matter) earlier and without having lost too much energy. The presence of lighter r-process elements was also confirmed by the direct observation of strontium ($Z = 38$) in the spectra of AT2017gfo (Watson et al. 2019). After a few days, the light of AT2017gfo turned from blue to red, pointing to the presence of lanthanides and actinides. See also further reviews and recent results by Horowitz et al. (2019); Shibata and Hotokezaka (2019); Metzger (2019); Cowan et al. (2021); Perego et al. (2021); Shibata et al. (2021); Fujibayashi et al. (2022).

Based on these considerations, three components of neutron star merger ejecta contribute to the overall nucleosynthesis site (see Fig. 28): (i) dynamical ejecta including compressed and shock heated material from the initial collision as well as possible—cold—tidal spiral arm-type ejecta, (ii) winds driven by neutrinos (emitted from the central hot very massive neutron star and the accretion disk) and potentially also by magnetic fields and (iii) finally mass outflow from the accretion disk (see the series of Figs. 29, 30, 31, and 32) . A common feature of these scenarios is that matter reaches NSE with Y_e given by weak reactions or in the cold dynamical ejecta component by beta equilibrium in the cold neutron stars before merger.

Combining the three types of ejecta discussed above with kilonova lightcurve and spectra observations, there is no doubt that neutron star mergers are indeed a major r-process source. The blue emission, that was observed after one day, points to the production of a light (lanthanide-free) r-process (Evans et al. 2017), while the late ($\sim$ 1 week) red emission is the natural expectation for heavy (lanthanides and beyond) r-process ejecta. This heavy r-process is the unavoidable result of decompressing neutron star matter from its initial, very low ($Y_e < 0.1$) β-equilibrium electron fraction (Lattimer and Schramm 1976; Freiburghaus et al. 1999b; Korobkin et al. 2012) and it is also supported by observational evidence from late-time near-infrared observations (Wu et al. 2019; Kasliwal et al. 2022). The early blue emission,

[9] https://indico.gsi.de/event/14501/timetable/#20221017.detailed.

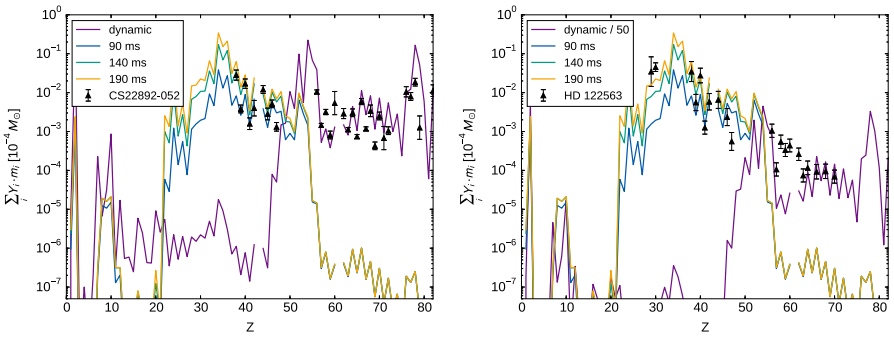

Fig. 31 Elemental abundance comparison between BNS merger models and metal poor star observations. The violet curve represents nucleosynthesis yields for tidally dominated dynamical ejecta (Korobkin et al. 2012), while the other curves yields from neutrino-driven wind ejecta for different massive NS lifetimes. Theoretical abundances are compared with two classes of metal poor stars. In the right panel dynamical ejecta have been diluted by a factor of 50 with respect to the neutrino-driven wind component. Images reproduced with permission from Martin et al. (2015), copyright by AAS

in turn, shows that a substantial fraction of the ejecta has been re-processed via weak interactions to larger Y_e-values, resulting in a light, lanthanide-free r-process (for the variation in nucleosynthesis conditions see Wanajo et al. 2014; Just et al. 2015; Martin et al. 2015; Wu et al. 2016; Bauswein et al. 2017; Miller et al. 2019; Barnes et al. 2021; Lund et al. 2022, and talks at the recent EMMI and IReNA Workshop "Remnants of Neutron Star Mergers"[9]). This is also supported by the identification of the light r-process element strontium (Watson et al. 2019). In summary, there is strong evidence that this neutron star merger event has produced at least a broad, and maybe the whole, r-process range. However, based on the observed lanthanide fraction $X_{\rm La}$, Ji et al. (2019) find that at least for the neutron star merger GW170817 this might not represent a typical solar r-process pattern.

8 Galactic chemical evolution (GCE)

We have gone in this article through a number of astrophysical sites from the Big Bang via stellar evolution of low and intermediate-mass stars to massive stars, their winds and explosive ejecta. We find that H, He, and Li are the products of the Bing Bang, spreading this abundance floor throughout the Universe before galaxy formation. Star formation in galaxies results then in the formation of the other elements. There exist many observations of individual objects, which hint at their ejecta compositions, from supernovae and their remnants (e.g. Arnett et al. 1989; McCray and Fransson 2016; Seitenzahl et al. 2019; Weinberger et al. 2020; Jerkstrand et al. 2020), from neutron star mergers (Abbott et al. 2017; Ji et al. 2019), from indirect investigations via meteoritic inclusions, pointing to the composition of ejecta and dust formation from stellar evolution or stellar explosions (Nittler et al. 1996; Zinner 1998; Zinner and Amari 1999; Lugaro and Gallino 2006; Zinner 2008b, a; Lugaro and Chieffi 2011; Nittler and Ciesla 2016; Kobayashi et al. 2020; Busso et al. 2021), just to name a few. However, there exists also an integrated view,

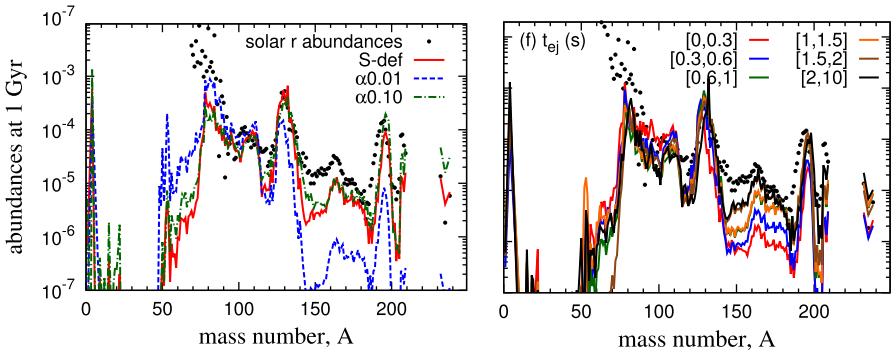

Fig. 32 Abundance comparison between BNS merger models and solar system r-process. Left panel: viscous disk ejecta with various viscosity paramters α, showing the intensity of r-processing. Right panel: top model of the left panel (that overall reproduces solar r-abundances) with integrated ejecta compositions as a function of integration time since merging. Images reproduced with permission from Wu et al. (2016), copyright by the authors

how all these additions changed the composition of the interstellar gas out of which the next generations of stars formed. We can follow this behaviour in Fig. 2. This evolution of element abundances in galaxies (termed usually also chemical evolution) has been pioneered in the 1960s to 1980s by Tinsley (1968); Truran and Cameron (1971); Talbot and Arnett (1971); Tinsley (1972); Audouze and Tinsley (1976); Tinsley (1980); Matteucci and Greggio (1986); Wheeler et al. (1989) and described in a number of books, e.g. Pagel (2009); Matteucci (2012).

The most massive stars have the shortest life span and enter their products first. Collapsars and hypernovae experience very energetic explosions and comparably high entropies. This does not lead to the regular NSE abundances, dominated by a composition of nuclei with the highest binding energies like Fe and Ni. In a milder form than for the Big Bang one finds high He abundances (the production of elements beyond He is hampered at high entropies or low densities for the relevant temperatures) and an alpha-rich freeze-out of explosive Si burning, that produces nuclei like ^{64}Zn (decaying from ^{64}Ge, which was built by further alpha-captures on ^{56}Ni and ^{60}Zn). This is seen in Fig. 2 for low metallicities around [Fe/H]= −3 with the upturn of Zn and Co and the downturn of Mn.

Regular core-collapse supernovae, being the next massive stars and next fastest source in galactic evolution, produce lots of O, Ne, Mg in the outer zones during stellar evolution (see Fig. 22) and Si, S, Ar, Ca, as well as Ti and ^{56,57,58}Ni (^{56,57}Ni decaying to Fe) in the explosively processed zones during the passing of the explosion shock wave. However, the ratio of these "alpha-elements" (O, Ne, Mg, Si, S, Ar, Ca, Ti) to Fe is about a factor of 3 higher than in the solar composition ([X/Fe] = 0.5 corresponds to a factor of 3, which can be seen in Fig. 2 for [Fe/H]<-1). C is also produced by these massive stars in He burning, as well as N in H burning due to the proton capture on ^{14}N being the slowest reaction in the CNO cycle (acting on pre-existing CNO). However, with low- and intermediate-mass stars dominating the so-called initial mass function IMF (the distribution of star formation as a function of

initial mass), due to a decline as a function of initial mass close to $M^{-2.3}$ (initially introduced in Salpeter 1955), they are the main contributors to C and N, which show a different behaviour at these low metallicities.

It remains to be mentioned that the abundances of B and Be are due to galactic cosmic ray (GCR) spallation reactions involving C and heavier nuclei, similar to what is shown for ^{6}Li and other nuclei in Fig. 7. These nuclei were initially attributed to an x-process of unknown origin (Burbidge et al. 1957).

As discussed already with respect to the contributions from the most massive and massive stars, the understanding of the combination of contributing stellar sites is coming from their stellar life times and galactic nucleosynthesis contributions as a function of time. The impact of type Ia supernovae is delayed due to two facts: (a) white dwarf progenitors are low- and intermediate-mass stars with a comparably slow evolution and (b) the delay due to binary interaction until accretion/merging sets in. Thus, their impact is only seen at about [Fe/H]$= -1$, shown by a downturn of the [alpha/Fe]-ratios, driven by the dominant production of Fe (at a galactic age of about 1 Gyr). It should also be mentioned that some heavier alpha elements (Si, S, Ar, Ca, Ti) are also part of type Ia ejecta, but less important than the contribution from core-collapse supernovae. They result in this case from explosive burning (rather than the ejection of hydrostatically evolved shells of massive stars with O, Ne, and Mg), For type Ia supernovoae an important additional contribution to the dominant Fe production is related to Mn (from ^{55}Co-decay), adding to the Mn production. Further aspects, testing the role of type Ia supernovae, and their possible subsites (single vs. double degenerate, Chandrasekhar mass vs. sub-Chandrasekhar and He-detonation scenarios) have been discussed in Seitenzahl and Townsley (2017); Hoeflich (2017); Leung and Nomoto (2018); Mishenina et al. (2015); Tsujimoto and Nishimura (2018); Palla (2021); Gronow et al. (2021); Lach et al. (2022). When having a look at Fig. 2, one sees (i) the impact of the strong Fe-production (mainly from ^{56}Ni-decay) at metallicities of [Fe/H]$= -1$. The slow stellar evolution of stars turning into white dwarfs with originally low and intermediate masses $< 8\,M_{\odot}$ delays this process, plus the evolution of the binary system to mass transfer or a merger. This can be seen in the [O/Fe], [Mg/Fe], [Si/Fe], [S/Fe], [Ca/Fe], [Ti/Fe] downturns at [Fe/H]$= -1$. On the other hand Mn is rising at this point, i.e. type Ia supernovae must be a strong contributor of Mn.

Because Chandrasekhar as well as sub-Chandrasekhar models of type Ia supernovae can contribute ^{55}Mn (either in the inner electron-capture dominated parts or due to reduced Y_e because of higher metallicities) both types of scenarios could therefore explain the rise of [Mn/Fe] due to the onset of type Ia supernovae in galactic evolution for metallicities [Fe/H] > -1. Similar aspects are discussed by Palla (2021) and Gronow et al. (2021) also for V, Cr, and Ni. Another feature that still needs to be explained is the behaviour of [Zn/Fe] (see also Fig. 2), which stays constant during galactic evolution across the [Fe/H]$= -1$ boundary, dominated by core-collapse supernovae or type Ia supernovae, respectively. The Zn in core-collapse supernovae is made in high entropy explosive Si burning, where matter is in an alpha-rich freeze-out processed beyond ^{56}Ni up to ^{60}Zn and ^{64}Ge (decaying to ^{64}Zn). Chandrasekhar-mass models seem not to be able to result in such conditions.

The open question is whether specific conditions of He detonations in sub-Chandrasekhar models might nevertheless be able to do this or whether binary merger double-degenerate systems can do so. In order for [Zn/Fe] to stay constant during galactic evolution across the [Fe/H]= −1 boundary, also a fraction of type Ia supernovae has to experience such conditions.

The understanding how the different stellar contributions enter the chemical evolution of elements in our Galaxy evolved over the years from the above mentioned early references to, e.g. Nomoto et al. (2013); Prantzos et al. (2018, 2020); Kobayashi et al. (2020); Matteucci (2021); Cescutti and Matteucci (2022). This involves specifically also the production of the heavier elements by sequences of neutron captures and beta-decays up to Pb and Bi or even Th, U, Pu and beyond, which has been discussed in the s-process and r-process sections. Here we want first to focus on the evolution of the s-process contributions. In the stellar evolution section we mentioned essentially two sources: (a) the weak s-process in core He burning of massive stars, based on the ^{22}Ne neutron source (a further option is C burning, see case (c) in Table 4 or Table 12 in Limongi and Chieffi 2003) and (b) the dominant main/strong s-process driven by the ^{13}C source (in combination with ^{22}Ne), which is based on the mixing of H into He burning zones, and therefore the neutron production is almost independent of metallicity. However the neutron/seed ratio, with seeds dependent on metallicity, increases towards lower metallicities. Therefore the abundance pattern is shifted to higher masses. This is observed as the high s / low s ratio, shown in Fig. 33 (Kamath and Van Winkel 2022, see also Magrini et al. 2018). The trend is not a very clean one, as also the weak s-process of massive stars contributes, as well as the effect of rotational mixing in massive stars that permits the production of primary N and consequently ^{22}Ne, the latter also not dependent on metallicity.

The relation of the s-process vs. r-process impact can also be viewed as a function of metallicity. As mentioned before, the dominant s-process contribution comes from low- and intermediate-mass stars with long evolutionary lifetimes, therefore entering late in galactic evolution. Although there exist still doubts on the origin(s) of the r-process, Fig. 34 indicates that at the lowest metallicities abundance features represent solar r-process ratios, before during the later evolution also s-contributions enter, leading eventually to the solar abundance ratios (see also the extended observational overview by Battistini and Bensby (2016)).

While the pioneering papers (Burbidge et al. 1957; Cameron 1957a) laid out also the underlying nuclear physics of the rapid neutron capture r-process, responsible for the heaviest elements in the Universe, the site was still unclear. For many years the subject gained maturity by improving nuclear input, astrophysical modelling, and observational efforts (Seeger et al. 1965; Hillebrandt 1978; Cowan et al. 1991; Kratz et al. 1993; Woosley et al. 1994; Takahashi et al. 1994; Hoffman et al. 1997; Freiburghaus et al. 1999a; Pfeiffer et al. 2001; Arnould et al. 2007; Qian and Wasserburg 2007; Farouqi et al. 2010; Roederer et al. 2010; Kratz et al. 2014; Cowan et al. 2021), starting from neutron density superpositions via adiabatic expansions of matter for a given Y_e, entropy S, and expansion time scale τ, to realistic astrophysical scenarios. Only in recent years these became more concrete, including neutron star

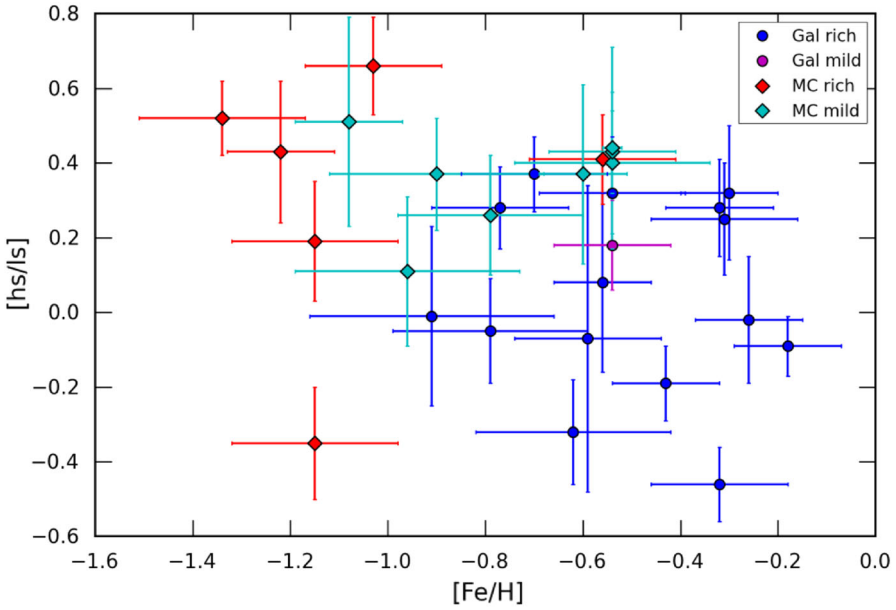

Fig. 33 Observed hs/ls ratios as a function of metallicity. A general tendency of the abundance pattern can be noticed, changing from supersolar to subsolar values for hs/ls. This is consistent with the dominant s-process origin from low- and intermediate-mass stars, where the ^{13}C neutron source is not dependent on metallicity, but the neutron to heavy seed ratio declines with metallicity. Image reproduced with permissions from Kamath and Van Winckel (2022), copyright by the authors

mergers (see e.g. Freiburghaus et al. 1999b; Just et al. 2015; Bauswein et al. 2017; Thielemann et al. 2017; Rosswog et al. 2018; Shibata and Hotokezaka 2019; Shibata et al. 2021; Barnes et al. 2021), magneto-rotational jet supernovae (see e.g. Winteler et al. 2012; Mösta et al. 2018; Nishimura et al. 2017; Reichert et al. 2021) and collapsars (fast rotating massive stars whose final core collapse ends in a black hole and mass ejection from jets and disks, see Siegel et al. 2019; Siegel 2019, 2022). The first site is related to stellar evolution (and explosions) in binary systems, while the latter two options are both related to the final collapse of massive stars. The original idea was that regular core collapse supernovae could be responsible for a strong r-process, i.e. reproducing solar r-process abundances (see e.g. Woosley et al. 1994; Takahashi et al. 1994) also up to the heaviest nuclei, within a high-entropy neutrino-powered wind. Recent supernova simulations, however, do not support the required conditions and it seems that, if at all, supernovae could only lead to a weak r-process, not producing the heavy r-process nuclei in solar proportions (Roberts et al. 2012; Martínez-Pinedo et al. 2012; Wu et al. 2014; Fischer et al. 2020a; Ghosh et al. 2022). Quark-deconfinement (QD) supernovae (Fischer et al. 2020b) were suggested as another weak r-process site.

As seen in Fig. 35, observations of low metallicity stars indicate the existence of a weak or limited r-process (dependent on the [Eu/Fe]-ratio, categorized into limited-r and r-enriched r-I and r-II stars), while most r-process enhanced stars show a solar r-process pattern. This goes together with a variation of e.g. the Sr/Eu ratio, ranging

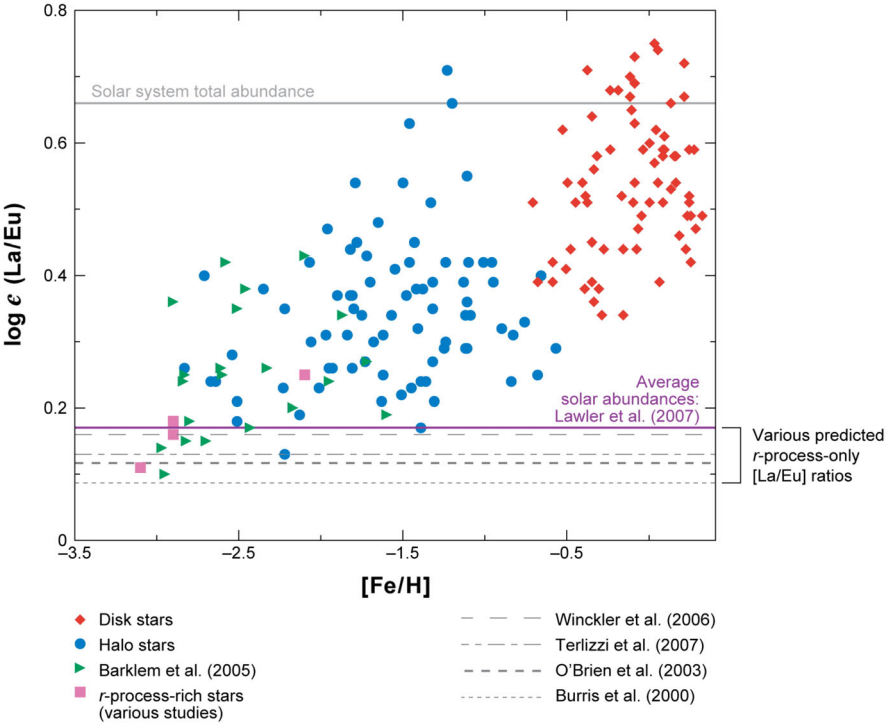

Sneden C, et al. 2008.
Annu. Rev. Astron. Astrophys. 46:241–88

Fig. 34 Observed La/Eu ratios as a function of metallicity. A general tendency can be noticed that the abundance ratio is at low metallicities dominated by the r-process contribution while the combination with the delayed s-process leads finally to solar ratios. Image reproduced with permission from Sneden et al. (2008), copyright by Annual Reviews

from about 1120 down to 0.5 (Hansen et al. 2018), and indicating the different decline of the abundance curve as a function of A. Some of the r-process enriched stars show an "actinide boost", i.e. their Th or U to Eu ratio is supersolar (see e.g. Roederer et al. 2010; Holmbeck et al. 2018, 2019b, a).

Summarizing the discussion above: we have a number of suggested r-process sites, but only one of them is proven by a direct observation of the explosive event. Observations of low metallicity stars show essentially three types of patterns, a weak or limited r-process, a strong solar-type r-process, and an actinide-boosted r-process (for reviews and impact on galactic chemical evolution see e.g. Matteucci et al. (2014); Wehmeyer et al. (2015); Cescutti et al. (2015); van de Voort et al. (2020); Perego et al. (2021); Cowan et al. (2021); Thielemann et al. (2022); Farouqi et al. (2022)). Whether the latter two types are produced in different sites or result from variations within the same site (e.g. neutron star mergers) is still debated. The question is now how to identify features that can point back to individual sites. In terms of chemical evolution models it is important to utilize inhomogeneous models

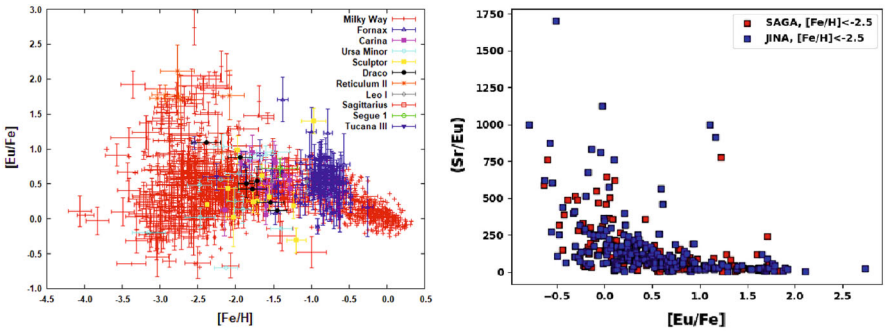

Fig. 35 Left: [Eu/Fe] ratios of 1572 stars with Eu detections from the SAGA database (Suda et al. 2008). A huge scatter can be observed before at about [Fe/H]$= -2$ an averaging (smaller spread) sets in, continues with a different gradient when SNe Ia start to contribute at -1. Right: Sr/Eu ratios for all stars with [Fe/H]< -2.5, show a drastic change at about [Eu/Fe]$= 0 - 0.3$, i.e. the division between limited-r stars and r-enriched stars (for these observational classifications and the definition of actinide boost stars see e.g. Schatz et al. 2002; Roederer et al. 2009, 2010; Mashonkina et al. 2014; Roederer 2017; Holmbeck et al. 2018; Hansen et al. 2018; Sakari et al. 2018; Holmbeck et al. 2020; Ezzeddine et al. 2020). Notice that some points are identical for SAGA and JINA and only the entry plotted for JINA—in blue—is visible, especially the value of about 1100 for [Eu/Fe] ≈ 0

that do not make use of the instantaneous mixing approximation IMA and can treat the impact of rare events, leading to a sizable spread in abundance ratios (see Fig. 35). A promising approach is to look for correlations among different elements. Comparing the abundances of Fe, Ge, Zr, and r-process Eu in low metallicity stars led to a strong correlation of Ge with Fe, indicating the same nucleosynthesis origin (core-collapse supernovae), a weak correlation of Zr with Fe, indicating that other sites than regular core-collapse supernovae (without or with low Fe ejection) contribute as well, and no correlation between Eu and Fe, pointing essentially to a pure r-process origin with negligible Fe ejection (Cowan et al. 2005). More recent data from the SAGA and JINA databases (Suda et al. 2008; Abohalima and Frebel 2018) permit a correlation between Eu and Fe for [Eu/Fe]<0–0.3, i.e. for stars with lower than average r-process enrichment that also show high [Sr/Fe] values (Fig. 35, right panel). Interpreted in a straightforward way this would point to a negligible Fe/Eu ratio (in comparison to solar ratios) in the major r-process sources (like neutron star mergers and collapsars), while a noticeable co-production of Fe with Eu is possible in less strong r-process sources, e.g. with a weak r-process (probably pointing to rare supernova types). The latter options have been discussed in more detail in Thielemann et al. (2022); Farouqi et al. (2022), requiring further and continuous consistency checks through observations, modelling of the contributing objects, and the treatment of their impact in galactic evolution.

9 Summary and future

This has been a long and maybe (but hopefully not) fatiguing journey through the chart of nuclei and periodic table of the elements, but hopefully it gave an impression how we arrived at the abundance pattern of elements and isotopes on earth, in the

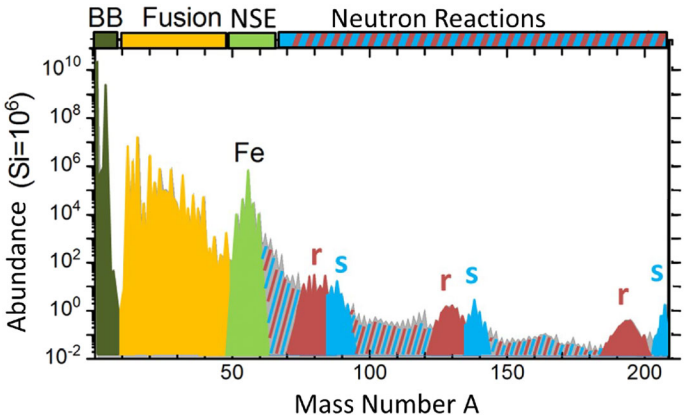

Fig. 36 Solar abundances as a function of mass number A, divided in the responsible processes from Big Bang nucleosynthesis, fusion reactions in the evolution of stars and their explosions, including conditions that lead to a full chemical equilibrium of abundances for nuclei with the highest binding energies (nuclear statistical equilibrium NSE), and s- and r-process contributions. The abundances of p-nuclei are too small to be visible in this plot. Image courtesy of F. Käppeler

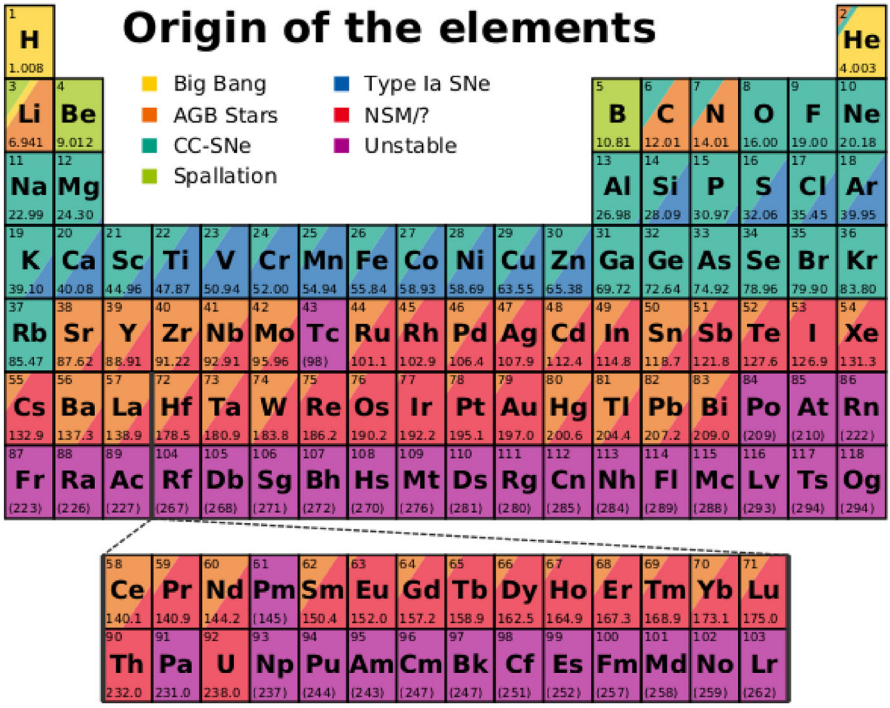

Fig. 37 The periodic table of the elements, where the processes of the preceding figure are translated into stellar sites. It should be noticed that the s- and r-process should be divided into weak and main components, where the weak components are related to different sites than indicated in the plot, like massive stars for the weak s-process and probably rare classes of supernovae for the weak r-process. Image courtesy of M. Reichert

solar system, the Milky Way and the Universe. It remains to be mentioned, that the abundances of B and Be are due to galactic cosmic ray (GCR) spallation reactions involving C and heavier nuclei, similar to what is shown for ^{6}Li and other nuclei in Fig. 7 (Prantzos 2012). These nuclei were initially attributed to an x-process of unknown origin (Burbidge et al. 1957).

We want to conclude with a summary of all these nucleosynthesis process contributions to the elements and isotopes known on Earth with two figures (Figs. 36 and 37), which hopefully provide an excellent overview on the topic of this review. Future progress depends on many efforts in the research areas discussed in this review: starting with extended input from a variety of nuclear physics (experimental and theoretical reaction determinations, at lowest energies in underground labs, far from stability in radioactive isotope facilities, weak interactions from decays to electron capture and neutrino interactions with nuclei, the nuclear equation of state), stellar evolution modelling (including radiation transport, the impact of rotation, the advent of multi-D modelling that will improve the treatment of convection and mixing and magnetic fields), the treatment of explosive events (with all aspects from neutrino transport, the combination of hydrodynamics with nuclear energy generation and losses with their different timescales, the high density equation of state, the numerical problems related to the transition from quasistatic hydrostatic evolution to a sudden onset of explosions in some sites like novae, X-ray burst and type Ia supernovae, the correct and efficient numerical treatment of environments were general relativity plays an important role), the prediction of light curves, spectra, and gravitational wave emission, the observation of individual stars (during their evolution and in catastrophic end stages), the abundance determinations of stars in galaxies like the Milky Way as well as dwarf galaxies, which serve as the witnesses of the evolution of the elements throughout our universe, from the Big Bang to the role of stars in galaxies, and finally the information from gamma-ray detections of unstable isotopes in remnants of explosions or interstellar space, as well as the isotopic composition of meteoritic grains and deep-sea sediments which can give us information about the composition of individual event ejecta and the recent addition of such ejecta to the solar system or even the Earth environment. On all these fronts, we expect further progress in theory as well as experimental and observational facilities.

Acknowledgements This work benefitted from support by the Deutsche Forschungsgemeinschaft (DFG, German Research Foundation)—Project-ID 279384907—SFB 1245, the ERC Starting Grant EUROPIUM-677912, the European COST Action CA16117 Chemical Elements as Tracers of the Evolution of the Cosmos (ChETEC), and the International Research Network for Nuclear Astrophysics (IReNA). We also want to thank a large number of colleagues for exchange and collaborations on issues which relate to the topics of the present review, especially the referees Marco Limongi and Maurizo Busso for their very constructive advice and the Editor-in-Chief Francesca Matteucci and the Publishing Editor Frank Schulz for their patience and support.

Funding Open access funding provided by University of Basel.

Open Access This article is licensed under a Creative Commons Attribution 4.0 International License, which permits use, sharing, adaptation, distribution and reproduction in any medium or format, as long as you give appropriate credit to the original author(s) and the source, provide a link to the Creative

Commons licence, and indicate if changes were made. The images or other third party material in this article are included in the article's Creative Commons licence, unless indicated otherwise in a credit line to the material. If material is not included in the article's Creative Commons licence and your intended use is not permitted by statutory regulation or exceeds the permitted use, you will need to obtain permission directly from the copyright holder. To view a copy of this licence, visit http://creativecommons.org/licenses/by/4.0/.

References

Abbott BP et al (2017) GW170817: observation of gravitational waves from a binary neutron star inspiral. Phys Rev Lett 119:161101. https://doi.org/10.1103/PhysRevLett.119.161101

Abohalima A, Frebel A (2018) JINAbase-a database for chemical abundances of metal-poor stars. Astrophys J Suppl 238(2):36. https://doi.org/10.3847/1538-4365/aadfe9 .arXiv:1711.04410 [astro-ph.SR]

Adelberger EG, Garcia A, Robertson RGH, Snover KA, Balantekin AB, Heeger K, Ramsey-Musolf MJ, Bemmerer D, Junghans A, Bertulani CA, Chen JW, Costantini H, Prati P, Couder M, Uberseder E, Wiescher M, Cyburt R, Davids B, Freedman SJ, Gai M, Gazit D, Gialanella L, Imbriani G, Greife U, Hass M, Haxton WC, Itahashi T, Kubodera K, Langanke K, Leitner D, Leitner M, Vetter P, Winslow L, Marcucci LE, Motobayashi T, Mukhamedzhanov A, Tribble RE, Nollett KM, Nunes FM, Park TS, Parker PD, Schiavilla R, Simpson EC, Spitaleri C, Strieder F, Trautvetter HP, Suemmerer K, Typel S (2011) Solar fusion cross sections. II. The pp chain and CNO cycles. Rev Mod Phys 83(1):195–246. https://doi.org/10.1103/RevModPhys.83.195. arXiv:1004.2318 [nucl-ex]

Aerts C (2021) Probing the interior physics of stars through asteroseismology. Rev Mod Phys 93 (1):015001. https://doi.org/10.1103/RevModPhys.93.015001. arXiv:1912.12300 [astro-ph.SR]

Aliotta M, Buompane R, Couder M, Couture A, deBoer RJ, Formicola A, Gialanella L, Glorius J, Imbriani G, Junker M, Langer C, Lennarz A, Litvinov YA, Liu WP, Lugaro M, Matei C, Meisel Z, Piersanti L, Reifarth R, Robertson D, Simon A, Straniero O, Tumino A, Wiescher M, Xu Y (2022) The status and future of direct nuclear reaction measurements for stellar burning. J Phys G 49(1):010501. https://doi.org/10.1088/1361-6471/ac2b0f. arXiv:2109.14418 [nucl-ex]

Aloy MÁ, Obergaulinger M (2021) Magnetorotational core collapse of possible GRB progenitors - II. Formation of protomagnetars and collapsars. MNRAS 500(4):4365–4397. https://doi.org/10.1093/mnras/staa3273. arXiv:2008.03779 [astro-ph.HE]

Ando S, Cyburt RH, Hong SW, Hyun CH (2006) Radiative neutron capture on a proton at big-bang nucleosynthesis energies. Phys Rev C 74(2):025809. https://doi.org/10.1103/PhysRevC.74.025809. arXiv:nucl-th/0511074

Angulo C, Arnould M, Rayet M, Descouvemont P, Baye D, Leclercq-Willain C, Coc A, Barhoumi S, Aguer P, Rolfs C, Kunz R, Hammer JW, Mayer A, Paradellis T, Kossionides S, Chronidou C, Spyrou K, degl'Innocenti S, Fiorentini G, Ricci B, Zavatarelli S, Providencia C, Wolters H, Soares J, Grama C, Rahighi J, Shotter A, Lamehi Rachti M, (1999) A compilation of charged-particle induced thermonuclear reaction rates. Nucl Phys A 656(1):3–183. https://doi.org/10.1016/S0375-9474(99)00030-5

Arcones A, Bliss J (2014) Nucleosynthesis of elements between Sr and Ag in neutron- and proton-rich neutrino-driven winds. J Phys G 41(4):044005. https://doi.org/10.1088/0954-3899/41/4/044005. arXiv:1312.0434 [astro-ph.SR]

Arcones A, Martínez-Pinedo G (2011) Dynamical *r*-process studies within the neutrino-driven wind scenario and its sensitivity to the nuclear physics input. Phys Rev C 83:045809. https://doi.org/10.1103/PhysRevC.83.045809

Arcones A, Thielemann FK (2013) Neutrino-driven wind simulations and nucleosynthesis of heavy elements. J Phys G 40:013201. https://doi.org/10.1088/0954-3899/40/1/013201

Arnett WD (1969) A possible model of supernovae: detonation of ^{12}C. Astrophys Space Sci 5(2):180–212. https://doi.org/10.1007/BF00650291

Arnett WD (1977) Advanced evolution of massive stars. VII. Silicon burning. Astrophys J Suppl 35:145–159. https://doi.org/10.1086/190472

Arnett WD, Truran JW, Woosley SE (1971) Nucleosynthesis in supernova models. II. The ^{12}C detonation model. Astrophys J 165:87. https://doi.org/10.1086/150878

Arnett WD, Bahcall JN, Kirshner RP, Woosley SE (1989) Supernova 1987A. Annu Rev Astron Astrophys 27:629–700. https://doi.org/10.1146/annurev.aa.27.090189.003213

Arnett WD, Meakin C, Hirschi R, Cristini A, Georgy C, Campbell S, Scott LJA, Kaiser EA, Viallet M, Mocák M (2019) 3D Simulations and MLT. I. Renzini's Critique. Astrophys J 882(1):18. https://doi.org/10.3847/1538-4357/ab21d9. arXiv:1810.04653 [astro-ph.SR]

Arnould M (1972) Influence of the excited states of target nuclei in the vicinity of the iron peak on stellar reaction rates. Astron Astrophys 19:92

Arnould M, Goriely S (2003) The p-process of stellar nucleosynthesis: astrophysics and nuclear physics status. Phys Rep 384(1–2):1–84. https://doi.org/10.1016/S0370-1573(03)00242-4

Arnould M, Goriely S, Takahashi K (2007) The r-process of stellar nucleosynthesis: astrophysics and nuclear physics achievements and mysteries. Phys Rep 450:97–213. https://doi.org/10.1016/j.physrep.2007.06.002

Asplund M, Grevesse N, Sauval AJ, Scott P (2009) The chemical composition of the sun. Annu Rev Astron Astrophys 47:481–522. https://doi.org/10.1146/annurev.astro.46.060407.145222

Asplund M, Amarsi AM, Grevesse N (2021) The chemical make-up of the Sun: a 2020 vision. Astron Astrophys 653:A141. https://doi.org/10.1051/0004-6361/202140445. arXiv:2105.01661 [astro-ph.SR]

Audouze J, Tinsley BM (1976) Chemical evolution of galaxies. Annu Rev Astron Astrophys 14:43–79. https://doi.org/10.1146/annurev.aa.14.090176.000355

Aver E, Olive KA, Porter RL, Skillman ED (2013) The primordial helium abundance from updated emissivities. J Cosmol Astropart Phys 11:017. https://doi.org/10.1088/1475-7516/2013/11/017. arXiv:1309.0047

Aver E, Olive KA, Skillman ED (2015) The effects of He I λ10830 on helium abundance determinations. J Cosmol Astropart Phys 7:011. https://doi.org/10.1088/1475-7516/2015/07/011. arXiv:1503.08146

Aver E, Berg DA, Olive KA, Pogge RW, Salzer JJ, Skillman ED (2021) Improving helium abundance determinations with Leo P as a case study. J Cosmol Astropart Phys 3:027. https://doi.org/10.1088/1475-7516/2021/03/027. arXiv:2010.04180 [astro-ph.CO]

Bahcall JN, Pinsonneault MH (2004) What do we (not) know theoretically about solar neutrino fluxes? Phys Rev Lett 92(12):121301. https://doi.org/10.1103/PhysRevLett.92.121301.. arXiv:astro-ph/0402114 [astro-ph]

Bahcall JN, Basu S, Pinsonneault M, Serenelli AM (2005) Helioseismological implications of recent solar abundance determinations. Astrophys J 618(2):1049–1056. https://doi.org/10.1086/426070. arXiv:astro-ph/0407060 [astro-ph]

Bahcall JN, Serenelli AM, Basu S (2006) 10,000 standard solar models: a Monte Carlo simulation. Astrophys J Suppl 165(1):400–431. https://doi.org/10.1086/504043. arXiv:astro-ph/0511337 [astro-ph]

Baiotti L, Rezzolla L (2017) Binary neutron star mergers: a review of Einstein's richest laboratory. Rep Prog Phys 80:096901. https://doi.org/10.1088/1361-6633/aa67bb

Balasi KG, Langanke K, Martínez-Pinedo G (2015) Neutrino-nucleus reactions and their role for supernova dynamics and nucleosynthesis. Prog Part Nucl Phys 85:33–81. https://doi.org/10.1016/j.ppnp.2015.08.001.. arXiv:1503.08095 [nucl-th]

Balbus SA, Hawley JF (1998) Instability, turbulence, and enhanced transport in accretion disks. Rev Mod Phys 70:1–53

Bania TM, Rood RT, Balser DS (2002) The cosmological density of baryons from observations of ^{3} He$^+$ in the Milky Way. Nature 415:54–57. https://doi.org/10.1038/415054a

Bao ZY, Beer H, Käppeler F, Voss F, Wisshak K (1997) Stellar cross sections for s-process studies. Nucl Phys A 621:595–598. https://doi.org/10.1016/S0375-9474(97)00310-2

Bao ZY, Beer H, Käppeler F, Voss F, Wisshak K, Rauscher T (2000) Neutron cross sections for nucleosynthesis studies. At Nucl Data Tables 76(1):70–154. https://doi.org/10.1006/adnd.2000.0838

Barnes J, Zhu YL, Lund KA, Sprouse TM, Vassh N, McLaughlin GC, Mumpower MR, Surman R (2021) Kilonovae across the nuclear physics landscape: the impact of nuclear physics uncertainties on r-process-powered emission. Astrophys J 918(2):44. https://doi.org/10.3847/1538-4357/ac0aec. arXiv:2010.11182 [astro-ph.HE]

Battino U, Pignatari M, Travaglio C, Lederer-Woods C, Denissenkov P, Herwig F, Thielemann F, Rauscher T (2020) Heavy elements nucleosynthesis on accreting white dwarfs: building seeds for the p-process.

MNRAS 497(4):4981–4998. https://doi.org/10.1093/mnras/staa2281. arXiv:2007.13677 [astro-ph.SR]

Baumann D (2018) TASI lectures on primordial cosmology. arXiv e-prints arXiv:1807.03098 [hep-th]

Bauswein A, Just O, Janka HT, Stergioulas N (2017) Neutron-star radius constraints from GW170817 and future detections. Astrophys J Lett 850:L34. https://doi.org/10.3847/2041-8213/aa9994

Beloborodov AM (2003) Nuclear composition of gamma-ray burst fireballs. Astrophys J 588:931–944. https://doi.org/10.1086/374217

Beutler F, Blake C, Colless M, Jones DH, Staveley-Smith L, Campbell L, Parker Q, Saunders W, Watson F (2011) The 6dF galaxy survey: baryon acoustic oscillations and the local Hubble constant. MNRAS 416(4):3017–3032. https://doi.org/10.1111/j.1365-2966.2011.19250.x. arXiv:1106.3366 [astro-ph.CO]

Bisterzo S, Travaglio C, Wiescher M, Käppeler F, Gallino R (2017) Galactic chemical evolution: the impact of the ^{13}C-pocket structure on the s-process distribution. Astrophys J 835:97. https://doi.org/10.3847/1538-4357/835/1/97

Bliss J, Arcones A, Qian YZ (2018) Production of Mo and Ru isotopes in neutrino-driven winds: implications for solar abundances and presolar grains. Astrophys J 866(2):105. https://doi.org/10.3847/1538-4357/aade8d. arXiv:1804.03947 [astro-ph.HE]

Bliss J, Arcones A, Montes F, Pereira J (2020) Nuclear physics uncertainties in neutrino-driven, neutron-rich supernova ejecta. Phys Rev C 101(5):055807. https://doi.org/10.1103/PhysRevC.101.055807. arXiv:2001.02085 [nucl-ex]

Boesgaard AM, Steigman G (1985) Big bang nucleosynthesis–theories and observations. Annu Rev Astron Astrophys 23:319–378. https://doi.org/10.1146/annurev.aa.23.090185.001535

Borexino Collaboration (2020) Experimental Evidence of neutrinos produced in the CNO fusion cycle in the sun. Nature 587(11):577–582. https://doi.org/10.1038/s41586-020-2934-0. arXiv:2006.15115 [hep-ex]

Bovard L, Martin D, Guercilena F, Arcones A, Rezzolla L, Korobkin O (2017) *r*-process nucleosynthesis from matter ejected in binary neutron star mergers. Phys Rev D 96:124005. https://doi.org/10.1103/PhysRevD.96.124005

Bruno CG, Scott DA, Aliotta M, Formicola A, Best A, Boeltzig A, Bemmerer D, Broggini C, Caciolli A, Cavanna F, Ciani GF, Corvisiero P, Davinson T, Depalo R, Di Leva A, Elekes Z, Ferraro F, Fülöp Z, Gervino G, Guglielmetti A, Gustavino C, Gyürky G, Imbriani G, Junker M, Menegazzo R, Mossa V, Pantaleo FR, Piatti D, Prati P, Somorjai E, Straniero O, Strieder F, Szücs T, Takács MP, Trezzi D [LUNA Collaboration] (2016) Improved Direct Measurement of the 64.5 keV Resonance Strength in the ^{17}O (p ,α)^{14}N Reaction at LUNA. Phys Rev Lett 117(14):142502. https://doi.org/10.1103/PhysRevLett.117.142502. arXiv:1610.00483 [nucl-ex]

Buntain JF, Doherty CL, Lugaro M, Lattanzio JC, Stancliffe RJ, Karakas AI (2017) Partial mixing and the formation of 13C pockets in AGB stars: effects on the s-process elements. MNRAS 471(1):824–838

Burbidge EM, Burbidge GR, Fowler WA, Hoyle F (1957) Synthesis of the elements in stars. Rev Mod Phys 29:547–650. https://doi.org/10.1103/RevModPhys.29.547

Burrows A (2013) Colloquium: perspectives on core-collapse supernova theory. Rev Mod Phys 85:245–261. https://doi.org/10.1103/RevModPhys.85.245

Burrows A, Vartanyan D (2021) Core-collapse supernova explosion theory. Nature 589(7840):29–39. https://doi.org/10.1038/s41586-020-03059-w. arXiv:2009.14157 [astro-ph.SR]

Burrows A, Dessart L, Livne E, Ott CD, Murphy J (2007) Simulations of magnetically driven supernova and hypernova explosions in the context of rapid rotation. Astrophys J 664:416–434. https://doi.org/10.1086/519161. arXiv:astro-ph/0702539

Busso M, Vescovi D, Palmerini S, Cristallo S, Antonuccio-Delogu V (2021) s-processing in AGB stars revisited. III. Neutron captures from MHD mixing at different metallicities and observational constraints. Astrophys J 908(1):55. https://doi.org/10.3847/1538-4357/abca8e. arXiv:2011.07469 [astro-ph.SR]

Cameron AGW (1957) Nuclear reactions in stars and nucleogenesis. Publ Astron Soc Pac 69:201. https://doi.org/10.1086/127051

Cameron AGW (1957b) Stellar evolution, nuclear astrophysics, and nucleogenesis. Chalk River Lectures, CRL-41. Atomic Energy of Canada Ltd. https://www.osti.gov/biblio/4709881

Cameron AGW (2003) Some nucleosynthesis effects associated with r-process jets. Astrophys J 587:327–340. https://doi.org/10.1086/368110

Cescutti G, Matteucci F (2022) Impact of AGB stars on the chemical evolution of neutron-capture elements. Universe 8(3):173. https://doi.org/10.3390/universe8030173
Cescutti G, Romano D, Matteucci F, Chiappini C, Hirschi R (2015) The role of neutron star mergers in the chemical evolution of the Galactic halo. Astron Astrophys 577:A139. https://doi.org/10.1051/0004-6361/201525698. arXiv:1503.02954
Chandrasekhar S (1960) The stability of non-dissipative couette flow in hydromagnetics. Proc Natl Acad Sci 46(2):253–257. https://doi.org/10.1073/pnas.46.2.253
Chandrasekhar S (1984) On stars, their evolution and their stability. Rev Mod Phys 56(2):137–147. https://doi.org/10.1103/RevModPhys.56.137
Chen W, Beloborodov AM (2007) Neutrino-cooled accretion disks around spinning black holes. Astrophys J 657:383–399. https://doi.org/10.1086/508923. arXiv:astro-ph/0607145
Chiappini C, Frischknecht U, Meynet G, Hirschi R, Barbuy B, Pignatari M, Decressin T, Maeder A (2011) Imprints of fast-rotating massive stars in the Galactic Bulge. Nature 472(7344):454–457. https://doi.org/10.1038/nature10000
Chieffi A, Limongi M, Straniero O (1998) The evolution of a 25 $M_{\odot}$ Star from the main sequence up to the onset of the iron core collapse. Astrophys J 502(2):737–762. https://doi.org/10.1086/305921
Coc A, Vangioni E (2017) Primordial nucleosynthesis. Int J Mod Phys E 26:1741002. https://doi.org/10.1142/S0218301317410026. arXiv:1707.01004
Cooke RJ, Fumagalli M (2018) Measurement of the primordial helium abundance from the intergalactic medium. Nat Astron 2:957–961. https://doi.org/10.1038/s41550-018-0584-z. arXiv:1810.06561
Côté B, Eichler M, Arcones A, Hansen CJ, Simonetti P, Frebel A, Fryer CL, Pignatari M, Reichert M, Belczynski K, Matteucci F (2019) Neutron star mergers might not be the only source of r-process elements in the Milky Way. Astrophys J 875:106. https://doi.org/10.3847/1538-4357/ab10db
Cowan JJ, Thielemann FK, Truran JW (1991) The r-process and nucleochronology. Phys Rep 208:267–394. https://doi.org/10.1016/0370-1573(91)90070-3
Cowan JJ, Sneden C, Beers TC, Lawler JE, Simmerer J, Truran JW, Primas F, Collier J, Burles S (2005) Hubble Space Telescope observations of heavy elements in metal-poor galactic halo stars. Astrophys J 627:238–250. https://doi.org/10.1086/429952
Cowan JJ, Sneden C, Lawler JE, Aprahamian A, Wiescher M, Langanke K, Martínez-Pinedo G, Thielemann FK (2021) Origin of the heaviest elements: the rapid neutron-capture process. Rev Mod Phys 93(1):015002. https://doi.org/10.1103/RevModPhys.93.015002. arXiv:1901.01410 [astro-ph.HE]
Cristallo S, Straniero O, Gallino R, Piersanti L, Domínguez I, Lederer MT (2009) Evolution, nucleosynthesis, and yields of low-mass asymptotic giant branch stars at different metallicities. Astrophys J 696(1):797–820. https://doi.org/10.1088/0004-637X/696/1/797. arXiv:0902.0243 [astro-ph.SR]
Cseh B, Világos B, Roriz MP, Pereira CB, D'Orazi V, Karakas AI, Soós B, Drake NA, Junqueira S, Lugaro M (2022) Barium stars as tracers of s-process nucleosynthesis in AGB stars. I. 28 stars with independently derived AGB mass. Astron Astrophys 660:A128. https://doi.org/10.1051/0004-6361/202142468. arXiv:2201.13379 [astro-ph.SR]
Curtis S, Ebinger K, Fröhlich C, Hempel M, Perego A, Liebendörfer M, Thielemann FK (2019) PUSHing core-collapse supernovae to explosions in spherical symmetry. III. Nucleosynthesis yields. Astrophys J 870:2. https://doi.org/10.3847/1538-4357/aae7d2
Cyburt RH, Amthor AM, Ferguson R, Meisel Z, Smith K, Warren S, Heger A, Hoffman RD, Rauscher T, Sakharuk A, Schatz H, Thielemann FK, Wiescher M (2010) The JINA REACLIB database: its recent updates and impact on type-I X-ray bursts. Astrophys J Suppl 189(1):240–252. https://doi.org/10.1088/0067-0049/189/1/240
Cyburt RH, Fields BD, Olive KA, Yeh TH (2016) Big bang nucleosynthesis: present status. Rev Mod Phys 88(1):015004. https://doi.org/10.1103/RevModPhys.88.015004. arXiv:1505.01076
Dan M, Guillochon J, Brüggen M, Ramirez-Ruiz E, Rosswog S (2015) Thermonuclear detonations ensuing white dwarf mergers. MNRAS 454(4):4411–4428. https://doi.org/10.1093/mnras/stv2289. arXiv:1508.02402 [astro-ph.HE]
D'Antona F, Matteucci F (1991) Galactic evolution of lithium. Astron Astrophys 248:62
deBoer RJ, Görres J, Wiescher M, Azuma RE, Best A, Brune CR, Fields CE, Jones S, Pignatari M, Sayre D, Smith K, Timmes FX, Uberseder E (2017) The $^{12}C(\alpha,\gamma)^{16}O$ reaction and its implications for stellar helium burning. Rev Mod Phys 89(3):035007. https://doi.org/10.1103/RevModPhys.89.035007. arXiv:1709.03144 [nucl-ex]

Denissenkov PA, Tout CA (2003) Partial mixing and formation of the 13C pocket by internal gravity waves in asymptotic giant branch stars. MNRAS 340(3):722–732. https://doi.org/10.1046/j.1365-8711.2003.06284.x

Dessart L, Burrows A, Ott CD, Livne E, Yoon SC, Langer N (2006) Multidimensional simulations of the accretion-induced collapse of white dwarfs to neutron stars. Astrophys J 644(2):1063–1084. https://doi.org/10.1086/503626. arXiv:astro-ph/0601603 [astro-ph]

Diehl R, Korn A, Leibundgut B, Lugaro M, Wallner A (2022) Cosmic nucleosynthesis: a multi-messenger challenge. Progr Part Nucl Phys 127:103983. https://doi.org/10.1016/j.ppnp.2022.103983. arXiv:2206.12246 [astro-ph.HE]

Dillmann I, Rauscher T, Heil M, Käppeler F, Rapp W, Thielemann FK (2008) p-process simulations with a modified reaction library. J Phys G 35(1):014029. https://doi.org/10.1088/0954-3899/35/1/014029. arXiv:0805.4756 [astro-ph]

Doherty CL, Gil-Pons P, Siess L, Lattanzio JC (2017) Super-AGB stars and their role as electron capture supernova progenitors. Publ Astron Soc Aust 34:e056. https://doi.org/10.1017/pasa.2017.52. arXiv:1703.06895 [astro-ph.SR]

Drout MR et al (2017) Light curves of the neutron star merger GW170817/SSS17a: implications for r-process nucleosynthesis. Science 358:1570–1574. https://doi.org/10.1126/science.aaq0049

Dumont T, Charbonnel C, Palacios A, Borisov S (2021) Lithium depletion and angular momentum transport in F-type and G-type stars in Galactic open clusters. Astron Astrophys 654:A46. https://doi.org/10.1051/0004-6361/202141094. arXiv:2107.12060 [astro-ph.SR]

Ebinger K, Curtis S, Ghosh S, Fröhlich C, Hempel M, Perego A, Liebendörfer M, Thielemann FK (2020) PUSHing Core-collapse Supernovae to Explosions in Spherical Symmetry. IV. Explodability, Remnant properties, and nucleosynthesis yields of low-metallicity stars. Astrophys J 888(2):91. https://doi.org/10.3847/1538-4357/ab5dcb. https://arxiv.org/abs/1910.08958arXiv:1910.08958 [astro-ph.SR]

Eggenberger P, Ekström S, Georgy C, Martinet S, Pezzotti C, Nandal D, Meynet G, Buldgen G, Salmon S, Haemmerlé L, Maeder A, Hirschi R, Yusof N, Groh J, Farrell E, Murphy L, Choplin A (2021) Grids of stellar models with rotation. VI. Models from 0.8 to 120 $M_{\odot}$ at a metallicity Z = 0.006. Astron Astrophys 652:A137. https://doi.org/10.1051/0004-6361/202141222. https://arxiv.org/abs/2201.12262arXiv:2201.12262 [astro-ph.GA]

Eichler D, Livio M, Piran T, Schramm DN (1989) Nucleosynthesis, neutrino bursts and gamma-rays from coalescing neutron stars. Nature 340:126–128. https://doi.org/10.1038/340126a0

Eichler M, Arcones A, Kelic A, Korobkin O, Langanke K, Marketin T, Martínez-Pinedo G, Panov I, Rauscher T, Rosswog S, Winteler C, Zinner NT, Thielemann FK (2015) The role of fission in neutron star mergers and its impact on the r-process peaks. Astrophys J 808:30. https://doi.org/10.1088/0004-637X/808/1/30. arXiv:1411.0974 [astro-ph.HE]

Eichler M, Nakamura K, Takiwaki T, Kuroda T, Kotake K, Hempel M, Cabezón R, Liebendörfer M, Thielemann FK (2018) Nucleosynthesis in 2D core-collapse supernovae of 11.2 and 17.0 $M_{\odot}$ progenitors: implications for Mo and Ru production. J Phys G 45(1):014001. https://doi.org/10.1088/1361-6471/aa8891. https://arxiv.org/abs/1708.08393arXiv:1708.08393 [astro-ph.SR]

Eichler M, Sayar W, Arcones A, Rauscher T (2019) Probing the production of actinides under different r-process conditions. Astrophys J 879:47. https://doi.org/10.3847/1538-4357/ab24cf

Einstein A (1915) Die Feldgleichungen der Gravitation. Sitzungsber K Preuss Akad Wiss Berlin, pp 844–847

Ertl T, Janka HT, Woosley SE, Sukhbold T, Ugliano M (2016) A two-parameter criterion for classifying the explodability of massive stars by the neutrino-driven mechanism. Astrophys J 818(2):124. https://doi.org/10.3847/0004-637X/818/2/124. arXiv:1503.07522 [astro-ph.SR]

Evans PA et al (2017) Swift and NuSTAR observations of GW170817: detection of a blue kilonova. Science 358:1565–1570. https://doi.org/10.1126/science.aap9580

Ezzeddine R, Rasmussen K, Frebel A, Chiti A, Hinojisa K, Placco VM, Ji AP, Beers TC, Hansen TT, Roederer IU, Sakari CM, Melendez J (2020) The r-process alliance: first magellan/MIKE release from the southern search for r-process-enhanced stars. Astrophys J 898(2):150. https://doi.org/10.3847/1538-4357/ab9d1a. arXiv:2006.07731 [astro-ph.SR]

Farouqi K, Kratz K, Pfeiffer B, Rauscher T, Thielemann F, Truran JW (2010) Charged-particle and neutron-capture processes in the high-entropy wind of core-collapse supernovae. Astrophys J 712:1359–1377. https://doi.org/10.1088/0004-637X/712/2/1359

Farouqi K, Thielemann FK, Rosswog S, Kratz KL (2022) Correlations of r-process elements in very metal-poor stars as clues to their nucleosynthesis sites. Astron Astrophys 663:A70. https://doi.org/10.1051/0004-6361/202141038. arXiv:2107.03486 [astro-ph.SR]

Fernández R, Tchekhovskoy A, Quataert E, Foucart F, Kasen D (2019) Long-term GRMHD simulations of neutron star merger accretion discs: implications for electromagnetic counterparts. MNRAS 482:3373–3393. https://doi.org/10.1093/mnras/sty2932

Fields BD, Olive KA (2022) Implications of the non-observation of ^{6}Li in halo stars for the primordial ^{7}Li problem. arXiv e-prints arXiv:2204.03167 [astro-ph.GA]

Fischer T, Sagert I, Pagliara G, Hempel M, Schaffner-Bielich J, Rauscher T, Thielemann FK, Käppeli R, Martínez-Pinedo G, Liebendörfer M (2011) Core-collapse supernova explosions triggered by a quark-hadron phase transition during the early post-bounce phase. Astrophys J Suppl 194:39. https://doi.org/10.1088/0067-0049/194/2/39

Fischer T, Guo G, Dzhioev AA, Martínez-Pinedo G, Wu MR, Lohs A, Qian YZ (2020) Neutrino signal from proto-neutron star evolution: effects of opacities from charged-current-neutrino interactions and inverse neutron decay. Phys Rev C 101:025804. https://doi.org/10.1103/PhysRevC.101.025804

Fischer T, Wu MR, Wehmeyer B, Bastian NUF, Martínez-Pinedo G, Thielemann FK (2020) Core-collapse supernova explosions driven by the hadron-quark phase transition as a rare r-process site. Astrophys J 894(1):9. https://doi.org/10.3847/1538-4357/ab86b0. arXiv:2003.00972 [astro-ph.HE]

Fowler WA, Caughlan GR, Zimmerman BA (1967) Thermonuclear reaction rates. Annu Rev Astron Astrophys 5:525. https://doi.org/10.1146/annurev.aa.05.090167.002521

Freedman WL (2021) Measurements of the Hubble constant: tensions in perspective. Astrophys J 919 (1):16. https://doi.org/10.3847/1538-4357/ac0e95. arXiv:2106.15656 [astro-ph.CO]

Freiburghaus C, Rembges JF, Rauscher T, Kolbe E, Thielemann FK, Kratz KL, Pfeiffer B, Cowan JJ (1999) The astrophysical r-process: a comparison of calculations following adiabatic expansion with classical calculations based on neutron densities and temperatures. Astrophys J 516:381–398. https://doi.org/10.1086/307072

Freiburghaus C, Rosswog S, Thielemann FK (1999) R-process in neutron star mergers. Astrophys J 525: L121–L124. https://doi.org/10.1086/312343

Friedmann A (1922) Über die Krümmung des Raumes. Z Phys 10:377–386. https://doi.org/10.1007/BF01332580

Friedmann A (1924) Über die Möglichkeit einer Welt mit konstanter negativer Krümmung des Raumes. Z Phys 21(1):326–332. https://doi.org/10.1007/BF01328280

Frischknecht U, Hirschi R, Pignatari M, Maeder A, Meynet G, Chiappini C, Thielemann FK, Rauscher T, Georgy C, Ekström S (2016) s-process production in rotating massive stars at solar and low metallicities. MNRAS 456:1803–1825. https://doi.org/10.1093/mnras/stv2723. arXiv:1511.05730 [astro-ph.SR]

Fröhlich C, Martínez-Pinedo G, Liebendörfer M, Thielemann FK, Bravo E, Hix WR, Langanke K, Zinner NT (2006) Neutrino-induced nucleosynthesis of $A > 64$ nuclei: the *vp* process. Phys Rev Lett 96 (14):142502. https://doi.org/10.1103/PhysRevLett.96.142502. arXiv:astro-ph/0511376

Fujibayashi S, Kiuchi K, Wanajo S, Kyutoku K, Sekiguchi Y, Shibata M (2022) Comprehensive study of mass ejection and nucleosynthesis in binary neutron star mergers leaving short-lived massive neutron stars. arXiv e-prints arXiv:2205.05557 [astro-ph.HE]

Fuller GM, Fowler WA, Newman MJ (1985) Stellar weak interaction rates for intermediate-mass nuclei. IV. Interpolation procedures for rapidly varying lepton capture rates using effective log (ft)-values. Astrophys J 293:1–16. https://doi.org/10.1086/163208

Fülöp Z, Gyürky G, Somorjai E (2005) Data needs for the astrophysical p-process. Nucl Phys A 758:90–97. https://doi.org/10.1016/j.nuclphysa.2005.05.168

Fushiki I, Lamb DQ (1987) S-matrix calculation of the triple-alpha reaction. Astrophys J 317:368. https://doi.org/10.1086/165284

Garcia-Senz D, Cabezon RM, Arcones A, Relano A, Thielemann FK (2013) High-resolution simulations of the head-on collision of white dwarfs. MNRAS 436(4):3413–3429. https://doi.org/10.1093/mnras/stt1821. arXiv:1309.6884 [astro-ph.SR]

García-Senz D, Cabezón RM, Domínguez I, Thielemann FK (2016) Type Ia supernovae: can coriolis force break the symmetry of the gravitational confined detonation explosion mechanism? Astrophys J 819 (2):132. https://doi.org/10.3847/0004-637X/819/2/132. arXiv:1507.05830 [astro-ph.HE]

Ghosh S, Wolfe N, Fröhlich C (2022) PUSHing Core-collapse Supernovae to Explosions in Spherical Symmetry. V. Equation of state dependency of explosion properties, nucleosynthesis yields, and

compact remnants. Astrophys J 929(1):43. https://doi.org/10.3847/1538-4357/ac4d20. https://arxiv.org/abs/2107.13016arXiv:2107.13016 [astro-ph.HE]
Gil-Pons P, Doherty CL, Gutiérrez JL, Siess L, Campbell SW, Lau HB, Lattanzio JC (2018) Primordial to extremely metal-poor AGB and Super-AGB stars: white dwarf or supernova progenitors? Publ Astron Soc Aust 35:e038. https://doi.org/10.1017/pasa.2018.42. arXiv:1810.00982 [astro-ph.SR]
Giraud S, Zegers RGT, Brown BA, Gabler J-M, Lesniak J, Rebenstock J, Ney EM, Engel J, Ravlić A, Paar N (2022) Finite-temperature electron-capture rates for neutron-rich nuclei near $N = 50$ and effects on core-collapse supernova simulations. Phys Rev C 105(5). https://doi.org/10.1103/PhysRevC.105.055801
Goldstein DA, Kasen D (2018) Evidence for sub-chandrasekhar mass type Ia supernovae from an extensive survey of radiative transfer models. Astrophys J Lett 852(2):L33. https://doi.org/10.3847/2041-8213/aaa409. arXiv:1801.00789 [astro-ph.HE]
Gómez Iñesta Á, Iliadis C, Coc A (2017) Bayesian estimation of thermonuclear reaction rates for deuterium+deuterium reactions. Astrophys J 849:134. https://doi.org/10.3847/1538-4357/aa9025. arXiv:1710.01647 [astro-ph.IM]
Gonzalez FM, Fries EM, Cude-Woods C, Bailey T, Blatnik M, Broussard LJ, Callahan NB, Choi JH, Clayton SM, Currie SA, Dawid M, Dees EB, Filippone BW, Fox W, Geltenbort P, George E, Hayen L, Hickerson KP, Hoffbauer MA, Hoffman K, Holley AT, Ito TM, Komives A, Liu CY, Makela M, Morris CL, Musedinovic R, O'Shaughnessy C, Pattie RW, Ramsey J, Salvat DJ, Saunders A, Sharapov EI, Slutsky S, Su V, Sun X, Swank C, Tang Z, Uhrich W, Vanderwerp J, Walstrom P, Wang Z, Wei W, Young AR [UCN τ Collaboration] (2021) Improved neutron lifetime measurement with UCN τ. Phys Rev Lett 127(16):162501. https://doi.org/10.1103/PhysRevLett.127.162501. arXiv:2106.10375 [nucl-ex]
Goriely S (2015) The fundamental role of fission during r-process nucleosynthesis in neutron star mergers. Eur Phys J A 51:22. https://doi.org/10.1140/epja/i2015-15022-3
Goriely S, José J, Hernanz M, Rayet M, Arnould M (2002) He-detonation in sub-chandrasekhar CO white dwarfs: a new insight into energetics and p-process nucleosynthesis. Astron Astrophys 383:L27–L30. https://doi.org/10.1051/0004-6361:20020088. arXiv:astro-ph/0201199 [astro-ph]
Goriely S, Hilaire S, Koning AJ (2008) Improved predictions of nuclear reaction rates with the TALYS reaction code for astrophysical applications. Astron Astrophys 487(2):767–774. https://doi.org/10.1051/0004-6361:20078825. arXiv:0806.2239 [astro-ph]
Goriely S, Hilaire S, Koning AJ, Sin M, Capote R (2009) Towards a prediction of fission cross sections on the basis of microscopic nuclear inputs. Am Phys Soc 79:024612
Görres J, Wiescher M, Thielemann FK (1995) Bridging the waiting points: the role of two-proton capture reactions in the rp process. Phys Rev C 51(1):392–400. https://doi.org/10.1103/PhysRevC.51.392
Greiner J et al (2015) A very luminous magnetar-powered supernova associated with an ultra-long γ-ray burst. Nature 523:189–192. https://doi.org/10.1038/nature14579
Grohs E, Fuller GM, Kishimoto CT, Paris MW, Vlasenko A (2016) Neutrino energy transport in weak decoupling and big bang nucleosynthesis. Phys Rev D 93(8):083522. https://doi.org/10.1103/PhysRevD.93.083522. arXiv:1512.02205
Grohs E, Bond JR, Cooke RJ, Fuller GM, Meyers J, Paris MW (2019) Big bang nucleosynthesis and neutrino cosmology. Bull AAS 51(3):412. https://arxiv.org/abs/1903.09187arXiv:1903.09187 [astro-ph.CO]
Gronow S, Côté B, Lach F, Seitenzahl IR, Collins CE, Sim SA, Röpke FK (2021) Metallicity-dependent nucleosynthetic yields of Type Ia supernovae originating from double detonations of sub-M_{Ch} white dwarfs. Astron Astrophys 656:A94. https://doi.org/10.1051/0004-6361/202140881. arXiv:2103.14050 [astro-ph.HE]
Güray RT, Özkan N, Yalçın C, Rauscher T, Gyürky G, Farkas J, Fülöp Z, Halász Z, Somorjai E (2015) Measurements of ^{152}Gd(p,γ)^{153}Tb and ^{152}Gd(p, n)^{152}Tb reaction cross sections for the astrophysical γ process. Phys Rev C 91(5):055809. https://doi.org/10.1103/PhysRevC.91.055809. arXiv:1504.07820 [nucl-ex]
Guth AH (2014) The big bang and cosmic inflation. In: Ekspong G (ed) The oskar klein memorial lectures: 1988–1999. World Scientific, pp 159–206. https://doi.org/10.1142/9789814571616_0012
Gyürky G, Kiss GG, Elekes Z, Fülöp Z, Somorjai E, Palumbo A, Görres J, Lee HY, Rapp W, Wiescher M, Özkan N, Güray RT, Efe G, Rauscher T (2006) α-induced cross sections of Cd106 for the astrophysical p process. Phys Rev C 74(2):025805. https://doi.org/10.1103/PhysRevC.74.025805. arXiv:nucl-ex/0605034 [nucl-ex]

Gyürky GY, Elekes Z, Farkas J, Fülöp ZS, Kiss GG, Somorjai E, Szücs T, Güray RT, Özkan N, Yalçin C, Rauscher T (2010) Alpha-induced reactions for the astrophysical p-process: the case of ^{151}Eu. J Phys Conf Ser 202:012004. https://doi.org/10.1088/1742-6596/202/1/012004. arXiv:0910.3496 [nucl-ex]

Gyürky G, Halász Z, Kiss GG, Szücs T, Fülöp Z (2022) Activation cross section measurement of the $^{14}N(p,\gamma)^{15}O$ astrophysical key reaction. Phys Rev C 105:L022801. https://doi.org/10.1103/PhysRevC.105.L022801

Halevi G, Mösta P (2018) r-process nucleosynthesis from three-dimensional jet-driven core-collapse supernovae with magnetic misalignments. MNRAS 477(2):2366–2375. https://doi.org/10.1093/mnras/sty797. arXiv:1801.08943 [astro-ph.HE]

Hansen CJ, Montes F, Arcones A (2014) How many nucleosynthesis processes exist at low metallicity? Astrophys J 797:123. https://doi.org/10.1088/0004-637X/797/2/123. arXiv:1408.4135 [astro-ph.SR]

Hansen TT, Holmbeck EM, Beers TC, Placco VM, Roederer IU, Frebel A, Sakari CM, Simon JD, Thompson IB (2018) The r-process alliance: first release from the southern search for r-process-enhanced stars in the galactic halo. Astrophys J 858:92. https://doi.org/10.3847/1538-4357/aabacc

Harris JA, Hix WR, Chertkow MA, Lee CT, Lentz EJ, Messer OEB (2017) Implications for post-processing nucleosynthesis of core-collapse supernova models with lagrangian particles. Astrophys J 843(1):2. https://doi.org/10.3847/1538-4357/aa76de. arXiv:1701.08876 [astro-ph.SR]

Haxton WC, Serenelli AM (2008) CN cycle solar neutrinos and the sun's primordial core metallicity. Astrophys J 687(1):678–691. https://doi.org/10.1086/591787. arXiv:0805.2013 [astro-ph]

Heger A, Woosley SE (2010) Nucleosynthesis and evolution of massive metal-free stars. Astrophys J 724:341–373. https://doi.org/10.1088/0004-637X/724/1/341. arXiv:0803.3161

Heger A, Fryer CL, Woosley SE, Langer N, Hartmann DH (2003) How massive single stars end their life. Astrophys J 591(1):288–300. https://doi.org/10.1086/375341. arXiv:astro-ph/0212469 [astro-ph]

Heger A, Kolbe E, Haxton WC, Langanke K, Martínez-Pinedo G, Woosley SE (2005) Neutrino nucleosynthesis. Phys Lett B 606(3–4):258–264. https://doi.org/10.1016/j.physletb.2004.12.017. arXiv:astro-ph/0307546 [astro-ph]

Hillebrandt W (1978) The rapid neutron-capture process and the synthesis of heavy and neutron-rich elements. Space Sci Rev 21:639–702. https://doi.org/10.1007/BF00186236

Hillebrandt W, Kodama T, Takahashi K (1976) R-process nucleosynthesis–a dynamical model. Astron Astrophys 52:63–68

Hillebrandt W, Kromer M, Röpke FK, Ruiter AJ (2013) Towards an understanding of Type Ia supernovae from a synthesis of theory and observations. Front Phys 8(2):116–143. https://doi.org/10.1007/s11467-013-0303-2. arXiv:1302.6420 [astro-ph.CO]

Hix WR, Meyer BS (2006) Thermonuclear kinetics in astrophysics. Nucl Phys A 777:188–207. https://doi.org/10.1016/j.nuclphysa.2004.10.009

Hix WR, Thielemann FK (1996) Silicon burning. I. Neutronization and the physics of quasi-equilibrium. Astrophys J 460:869. https://doi.org/10.1086/177016. arXiv:astro-ph/9511088 [astro-ph]

Hix WR, Thielemann FK (1999) Silicon burning. II. Quasi-equilibrium and explosive burning. Astrophys J 511:862–875

Hix WR, Thielemann FK (1999) Computational methods for nucleosynthesis and nuclear energy generation. J Comput Appl Math 109:321–351. https://doi.org/10.1016/S0377-0427(99)00163-6

Hix WR, Parete-Koon ST, Freiburghaus C, Thielemann FK (2007) The QSE-reduced nuclear reaction network for silicon burning. Astrophys J 667:476–488. https://doi.org/10.1086/520672

Hoeflich P (2017) Explosion physics of thermonuclear supernovae and their signatures. In: Alsabti AW, Murdin P (eds) Handbook of supernovae. Springer, Cham, p 1151. https://doi.org/10.1007/978-3-319-21846-5_56

Hoffman RD, Woosley SE, Qian YZ (1997) Nucleosynthesis in neutrino-driven winds. II. Implications for heavy element synthesis. Astrophys J 482:951–962. https://doi.org/10.1086/304181

Höflich P, Wheeler JC, Thielemann FK (1998) Type Ia supernovae: influence of the initial composition on the nucleosynthesis, light curves, and spectra and consequences for the determination of Ω_M and Λ. Astrophys J 495(2):617–629. https://doi.org/10.1086/305327. arXiv:astro-ph/9709233 [astro-ph]

Holmbeck EM, Beers TC, Roederer IU, Placco VM, Hansen TT, Sakari CM, Sneden C, Liu C, Lee YS, Cowan JJ, Frebel A (2018) The r-process alliance: 2MASS J09544277+5246414, the most actinide-enhanced R-II star known. Astrophys J 859:L24. https://doi.org/10.3847/2041-8213/aac722

Holmbeck EM, Frebel A, McLaughlin GC, Mumpower MR, Sprouse TM, Surman R (2019) Actinide-rich and actinide-poor r-process-enhanced metal-poor stars do not require separate r-process progenitors. Astrophys J 881:5. https://doi.org/10.3847/1538-4357/ab2a01

Holmbeck EM, Sprouse TM, Mumpower MR, Vassh N, Surman R, Beers TC, Kawano T (2019) Actinide production in the neutron-rich ejecta of a neutron star merger. Astrophys J 870:23. https://doi.org/10.3847/1538-4357/aaefef

Holmbeck EM, Hansen TT, Beers TC, Placco VM, Whitten DD, Rasmussen KC, Roederer IU, Ezzeddine R, Sakari CM, Frebel A, Drout MR, Simon JD, Thompson IB, Bland-Hawthorn J, Gibson BK, Grebel EK, Kordopatis G, Kunder A, Meléndez J, Navarro JF, Reid WA, Seabroke G, Steinmetz M, Watson F, Wyse RFG (2020) The r-process alliance: fourth data release from the search for r-process-enhanced stars in the galactic halo. Astrophys J Suppl 249(2):30. https://doi.org/10.3847/1538-4365/ab9c19. arXiv:2007.00749 [astro-ph.SR]

Holmes JA, Woosley SE, Fowler WA, Zimmerman BA (1976) Tables of thermonuclear-reaction-rate data for neutron-induced reactions on heavy nuclei. At Data Nucl Data Tables 18:305. https://doi.org/10.1016/0092-640X(76)90011-5

Horowitz CJ (2002) Weak magnetism for antineutrinos in supernovae. Phys Rev D 65:043001. https://doi.org/10.1103/PhysRevD.65.043001

Horowitz CJ et al (2019) r-process nucleosynthesis: connecting rare-isotope beam facilities with the cosmos. J Phys G 46:083001. https://doi.org/10.1088/1361-6471/ab0849

Hotokezaka K, Nakar E, Gottlieb O, Nissanke S, Masuda K, Hallinan G, Mooley KP, Deller AT (2019) A Hubble constant measurement from superluminal motion of the jet in GW170817. Nat Astron 3:940–944. https://doi.org/10.1038/s41550-019-0820-1. arXiv:1806.10596 [astro-ph.CO]

Howard WM, Meyer BS, Woosley SE (1991) A new site for the astrophysical gamma-process. Astrophys J Lett 373:L5. https://doi.org/10.1086/186038

Hoyle F, Fowler WA (1960) Nucleosynthesis in supernovae. Astrophys J 132:565. https://doi.org/10.1086/146963

Iben JI, Truran JW (1978) On the surface composition of thermally pulsing stars of high luminosity and on the contribution of such stars to the element enrichment of the interstellar medium. Astrophys J 220:980–995. https://doi.org/10.1086/155986

Iben JI, Tutukov AV (1984) Supernovae of type I as end products of the evolution of binaries with components of moderate initial mass. Astrophys J Suppl 54:335–372. https://doi.org/10.1086/190932

Iliadis C (2007) Nuclear physics of stars. Wiley-VCH, Weinheim. https://doi.org/10.1002/9783527692668

Imbriani G, Limongi M, Gialanella L, Terrasi F, Straniero O, Chieffi A (2001) The $^{12}C(\alpha,\gamma)^{16}O$ reaction rate and the evolution of stars in the mass range $0.8 \leq M/M_{\odot} \leq 25$. Astrophys. J. 558(2):903–915. https://doi.org/10.1086/322288. arXiv:astro-ph/0107172 [astro-ph]

Iwamoto K et al (1998) A hypernova model for the supernova associated with the γ-ray burst of 25 April 1998. Nature 395:672–674. https://doi.org/10.1038/27155

Izzo L, Della Valle M, Mason E, Matteucci F, Romano D, Pasquini L, Vanzi L, Jordan A, Fernandez JM, Bluhm P, Brahm R, Espinoza N, Williams R (2015) Early optical spectra of Nova V1369 Cen show the presence of lithium. Astrophys J Lett 808(1):L14. https://doi.org/10.1088/2041-8205/808/1/L14. arXiv:1506.08048 [astro-ph.SR]

Janka HT, Melson T, Summa A (2016) Physics of core-collapse supernovae in three dimensions: a sneak preview. Annu Rev Nucl Part Sci 66:341–375. https://doi.org/10.1146/annurev-nucl-102115-044747

Jerkstrand A, Wongwathanarat A, Janka HT, Gabler M, Alp D, Diehl R, Maeda K, Larsson J, Fransson C, Menon A, Heger A (2020) Properties of gamma-ray decay lines in 3D core-collapse supernova models, with application to SN 1987A and Cas A. MNRAS 494(2):2471–2497. https://doi.org/10.1093/mnras/staa736. arXiv:2003.05156 [astro-ph.HE]

Ji AP, Drout MR, Hansen TT (2019) The lanthanide fraction distribution in metal-poor stars: a test of neutron star mergers as the dominant r-process site. Astrophys J 882:40. https://doi.org/10.3847/1538-4357/ab3291

Jiang JA, Doi M, Maeda K, Shigeyama T, Nomoto K, Yasuda N, Jha SW, Tanaka M, Morokuma T, Tominaga N, Ivezić Ž, Ruiz-Lapuente P, Stritzinger MD, Mazzali PA, Ashall C, Mould J, Baade D, Suzuki N, Connolly AJ, Patat F, Wang L, Yoachim P, Jones D, Furusawa H, Miyazaki S (2017) A hybrid type Ia supernova with an early flash triggered by helium-shell detonation. Nature 550(7674):80–83. https://doi.org/10.1038/nature23908. arXiv:1710.01824 [astro-ph.HE]

Jose J (2016) Stellar explosions: hydrodynamics and nucleosynthesis. CRC Press, Boca Raton. https://doi.org/10.1201/b19165

José J, Coc A (2005) Nucleosynthesis in classical novae. Nucl Phys News 15:1–6

José J, Hernanz M, Amari S, Lodders K, Zinner E (2004) The imprint of nova nucleosynthesis in presolar grains. Astrophys J 612(1):414–428. https://doi.org/10.1086/422569. arXiv:astro-ph/0405332 [astro-ph]

Just O, Bauswein A, Pulpillo RA, Goriely S, Janka HT (2015) Comprehensive nucleosynthesis analysis for ejecta of compact binary mergers. MNRAS 448:541–567. https://doi.org/10.1093/mnras/stv009

Kaiser EA, Hirschi R, Arnett WD, Georgy C, Scott LJA, Cristini A (2020) Relative importance of convective uncertainties in massive stars. MNRAS 496(2):1967–1989. https://doi.org/10.1093/mnras/staa1595. arXiv:2006.01877 [astro-ph.SR]

Kamath D, Van Winckel H (2022) Post-AGB stars as tracers of AGB nucleosynthesis: an update. Universe 8(4):233. https://doi.org/10.3390/universe8040233

Kappeler F, Beer H, Wisshak K (1989) s-process nucleosynthesis-nuclear physics and the classical model. Rep Prog Phys 52:945–1013. https://doi.org/10.1088/0034-4885/52/8/002

Käppeler F, Thielemann FK, Wiescher M (1998) Current quests in nuclear astrophysics and experimental approaches. Annu Rev Nucl Part Sci 48:175–251. https://doi.org/10.1146/annurev.nucl.48.1.175

Käppeler F, Gallino R, Bisterzo S, Aoki W (2011) The s process: nuclear physics, stellar models, and observations. Rev Mod Phys 83(1):157–194. https://doi.org/10.1103/RevModPhys.83.157. arXiv:1012.5218 [astro-ph.SR]

Karakas AI, Lattanzio JC (2014) The dawes review 2: nucleosynthesis and stellar yields of low- and intermediate-mass single stars. Publ Astron Soc Aust 31:e030. https://doi.org/10.1017/pasa.2014.21

Karakas AI, Lugaro M (2016) Stellar yields from metal-rich asymptotic giant branch models. Astrophys J 825(1):26. https://doi.org/10.3847/0004-637X/825/1/26. arXiv:1604.02178 [astro-ph.SR]

Karakas AI, Lugaro M, Carlos M, Cseh B, Kamath D, García-Hernández DA (2018) Heavy-element yields and abundances of asymptotic giant branch models with a Small Magellanic Cloud metallicity. MNRAS 477(1):421–437. https://doi.org/10.1093/mnras/sty625. arXiv:1803.02028 [astro-ph.SR]

Kasen D, Metzger B, Barnes J, Quataert E, Ramirez-Ruiz E (2017) Origin of the heavy elements in binary neutron-star mergers from a gravitational-wave event. Nature 551:80–84. https://doi.org/10.1038/nature24453

Kasliwal MM et al (2017) Illuminating gravitational waves: a concordant picture of photons from a neutron star merger. Science 358:1559–1565. https://doi.org/10.1126/science.aap9455

Kasliwal MM, Kasen D, Lau RM, Perley DA, Rosswog S, Ofek EO, Hotokezaka K, Chary RR, Sollerman J, Goobar A, Kaplan DL (2022) Spitzer mid-infrared detections of neutron star merger GW170817 suggests synthesis of the heaviest elements. MNRAS Lett 510(1):L7–L12. https://doi.org/10.1093/mnrasl/slz007. arXiv:1812.08708 [astro-ph.HE]

Kawano L, Schramm D, Steigman G (1988) Primordial lithium–new reaction rates, new abundances, new constraints. Astrophys J 327:750–754. https://doi.org/10.1086/166232

Khokhlov A, Mueller E, Hoeflich P (1993) Light curves of type Ia supernova models with different explosion mechanisms. Astron Astrophys 270:223–248

Kippenhahn R, Weigert A, Weiss A (2013) Stellar structure and evolution, 2nd edn. Springer, Berlin Heidelberg. https://doi.org/10.1007/978-3-642-30304-3

Kirsebom OS et al (2019) Discovery of an exceptionally strong β -decay transition of ^{20}F and implications for the fate of intermediate-mass stars. Phys Rev Lett 123:262701. https://doi.org/10.1103/PhysRevLett.123.262701

Kirsebom OS et al (2019) Measurement of the $2^+ \rightarrow 0^+$ ground-state transition in the β decay of ^{20}F. Phys Rev C 100:065805. https://doi.org/10.1103/PhysRevC.100.065805

Kiss GG, Szücs T, Török Z, Korkulu Z, Gyürky G, Halász Z, Fülöp Z, Somorjai E, Rauscher T (2012) Investigation of α-induced reactions on ^{127}I for the astrophysical γ process. Phys Rev C 86 (3):035801. https://doi.org/10.1103/PhysRevC.86.035801. arXiv:1209.1238 [nucl-ex]

Kobayashi C, Karakas AI, Lugaro M (2020) The origin of elements from carbon to uranium. Astrophys J 900(2):179. https://doi.org/10.3847/1538-4357/abae65. arXiv:2008.04660 [astro-ph.GA]

Kolb EW, Turner MS (1990) The Early Universe. Frontiers in physics, Westview Press, Boulder, CO. https://doi.org/10.1201/9780429492860

Korkulu Z, Özkan N, Kiss GG, Szücs T, Gyürky G, Fülöp Z, Güray RT, Halász Z, Rauscher T, Somorjai E, Török Z, Yalçın C (2018) Investigation of α-induced reactions on Sb isotopes relevant to the astrophysical γ process. Phys Rev C 97(4):045803. https://doi.org/10.1103/PhysRevC.97.045803. arXiv:1803.07791 [nucl-ex]

Korn AJ (2020) How stars in globular clusters reveal the depletion of the Spite plateau of lithium. Mem SAIt 91:105. arXiv:2111.00913 [astro-ph.SR]

Korobkin O, Rosswog S, Arcones A, Winteler C (2012) On the astrophysical robustness of the neutron star merger r-process. MNRAS 426:1940–1949. https://doi.org/10.1111/j.1365-2966.2012.21859.x

Kotake K, Takiwaki T, Suwa Y, Iwakami Nakano W, Kawagoe S, Masada Y, Fujimoto Si (2012) Multimessengers from core-collapse supernovae: multidimensionality as a key to bridge theory and observation. Adv Astron 2012:428757. https://doi.org/10.1155/2012/428757. arXiv:1204.2330 [astro-ph.HE]

Kramer M (2009) Pulsars & Magnetars. In: Strassmeier KG, Kosovichev AG, Beckman JE (eds) Cosmic magnetic fields: from planets, to stars and galaxies. IAU Symposium, vol 259. pp 485–492. https://doi.org/10.1017/S1743921309031159

Kratz KL, Gabelmann H, Hillebrandt W, Pfeiffer B, Schlosser K, Thielemann FK (1986) The beta-decay half-life of cd-130(48)82 and its importance for astrophysical r-process scenarios. Z Phys A 325:489–490

Kratz K, Bitouzet J, Thielemann F, Moeller P, Pfeiffer B (1993) Isotopic r-process abundances and nuclear structure far from stability–implications for the r-process mechanism. Astrophys J 403:216–238. https://doi.org/10.1086/172196

Kratz KL, Farouqi K, Möller P (2014) A High-entropy-wind r-process Study Based on Nuclear-structure Quantities from the New Finite-range Droplet Model Frdm (2012). Astrophys J 792:6. https://doi.org/10.1088/0004-637X/792/1/6

Kuroda T, Arcones A, Takiwaki T, Kotake K (2020) Magnetorotational explosion of a massive star supported by neutrino heating in general relativistic three-dimensional simulations. Astrophys J 896 (2):102. https://doi.org/10.3847/1538-4357/ab9308. arXiv:2003.02004 [astro-ph.HE]

Lach F, Callan FP, Bubeck D, Röpke FK, Sim SA, Schrauth M, Ohlmann ST, Kromer M (2022) Type Iax supernovae from deflagrations in Chandrasekhar mass white dwarfs. Astron Astrophys 658:A179. https://doi.org/10.1051/0004-6361/202141453. arXiv:2109.02926 [astro-ph.SR]

Langanke K, Martínez-Pinedo G (2003) Nuclear weak-interaction processes in stars. Rev Mod Phys 75:819–862. https://doi.org/10.1103/RevModPhys.75.819

Langanke K, Martínez-Pinedo G, von Neumann-Cosel P, Richter A (2004) Supernova inelastic neutrino-nucleus cross sections from high-resolution electron scattering experiments and shell-model calculations. Phys Rev Lett 93(20):202501. https://doi.org/10.1103/PhysRevLett.93.202501. arXiv:nucl-th/0402001 [nucl-th]

Langanke K, Martínez-Pinedo G, Müller B, Janka HT, Marek A, Hix WR, Juodagalvis A, Sampaio JM (2008) Effects of inelastic neutrino-nucleus scattering on supernova dynamics and radiated neutrino spectra. Phys Rev Lett 100(1):011101. https://doi.org/10.1103/PhysRevLett.100.011101. arXiv:0706.1687 [astro-ph]

Langanke K, Martínez-Pinedo G, Petermann I, Thielemann FK (2011) Nuclear quests for supernova dynamics and nucleosynthesis. Prog Part Nucl Phys 66(2):319–328. https://doi.org/10.1016/j.ppnp.2011.01.027

Langanke K, Martínez-Pinedo G, Zegers RGT (2021) Electron capture in stars. Rep Progress Phys 84 (6):066301. https://doi.org/10.1088/1361-6633/abf207. arXiv:2009.01750 [nucl-th]

Langer N, Braun H, Fliegner J (1995) The production of circumstellar ^{26}Al by massive stars. Astrophys Space Sci 224(1–2):275–278. https://doi.org/10.1007/BF00667858

Lara JF, Kajino T, Mathews GJ (2006) Inhomogeneous big bang nucleosynthesis revisited. Phys Rev D 73 (8):083501. https://doi.org/10.1103/PhysRevD.73.083501. arXiv:astro-ph/0603817

Lattimer JM, Schramm DN (1974) Black-hole-neutron-star collisions. Astrophys J Lett 192:L145–L147. https://doi.org/10.1086/181612

Lattimer JM, Schramm DN (1976) The tidal disruption of neutron stars by black holes in close binaries. Astrophys J 210:549–567. https://doi.org/10.1086/154860

LeBlanc JM, Wilson JR (1970) A numerical example of the collapse of a rotating magnetized star. Astrophys J 161:541. https://doi.org/10.1086/150558

LeBlanc JM, Wilson JR (1970) A numerical example of the collapse of a rotating magnetized star. Astrophys J 161:541. https://doi.org/10.1086/150558

Lee WH, Ramirez-Ruiz E (2007) The progenitors of short gamma-ray bursts. New J Phys 9:17–17. https://doi.org/10.1088/1367-2630/9/1/017

Lemaître G (1927) Un Univers homogène de masse constante et de rayon croissant rendant compte de la vitesse radiale des nébuleuses extra-galactiques. Ann Soc Sci Bruxelles 47:49–59

Lemaître G (1931) Expansion of the universe, a homogeneous universe of constant mass and increasing radius accounting for the radial velocity of extra-galactic nebulae. MNRAS 91:483–490. https://doi.org/10.1093/mnras/91.5.483

Leung SC, Nomoto K (2018) Explosive nucleosynthesis in near-chandrasekhar-mass white dwarf models for type Ia supernovae: dependence on model parameters. Astrophys J 861(2):143. https://doi.org/10.3847/1538-4357/aac2df. arXiv:1710.04254 [astro-ph.SR]

Leung SC, Nomoto K (2019) Final evolution of super-AGB stars and supernovae triggered by electron capture. Publ Astron Soc Aust 36:e006. https://doi.org/10.1017/pasa.2018.49

Leung SC, Nomoto K, Suzuki T (2020) Electron-capture supernovae of super-AGB stars: sensitivity on input physics. Astrophys J 889(1):34. https://doi.org/10.3847/1538-4357/ab5d2f. arXiv:1901.11438 [astro-ph.HE]

Limongi M, Chieffi A (2003) Evolution, explosion, and nucleosynthesis of core-collapse supernovae. Astrophys J 592(1):404–433. https://doi.org/10.1086/375703. arXiv:astro-ph/0304185 [astro-ph]

Limongi M, Chieffi A (2006) The nucleosynthesis of ^{26}Al and ^{60}Fe in solar metallicity stars extending in mass from 11 to 120 $M_{\odot}$: the hydrostatic and explosive contributions. Astrophys J 647(1):483–500. https://doi.org/10.1086/505164. arXiv:astro-ph/0604297 [astro-ph]

Limongi M, Chieffi A (2018) Presupernova evolution and explosive nucleosynthesis of rotating massive stars in the metallicity range -3 $\leq$ [Fe/H] $\leq$ 0. Astrophys J Suppl 237(1):13. https://doi.org/10.3847/1538-4365/aacb24. arXiv:1805.09640 [astro-ph.SR]

Lippuner J, Roberts LF (2017) SkyNet: a modular nuclear reaction network library. Astrophys J Suppl 233:18. https://doi.org/10.3847/1538-4365/aa94cb

Lippuner J, Fernández R, Roberts LF, Foucart F, Kasen D, Metzger BD, Ott CD (2017) Signatures of hypermassive neutron star lifetimes on r-process nucleosynthesis in the disc ejecta from neutron star mergers. MNRAS 472:904–918. https://doi.org/10.1093/mnras/stx1987

Liu W, Li Z, He J, Tang X, Lian G, Su J, Shen Y, An Z, Chao F, Chang J, Chen L, Chen H, Chen X, Chen Y, Chen Z, Cheng J, Cui B, Fang X, Fu C, Gan L, Guo B, Han Z, Guo X, He G, He J, Heger A, Hou S, Huang H, Huang N, Jia B, Jiang L, Kubono S, Li J, Li M, Li K, Li E, Li T, Li Y, Lugaro M, Luo X, Ma H, Ma S, Mei D, Nan W, Nan W, Qi N, Qian Y, Qin J, Ren J, Shang C, Sun L, Sun W, Tan W, Tanihata I, Wang S, Wang P, Wang Y, Wu Q, Xu S, Yang Y, Yu X, Yue Q, Zeng S, Zhang L, Zhang H, Zhang H, Zhang L, Zhang N, Zhang P, Zhang Q, Zhang T, Zhang X, Zhang X, Zhao W, Zhou J, Zhou Y [JUNA Collaboration] (2022) Commissioning of underground nuclear astrophysics experiment JUNA in China. Eur Phys J Web Conf 260:08001. https://doi.org/10.1051/epjconf/202226008001

Lodders K (2021) Relative atomic solar system abundances, mass fractions, and atomic masses of the elements and their isotopes, composition of the solar photosphere, and compositions of the major chondritic meteorite groups. Space Sci Rev 217(3):44. https://doi.org/10.1007/s11214-021-00825-8

Lugaro M, Chieffi A (2011) Radioactivites in low- and intermediate-mass stars. In: Diehl R, Hartmann DH, Prantzos N (eds) Astronomy with radioactivities. Lecture notes in physics, vol 812. Springer, Berlin Heidelberg, pp 83–152. https://doi.org/10.1007/978-3-642-12698-7_3

Lugaro M, Gallino R (2006) Presolar grains and AGB stars. In: Montmerle T, Kahane C (eds) EAS publications series. EAS Publications Series, vol 19. pp 199–219. https://doi.org/10.1051/eas:2006033

Lund KA, Engel J, McLaughlin GC, Mumpower MR, Ney EM, Surman R (2022) The influence of beta decay rates on r-process observables. arXiv e-prints https://arxiv.org/abs/2208.06373[astro-ph.HE]

Luo Y, Kajino T, Kusakabe M, Mathews GJ (2019) Big bang nucleosynthesis with an inhomogeneous primordial magnetic field strength. Astrophys J 872:172. https://doi.org/10.3847/1538-4357/ab0088. arXiv:1810.08803

Macklin RL, Gibbons JH (1965) Neutron capture data at stellar temperatures. Rev Mod Phys 37:166–176. https://doi.org/10.1103/RevModPhys.37.166

Maeda K, Terada Y (2016) Progenitors of type Ia supernovae. Int J Mod Phys D 25(10):1630024. https://doi.org/10.1142/S021827181630024X. arXiv:1609.03639 [astro-ph.SR]

Maeda K, Röpke FK, Fink M, Hillebrandt W, Travaglio C, Thielemann FK (2010) Nucleosynthesis in two-dimensional delayed detonation models of type Ia supernova explosions. Astrophys J 712(1):624–638. https://doi.org/10.1088/0004-637X/712/1/624. arXiv:1002.2153 [astro-ph.SR]

Maeder A, Meynet G (2012) Rotating massive stars: from first stars to gamma ray bursts. Rev Mod Phys 84(1):25–63. https://doi.org/10.1103/RevModPhys.84.25

Magrini L, Spina L, Randich S, Friel E, Kordopatis G, Worley C, Pancino E, Bragaglia A, Donati P, Tautvaišienė G, Bagdonas V, Delgado-Mena E, Adibekyan V, Sousa SG, Jiménez-Esteban FM, Sanna

N, Roccatagliata V, Bonito R, Sbordone L, Duffau S, Gilmore G, Feltzing S, Jeffries RD, Vallenari A, Alfaro EJ, Bensby T, Francois P, Koposov S, Korn AJ, Recio-Blanco A, Smiljanic R, Bayo A, Carraro G, Casey AR, Costado MT, Damiani F, Franciosini E, Frasca A, Hourihane A, Jofré P, de Laverny P, Lewis J, Masseron T, Monaco L, Morbidelli L, Prisinzano L, Sacco G, Zaggia S (2018) The *Gaia*-ESO Survey: the origin and evolution of s-process elements. Astron Astrophys 617:A106. https://doi.org/10.1051/0004-6361/201832841

Malaney RA, Mathews GJ (1993) Probing the early universe: a review of primordial nucleosynthesis beyond the standard big bang. Phys Rep 229:145–219. https://doi.org/10.1016/0370-1573(93)90134-Y

Maoz D, Mannucci F, Nelemans G (2014) Observational clues to the progenitors of type Ia supernovae. Annu Rev Astron Astrophys 52:107–170. https://doi.org/10.1146/annurev-astro-082812-141031. arXiv:1312.0628 [astro-ph.CO]

Marketin T, Huther L, Martínez-Pinedo G (2016) Large-scale evaluation of β -decay rates of r-process nuclei with the inclusion of first-forbidden transitions. Phys Rev C 93:025805. https://doi.org/10.1103/PhysRevC.93.025805

Martin D, Perego A, Arcones A, Thielemann FK, Korobkin O, Rosswog S (2015) Neutrino-driven winds in the aftermath of a neutron star merger: nucleosynthesis and electromagnetic transients. Astrophys J 813:2. https://doi.org/10.1088/0004-637X/813/1/2

Martínez-Pinedo G, Fischer T, Lohs A, Huther L (2012) Charged-current weak interaction processes in hot and dense matter and its impact on the spectra of neutrinos emitted from protoneutron star cooling. Phys Rev Lett 109:251104. https://doi.org/10.1103/PhysRevLett.109.251104

Martínez-Pinedo G, Fischer T, Langanke K, Lohs A, Sieverding A, Wu MR (2017) Neutrinos and their impact on core-collapse supernova nucleosynthesis. In: Alsabti AW, Murdin P (eds) Handbook of supernovae. Springer, Cham, pp 1–37. https://doi.org/10.1007/978-3-319-20794-0_78-1

Mashonkina L, Christlieb N, Eriksson K (2014) The Hamburg/ESO R-process enhanced star survey (HERES). X. HE 2252-4225, one more r-process enhanced and actinide-boost halo star. Astron Astrophys 569:A43. https://doi.org/10.1051/0004-6361/201424017

Mathews GJ, Kusakabe M, Kajino T (2017) Introduction to big bang nucleosynthesis and modern cosmology. Int J Mod Phys E 26:1741001. https://doi.org/10.1142/S0218301317410014. arXiv:1706.03138

Matteucci F (2012) Chemical Evolution of Galaxies. Springer, Berlin Heidelberg. https://doi.org/10.1007/978-3-642-22491-1

Matteucci F (2021) Modelling the chemical evolution of the Milky Way. Annu Rev Astron Astrophys 29 (1):5. https://doi.org/10.1007/s00159-021-00133-8. arXiv:2106.13145 [astro-ph.GA]

Matteucci F, Greggio L (1986) Relative roles of type I and II supernovae in the chemical enrichment of the interstellar gas. Astron Astrophys 154:279–287

Matteucci F, Romano D, Arcones A, Korobkin O, Rosswog S (2014) Europium production: neutron star mergers versus core-collapse supernovae. MNRAS 438:2177–2185. https://doi.org/10.1093/mnras/stt2350

McCray R, Fransson C (2016) The remnant of supernova 1987A. Annu Rev Astron Astrophys 54:19–52. https://doi.org/10.1146/annurev-astro-082615-105405

McDonald AB (2004) Solar neutrinos. New J Phys 6(1):121. https://doi.org/10.1088/1367-2630/6/1/121. arXiv:astro-ph/0406253 [astro-ph]

McKinney JC, Tchekhovskoy A, Blandford RD (2013) Alignment of magnetized accretion disks and relativistic jets with spinning black holes. Science 339:49. https://doi.org/10.1126/science.1230811

McKinney JC, Tchekhovskoy A, Sadowski A, Narayan R (2014) Three-dimensional general relativistic radiation magnetohydrodynamical simulation of super-Eddington accretion, using a new code HARMRAD with M1 closure. MNRAS 441(4):3177–3208. https://doi.org/10.1093/mnras/stu762. arXiv:1312.6127 [astro-ph.CO]

McLaughlin GC, Surman R (2005) Prospects for obtaining an r process from gamma ray burst disk winds. Nucl Phys A 758:189–196. https://doi.org/10.1016/j.nuclphysa.2005.05.036.. arXiv:astro-ph/0407555 [astro-ph]

Meisel Z, George S, Ahn S, Bazin D, Brown BA, Browne J, Carpino JF, Chung H, Cyburt RH, Estradé A, Famiano M, Gade A, Langer C, Matoš M, Mittig W, Montes F, Morrissey DJ, Pereira J, Schatz H, Schatz J, Scott M, Shapira D, Smith K, Stevens J, Tan W, Tarasov O, Towers S, Wimmer K, Winkelbauer JR, Yurkon J, Zegers RGT (2020) Nuclear mass measurements map the structure of atomic nuclei and accreting neutron stars. Phys Rev C 101(5):052801. https://doi.org/10.1103/PhysRevC.101.052801. arXiv:2004.14101 [nucl-ex]

Mendoza-Temis JJ, Wu MR, Langanke K, Martínez-Pinedo G, Bauswein A, Janka HT (2015) Nuclear robustness of the *r* process in neutron-star mergers. Phys Rev C 92:055805. https://doi.org/10.1103/PhysRevC.92.055805

Metzger BD (2019) Kilonovae. Living Rev Relativ 23:1. https://doi.org/10.1007/s41114-019-0024-0

Metzger BD, Martínez-Pinedo G, Darbha S, Quataert E, Arcones A, Kasen D, Thomas R, Nugent P, Panov IV, Zinner NT (2010) Electromagnetic counterparts of compact object mergers powered by the radioactive decay of r-process nuclei. MNRAS 406:2650–2662. https://doi.org/10.1111/j.1365-2966.2010.16864.x

Meynet G, Arnould M, Prantzos N, Paulus G (1997) Contribution of wolf-rayet stars to the synthesis of ^{26}Al. I. The γ-ray connection. Astron Astrophys 320:460–468

Miller JM, Ryan BR, Dolence JC, Burrows A, Fontes CJ, Fryer CL, Korobkin O, Lippuner J, Mumpower MR, Wollaeger RT (2019) Full transport model of GW170817-like disk produces a blue kilonova. Phys Rev D 100(2):023008. https://doi.org/10.1103/PhysRevD.100.023008. arXiv:1905.07477 [astro-ph.HE]

Miller JM, Sprouse TM, Fryer CL, Ryan BR, Dolence JC, Mumpower MR, Surman R (2020) Full transport general relativistic radiation magnetohydrodynamics for nucleosynthesis in collapsars. Astrophys J 902(1):66. https://doi.org/10.3847/1538-4357/abb4e3. arXiv:1912.03378 [astro-ph.HE]

Mirizzi A, Tamborra I, Janka HT, Saviano N, Scholberg K, Bollig R, Hudepohl L, Chakraborty S (2016) Supernova neutrinos: production. Oscillations and detection. Riv Nuovo Cim 39(1–2):1. https://doi.org/10.1393/ncr/i2016-10120-8. arXiv:1508.00785 [astro-ph.HE]

Mishenina T, Gorbaneva T, Pignatari M, Thielemann FK, Korotin SA (2015) Mn abundances in the stars of the Galactic disc with metallicities $-1.0<$[Fe/H] <0.3. MNRAS 454(2):1585–1594. https://doi.org/10.1093/mnras/stv2038. arXiv:1509.05341 [astro-ph.GA]

Moghadasi A (2021) Study of ^{12}C+^{12}C reaction using the new optimized potential. New Astron 89:101649. https://doi.org/10.1016/j.newast.2021.101649

Mohr P, Fülöp Z, Gyürky G, Kiss GG, Szücs T (2020) Successful prediction of total α-induced reaction cross sections at astrophysically relevant sub-coulomb energies using a novel approach. Phys Rev Lett 124(25):252701. https://doi.org/10.1103/PhysRevLett.124.252701. arXiv:2006.03885 [nucl-th]

Möller P, Nix JR, Kratz KL (1997) Nuclear properties for astrophysical and radioactive-ion beam applications. At Data Nucl Data Tables 66:131–343. https://doi.org/10.1006/adnd.1997.0746

Möller P, Sierk AJ, Ichikawa T, Sagawa H (2016) Nuclear ground-state masses and deformations: FRDM (2012). At Data Nucl Data Tables 109:1–204. https://doi.org/10.1016/j.adt.2015.10.002

Montes F, Beers TC, Cowan J, Elliot T, Farouqi K, Gallino R, Heil M, Kratz K, Pfeiffer B, Pignatari M, Schatz H (2007) Nucleosynthesis in the early galaxy. Astrophys J 671:1685–1695. https://doi.org/10.1086/523084. arXiv:0709.0417

Moscoso J, de Souza RS, Coc A, Iliadis C (2021) Bayesian estimation of the D(p,γ)^{3}He thermonuclear reaction rate. Astrophys J 923(1):49. https://doi.org/10.3847/1538-4357/ac1db0. arXiv:2109.00049 [astro-ph.CO]

Mossa V, Stöckel K, Cavanna F, Ferraro F, Aliotta M, Barile F, Bemmerer D, Best A, Boeltzig A, Broggini C, Bruno CG, Caciolli A, Chillery T, Ciani GF, Corvisiero P, Csedreki L, Davinson T, Depalo R, Di Leva A, Elekes Z, Fiore EM, Formicola A, Fülöp Z, Gervino G, Guglielmetti A, Gustavino C, Gyürky G, Imbriani G, Junker M, Kievsky A, Kochanek I, Lugaro M, Marcucci LE, Mangano G, Marigo P, Masha E, Menegazzo R, Pantaleo FR, Paticchio V, Perrino R, Piatti D, Pisanti O, Prati P, Schiavulli L, Straniero O, Szücs T, Takács MP, Trezzi D, Viviani M, Zavatarelli S (2020) The baryon density of the Universe from an improved rate of deuterium burning. Nature 587(7833):210–213. https://doi.org/10.1038/s41586-020-2878-4

Mösta P, Richers S, Ott CD, Haas R, Piro AL, Boydstun K, Abdikamalov E, Reisswig C, Schnetter E (2014) Magnetorotational core-collapse supernovae in three dimensions. Astrophys J Lett 785:L29. https://doi.org/10.1088/2041-8205/785/2/L29. arXiv:1403.1230 [astro-ph.HE]

Mösta P, Roberts LF, Halevi G, Ott CD, Lippuner J, Haas R, Schnetter E (2018) r-process nucleosynthesis from three-dimensional magnetorotational core-collapse supernovae. Astrophys J 864:171. https://doi.org/10.3847/1538-4357/aad6ec

Mösta P, Radice D, Haas R, Schnetter E, Bernuzzi S (2020) A magnetar engine for short GRBs and kilonovae. Astrophys J Lett 901(2):L37. https://doi.org/10.3847/2041-8213/abb6ef. arXiv:2003.06043 [astro-ph.HE]

Mueller E, Arnett WD (1986) Carbon combustion supernovae: numerical studies of the final evolution of degenerate carbon-oxygen cores. Astrophys J 307:619. https://doi.org/10.1086/164448

Müller B (2016) The status of multi-dimensional core-collapse supernova models. Publ Astron Soc Aust 33:e048. https://doi.org/10.1017/pasa.2016.40

Müller B (2020) Hydrodynamics of core-collapse supernovae and their progenitors. Living Rev Comput Astrophys 6:3. https://doi.org/10.1007/s41115-020-0008-5. arXiv:2006.05083 [astro-ph.SR]

Murguia-Berthier A, Ramirez-Ruiz E, Montes G, De Colle F, Rezzolla L, Rosswog S, Takami K, Perego A, Lee WH (2017) The properties of short gamma-ray burst jets triggered by neutron star mergers. Astrophys J Lett 835(2):L34. https://doi.org/10.3847/2041-8213/aa5b9e. arXiv:1609.04828 [astro-ph.HE]

Nakamura T, Umeda H, Iwamoto K, Nomoto K, Hashimoto Ma, Hix WR, Thielemann FK (2001) Explosive nucleosynthesis in hypernovae. Astrophys J 555:880–899. https://doi.org/10.1086/321495

Nishimura S, Kotake K, Hashimoto Ma, Yamada S, Nishimura N, Fujimoto S, Sato K (2006) r-Process nucleosynthesis in magnetohydrodynamic jet explosions of core-collapse supernovae. Astrophys J 642:410–419. https://doi.org/10.1086/500786.astroph/0504100

Nishimura N, Takiwaki T, Thielemann FK (2015) The r-process nucleosynthesis in the various jet-like explosions of magnetorotational core-collapse supernovae. Astrophys J 810:109. https://doi.org/10.1088/0004-637X/810/2/109

Nishimura N, Sawai H, Takiwaki T, Yamada S, Thielemann FK (2017) The intermediate r-process in core-collapse supernovae driven by the magneto-rotational instability. Astrophys J 836:L21. https://doi.org/10.3847/2041-8213/aa5dee

Nishimura N, Rauscher T, Hirschi R, Murphy ASJ, Cescutti G, Travaglio C (2018) Uncertainties in the production of p nuclides in thermonuclear supernovae determined by Monte Carlo variations. MNRAS 474(3):3133–3139. https://doi.org/10.1093/mnras/stx3033. arXiv:1711.09098 [astro-ph.SR]

Nittler LR, Ciesla F (2016) Astrophysics with extraterrestrial materials. Annu Rev Astron Astrophys 54:53–93. https://doi.org/10.1146/annurev-astro-082214-122505

Nittler LR, Amari S, Zinner E, Woosley SE, Lewis RS (1996) Extinct ^{44}Ti in presolar graphite and SiC: proof of a supernova origin. Astrophys J Lett 462:L31. https://doi.org/10.1086/310021

Noebauer UM, Kromer M, Taubenberger S, Baklanov P, Blinnikov S, Sorokina E, Hillebrandt W (2017) Early light curves for Type Ia supernova explosion models. MNRAS 472(3):2787–2799. https://doi.org/10.1093/mnras/stx2093. arXiv:1706.03613 [astro-ph.HE]

Nomoto K (1982) Accreting white dwarf models for type I supernovae. I-Presupernova evolution and triggering mechanisms. Astrophys J 253:798–810. https://doi.org/10.1086/159682

Nomoto K, Kondo Y (1991) Conditions for accretion-induced collapse of white dwarfs. Astrophys J Lett 367:L19. https://doi.org/10.1086/185922

Nomoto K, Thielemann FK, Yokoi K (1984) Accreting white dwarf models for type I supern. III. Carbon deflagration supernovae. Astrophys J 286:644–658. https://doi.org/10.1086/162639

Nomoto K, Thielemann FK, Miyaji S (1985) The triple alpha reaction at low temperatures in accreting white dwarfs and neutron stars. Astron Astrophys 149(2):239–245

Nomoto K, Tominaga N, Umeda H, Kobayashi C, Maeda K (2006) Nucleosynthesis yields of core-collapse supernovae and hypernovae, and galactic chemical evolution. Nucl Phys A 777:424–458. https://doi.org/10.1016/j.nuclphysa.2006.05.008

Nomoto K, Tanaka M, Tominaga N, Maeda K (2010) Hypernovae, gamma-ray bursts, and first stars. New Astron Rev 54(3–6):191–200. https://doi.org/10.1016/j.newar.2010.09.022

Nomoto K, Kobayashi C, Tominaga N (2013) Nucleosynthesis in stars and the chemical enrichment of galaxies. Annu Rev Astron Astrophys 51:457–509. https://doi.org/10.1146/annurev-astro-082812-140956

Obergaulinger M, Aloy MÁ (2017) Protomagnetar and black hole formation in high-mass stars. MNRAS 469:L43–L47. https://doi.org/10.1093/mnrasl/slx046. arXiv:1703.09893 [astro-ph.SR]

Obergaulinger M, Aloy MÁ (2021) Magnetorotational core collapse of possible GRB progenitors–III. Three-dimensional models. MNRAS 503(4):4942–4963. https://doi.org/10.1093/mnras/stab295. arXiv:2008.07205 [astro-ph.HE]

Obergaulinger M, Cerdá-Durán P, Müller E, Aloy MA (2009) Semi-global simulations of the magneto-rotational instability in core collapse supernovae. Astron Astrophys 498(1):241–271. https://doi.org/10.1051/0004-6361/200811323. arXiv:0811.1652 [astro-ph]

Obergaulinger M, Janka HT, Aloy MA (2014) Magnetic field amplification and magnetically supported explosions of collapsing, non-rotating stellar cores. MNRAS 445:3169–3199. https://doi.org/10.1093/mnras/stu1969. arXiv:1405.7466 [astro-ph.SR]

O'Connor E, Ott CD (2011) Black hole formation in failing core-collapse supernovae. Astrophys J 730 (2):70. https://doi.org/10.1088/0004-637X/730/2/70. arXiv:1010.5550 [astro-ph.HE]
Olive KA, Schramm DN, Steigman G, Walker TP (1990) Big-bang nucleosynthesis revisited. Phys Rev B 236:454–460. https://doi.org/10.1016/0370-2693(90)90382-G
Otsuki K, Tagoshi H, Kajino T, Sy Wanajo (2000) General relativistic effects on neutrino-driven winds from young, hot neutron stars and r-process nucleosynthesis. Astrophys J 533(1):424–439. https://doi.org/10.1086/308632. arXiv:astro-ph/9911164 [astro-ph]
Pagel BEJ (2009) Nucleosynthesis and chemical evolution of galaxies, 2nd edn. Cambridge University Press, Cambridge. https://doi.org/10.1017/CBO9780511812170
Pakmor R, Kromer M, Taubenberger S, Springel V (2013) Helium-ignited violent mergers as a unified model for normal and rapidly declining type Ia supernovae. Astrophys J Lett 770(1):L8. https://doi.org/10.1088/2041-8205/770/1/L8. arXiv:1302.2913 [astro-ph.HE]
Palacios A, Meynet G, Vuissoz C, Knödlseder J, Schaerer D, Cerviño M, Mowlavi N (2005) New estimates of the contribution of Wolf–Rayet stellar winds to the Galactic ^{26}Al. Astron Astrophys 429:613–624. https://doi.org/10.1051/0004-6361:20041757.. arXiv:astro-ph/0409580 [astro-ph]
Palla M (2021) The effects of different Type Ia SN yields on Milky Way chemical evolution. MNRAS 503 (3):3216–3231. https://doi.org/10.1093/mnras/stab293. arXiv:2101.12679 [astro-ph.GA]
Panov IV, Korneev IY, Rauscher T, Martínez-Pinedo G, Kelic-Heil A, Zinner NT, Thielemann F (2010) Neutron-induced astrophysical reaction rates for translead nuclei. Astron Astrophys 513:A61. https://doi.org/10.1051/0004-6361/200911967
Peebles PJE (1966) Primordial helium abundance and the primordial fireball. II. Astrophys J 146:542. https://doi.org/10.1086/148918
Peebles PJE (1993) Principles of physical cosmology. Princeton University Press, Princeton
Perego A, Thielemann FK, Cescutti G (2021) *r*-process nucleosynthesis from compact binary mergers. In: Bambi C, Katsanevas S, Kokkotas KD (eds) Handbook of gravitational wave astronomy. Springer, Singapore. https://doi.org/10.1007/978-981-15-4702-7_13-1
Perlmutter S (2012) Nobel lecture: measuring the acceleration of the cosmic expansion using supernovae. Rev Mod Phys 84(3):1127–1149. https://doi.org/10.1103/RevModPhys.84.1127
Pfeiffer B, Kratz KL, Thielemann FK, Walters WB (2001) Nuclear structure studies for the astrophysical r-process. Nucl Phys A 693:282–324
Pignatari M, Göbel K, Reifarth R, Travaglio C (2016) The production of proton-rich isotopes beyond iron: the γ-process in stars. Int J Mod Phys E 25(4):1630003–232. https://doi.org/10.1142/S0218301316300034. arXiv:1605.03690 [astro-ph.SR]
Pisanti O, Mangano G, Miele G (2021) Mazzella P (2021) Primordial Deuterium after LUNA: concordances and error budget. J Cosmol Astropart Phys 4:020. https://doi.org/10.1088/1475-7516/2021/04/020. arXiv:2011.11537 [astro-ph.CO]
Pitrou C, Coc A, Uzan JP, Vangioni E (2018) Precision big bang nucleosynthesis with improved Helium-4 predictions. Phys Rep 754:1–66. https://doi.org/10.1016/j.physrep.2018.04.005.. arXiv:1801.08023
Pitrou C, Coc A, Uzan JP, Vangioni E (2021) A new tension in the cosmological model from primordial deuterium? MNRAS 502(2):2474–2481. https://doi.org/10.1093/mnras/stab135. arXiv:2011.11320 [astro-ph.CO]
Planck Collaboration, Aghanim N et al (2020) Planck 2018 results. VI. Cosmological parameters. Astron Astrophys 641:A6. https://doi.org/10.1051/0004-6361/201833910. arXiv:1807.06209 [astro-ph.CO]
Planck Collaboration, Aghanim N, et al (2021) Planck 2018 results. VI. Cosmological parameters (Corrigendum). Astron Astrophys 652:C4. https://doi.org/10.1051/0004-6361/201833910e
Prantzos N (2012) Production and evolution of Li, Be, and B isotopes in the galaxy. Astron Astrophys 542: A67. https://doi.org/10.1051/0004-6361/201219043. arXiv:1203.5662
Prantzos N, Abia C, Limongi M, Chieffi A, Cristallo S (2018) Chemical evolution with rotating massive star yields - I. The solar neighbourhood and the s-process elements. MNRAS 476(3):3432–3459. https://doi.org/10.1093/mnras/sty316. arXiv:1802.02824 [astro-ph.GA]
Prantzos N, Abia C, Cristallo S, Limongi M, Chieffi A (2020) Chemical evolution with rotating massive star yields II. A new assessment of the solar s- and r-process components. MNRAS 491(2):1832–1850. https://doi.org/10.1093/mnras/stz3154. arXiv:1911.02545 [astro-ph.GA]
Pruet J, Hoffman RD, Woosley SE, Janka HT, Buras R (2006) Nucleosynthesis in early supernova winds. II. The role of neutrinos. Astrophys J 644:1028–1039. https://doi.org/10.1086/503891
Qian Y, Wasserburg GJ (2007) Where, oh where has the r-process gone? Phys Rep 442:237–268. https://doi.org/10.1016/j.physrep.2007.02.006

Qian YZ, Woosley SE (1996) Nucleosynthesis in neutrino-driven winds. I. The physical conditions. Astrophys J 471:331–351. https://doi.org/10.1086/177973
Radice D, Galeazzi F, Lippuner J, Roberts LF, Ott CD, Rezzolla L (2016) Dynamical mass ejection from binary neutron star mergers. MNRAS 460:3255–3271. https://doi.org/10.1093/mnras/stw1227
Radice D, Abdikamalov E, Ott CD, Mösta P, Couch SM, Roberts LF (2018) Turbulence in core-collapse supernovae. J Phys G 45(5):053003. https://doi.org/10.1088/1361-6471/aab872. arXiv:1710.01282 [astro-ph.HE]
Rapp W, Görres J, Wiescher M, Schatz H, Käppeler F (2006) Sensitivity of p-process nucleosynthesis to nuclear reaction rates in a 25 $M_{\odot}$ supernova model. Astrophys J 653(1):474–489. https://doi.org/10.1086/508402.. arXiv:astro-ph/0608341 [astro-ph]
Raskin C, Timmes FX, Scannapieco E, Diehl S, Fryer C (2009) On Type Ia supernovae from the collisions of two white dwarfs. MNRAS 399(1):L156–L159. https://doi.org/10.1111/j.1745-3933.2009.00743.x. arXiv:0907.3915 [astro-ph.SR]
Rauscher T (2006) Branchings in the γ process path revisited. Phys Rev C 73(1):015804. https://doi.org/10.1103/PhysRevC.73.015804.. arXiv:astro-ph/0510710 [astro-ph]
Rauscher T (2011) The path to improved reaction rates for astrophysics. Int J Mod Phys E 20:1071–1169. https://doi.org/10.1142/S021830131101840X
Rauscher T, Thielemann FK (2000) Astrophysical reaction rates from statistical model calculations. At Data Nucl Data Tables 75:1–351. https://doi.org/10.1006/adnd.2000.0834
Rauscher T, Applegate JH, Cowan JJ, Thielemann FK, Wiescher M (1994) Production of heavy elements in inhomogeneous cosmologies. Astrophys J 429:499–530. https://doi.org/10.1086/174339
Rauscher T, Heger A, Hoffman RD, Woosley SE (2002) Nucleosynthesis in massive stars with improved nuclear and stellar physics. Astrophys J 576(1):323–348. https://doi.org/10.1086/341728. arXiv:astro-ph/0112478 [astro-ph]
Rauscher T, Dauphas N, Dillmann I, Fröhlich C, Fülöp Z, Gyürky G (2013) Constraining the astrophysical origin of the p-nuclei through nuclear physics and meteoritic data. Rep Progress Phys 76(6):066201. https://doi.org/10.1088/0034-4885/76/6/066201. arXiv:1303.2666 [astro-ph.SR]
Rauscher T, Nishimura N, Hirschi R, Cescutti G, Murphy ASJ, Heger A (2016) Uncertainties in the production of p nuclei in massive stars obtained from Monte Carlo variations. MNRAS 463(4):4153–4166. https://doi.org/10.1093/mnras/stw2266. arXiv:1606.05671 [astro-ph.HE]
Rayet M, Arnould M, Prantzos N (1990) The p-process revisited. Astron Astrophys 227(1):271–281
Rayet M, Arnould M, Hashimoto M, Prantzos N, Nomoto K (1995) The p-process in Type II supernovae. Astron Astrophys 298:517
Reeves H (1991) Big-bang nucleosynthesis and the quark-hadron phase transition. Phys Rep 201:335–354. https://doi.org/10.1016/0370-1573(91)90133-7
Reichert M, Obergaulinger M, Eichler M, Aloy MÁ, Arcones A (2021) Nucleosynthesis in magneto-rotational supernovae. MNRAS 501(4):5733–5745. https://doi.org/10.1093/mnras/stab029. arXiv:2010.02227 [astro-ph.HE]
Reichert M, Obergaulinger M, Aloy MÃ, Gabler M, Arcones A, Thielemann FK (2022) Magnetoro-tational supernovae: a nucleosynthetic analysis of sophisticated 3D models. Mon Not R Astron Soc. https://doi.org/10.1093/mnras/stac3185
Reifarth R, Lederer C, Käppeler F (2014) Neutron reactions in astrophysics. J Phys G 41:053101. https://doi.org/10.1088/0954-3899/41/5/053101
Rembges F, Freiburghaus C, Rauscher T, Thielemann FK, Schatz H, Wiescher M (1997) An approximation for the rp-process. Astrophys J 484(1):412–423. https://doi.org/10.1086/304300.. arXiv:astro-ph/9701217 [astro-ph]
Riess AG (2012) Nobel lecture: my path to the accelerating universe. Rev Mod Phys 84(3):1165–1175. https://doi.org/10.1103/RevModPhys.84.1165
Riess AG, Casertano S, Yuan W, Bowers JB, Macri L, Zinn JC, Scolnic D (2021) Cosmic distances calibrated to 1% precision with Gaia EDR3 parallaxes and Hubble Space Telescope photometry of 75 Milky Way Cepheids confirm tension with ΛCDM. Astrophys J Lett 908(1):L6. https://doi.org/10.3847/2041-8213/abdbaf. arXiv:2012.08534 [astro-ph.CO]
Roberts LF, Reddy S, Shen G (2012) Medium modification of the charged-current neutrino opacity and its implications. Phys Rev C 86(6):065803. https://doi.org/10.1103/PhysRevC.86.065803. arXiv:1205.4066 [astro-ph.HE]
Roederer IU (2017) The origin of the heaviest metals in most ultra-faint dwarf galaxies. Astrophys J 835:23. https://doi.org/10.3847/1538-4357/835/1/23

Roederer IU, Kratz KL, Frebel A, Christlieb N, Pfeiffer B, Cowan JJ, Sneden C (2009) The end of nucleosynthesis: production of lead and thorium in the early galaxy. Astrophys J 698:1963–1980. https://doi.org/10.1088/0004-637X/698/2/1963

Roederer IU, Sneden C, Lawler JE, Cowan JJ (2010) New abundance determinations of cadmium, lutetium, and osmium in the r-process enriched star BD +17 3248. Astrophys J 714:L123–L127. https://doi.org/10.1088/2041-8205/714/1/L123

Rolfs C, Rodney W (1988) Cauldrons in the cosmos: nuclear astrophysics. University of Chicago Press, Chicago

Romano D, Matteucci F, Ventura P, D'Antona F (2001) The stellar origin of ^{7}Li. Do AGB stars contribute a substantial fraction of the local Galactic lithium abundance? Astron Astrophys 374:646–655. https://doi.org/10.1051/0004-6361:20010751.. arXiv:astro-ph/0105483 [astro-ph]

Röpke FK, Sim SA (2018) Models for Type Ia supernovae and related astrophysical transients. Space Sci Rev 214(4):72. https://doi.org/10.1007/s11214-018-0503-8. arXiv:1805.07268 [astro-ph.SR]

Röpke FK, Kromer M, Seitenzahl IR, Pakmor R, Sim SA, Taubenberger S, Ciaraldi-Schoolmann F, Hillebrandt W, Aldering G, Antilogus P, Baltay C, Benitez-Herrera S, Bongard S, Buton C, Canto A, Cellier-Holzem F, Childress M, Chotard N, Copin Y, Fakhouri HK, Fink M, Fouchez D, Gangler E, Guy J, Hachinger S, Hsiao EY, Chen J, Kerschhaggl M, Kowalski M, Nugent P, Paech K, Pain R, Pecontal E, Pereira R, Perlmutter S, Rabinowitz D, Rigault M, Runge K, Saunders C, Smadja G, Suzuki N, Tao C, Thomas RC, Tilquin A, Wu C (2012) Constraining type Ia supernova models: SN 2011fe as a test case. Astrophys J Lett 750(1):L19. https://doi.org/10.1088/2041-8205/750/1/L19. arXiv:1203.4839 [astro-ph.SR]

Rosswog S, Liebendörfer M, Thielemann FK, Davies MB, Benz W, Piran T (1999) Mass ejection in neutron star mergers. Astron Astrophys 341:499–526

Rosswog S, Kasen D, Guillochon J, Ramirez-Ruiz E (2009) Collisions of white dwarfs as a new progenitor channel for type Ia supernovae. Astrophys J Lett 705(2):L128–L132. https://doi.org/10.1088/0004-637X/705/2/L128. arXiv:0907.3196 [astro-ph.HE]

Rosswog S, Feindt U, Korobkin O, Wu MR, Sollerman J, Goobar A, Martínez-Pinedo G (2017) Detectability of compact binary merger macronovae. Class Quantum Grav 34:104001. https://doi.org/10.1088/1361-6382/aa68a9

Rosswog S, Sollerman J, Feindt U, Goobar A, Korobkin O, Wollaeger R, Fremling C, Kasliwal MM (2018) The first direct double neutron star merger detection: implications for cosmic nucleosynthesis. Astron Astrophys 615:A132. https://doi.org/10.1051/0004-6361/201732117

Ruiter AJ, Ferrario L, Belczynski K, Seitenzahl IR, Crocker RM, Karakas AI (2019) On the formation of neutron stars via accretion-induced collapse in binaries. MNRAS 484(1):698–711. https://doi.org/10.1093/mnras/stz001. arXiv:1802.02437 [astro-ph.SR]

Ruiz M, Lang RN, Paschalidis V, Shapiro SL (2016) Binary neutron star mergers: a jet engine for short gamma-ray bursts. Astrophys J Lett 824(1):L6. https://doi.org/10.3847/2041-8205/824/1/L6. arXiv:1604.02455 [astro-ph.HE]

Ruiz M, Tsokaros A, Paschalidis V, Shapiro SL (2019) Effects of spin on magnetized binary neutron star mergers and jet launching. Phys Rev D 99(8):084032. https://doi.org/10.1103/PhysRevD.99.084032. arXiv:1902.08636 [astro-ph.HE]

Sakari CM et al (2018) The R-process alliance: first release from the northern search for r-process-enhanced metal-poor stars in the galactic halo. Astrophys J 868:110. https://doi.org/10.3847/1538-4357/aae9df

Salpeter EE (1955) The luminosity function and stellar evolution. Astrophys J 121:161. https://doi.org/10.1086/145971

Sanders RH (1967) S-process nucleosynthesis in thermal relaxation cycles. Astrophys J 150:971. https://doi.org/10.1086/149397

Sbordone L, Bonifacio P, Caffau E, Ludwig HG, Behara NT, González Hernández JI, Steffen M, Cayrel R, Freytag B, van't Veer C, Molaro P, Plez B, Sivarani T, Spite M, Spite F, Beers TC, Christlieb N, François P, Hill V (2010) The metal-poor end of the Spite plateau. I. Stellar parameters, metallicities, and lithium abundances. Astron Astrophys 522:A26. https://doi.org/10.1051/0004-6361/200913282. arXiv:1003.4510

Schatz H, Aprahamian A, Goerres J, Wiescher M, Rauscher T, Rembges JF, Thielemann FK, Pfeiffer B, Moeller P, Kratz KL, Herndl H, Brown BA, Rebel H (1998) rp-Process nucleosynthesis at extreme temperature and density conditions. Phys Rep 294:167–264. https://doi.org/10.1016/S0370-1573(97)00048-3

Schatz H, Toenjes R, Pfeiffer B, Beers TC, Cowan JJ, Hill V, Kratz KL (2002) Thorium and uranium chronometers applied to CS 31082–001. Astrophys J 579:626–638. https://doi.org/10.1086/342939

Seeger PA, Fowler WA, Clayton DD (1965) Nucleosynthesis of heavy elements by neutron capture. Astrophys J Suppl 11:121. https://doi.org/10.1086/190111

Seitenzahl IR, Townsley DM (2017) Nucleosynthesis in thermonuclear supernovae. In: Alsabti AW, Murdin P (eds) Handbook of supernovae. Springer, Cham, p 1955. https://doi.org/10.1007/978-3-319-21846-5_87

Seitenzahl IR, Ghavamian P, Laming JM, Vogt FPA (2019) Optical tomography of chemical elements synthesized in type Ia supernovae. Phys Rev Lett 123(4):041101. https://doi.org/10.1103/PhysRevLett.123.041101. arXiv:1906.05972 [astro-ph.SR]

Shen KJ, Boubert D, Gänsicke BT, Jha SW, Andrews JE, Chomiuk L, Foley RJ, Fraser M, Gromadzki M, Guillochon J, Kotze MM, Maguire K, Siebert MR, Smith N, Strader J, Badenes C, Kerzendorf WE, Koester D, Kromer M, Miles B, Pakmor R, Schwab J, Toloza O, Toonen S, Townsley DM, Williams BJ (2018) Three hypervelocity white dwarfs in Gaia DR2: evidence for dynamically driven double-degenerate double-detonation type Ia supernovae. Astrophys J 865(1):15. https://doi.org/10.3847/1538-4357/aad55b. arXiv:1804.11163 [astro-ph.SR]

Shibagaki S, Kajino T, Mathews GJ, Chiba S, Nishimura S, Lorusso G (2016) Relative contributions of the weak, main, and fission-recycling r-process. Astrophys J 816:79. https://doi.org/10.3847/0004-637X/816/2/79

Shibata M, Hotokezaka K (2019) Merger and mass ejection of neutron star binaries. Annu Rev Nucl Part Sci 69:41–64. https://doi.org/10.1146/annurev-nucl-101918-023625

Shibata M, Fujibayashi S, Sekiguchi Y (2021) Long-term evolution of neutron-star merger remnants in general relativistic resistive magnetohydrodynamics with a mean-field dynamo term. Phys Rev D 104 (6):063026. https://doi.org/10.1103/PhysRevD.104.063026. arXiv:2109.08732 [astro-ph.HE]

Siegel DM (2019) GW170817-the first observed neutron star merger and its kilonova: implications for the astrophysical site of the r-process. Eur Phys J A 55(11):203. https://doi.org/10.1140/epja/i2019-12888-9. arXiv:1901.09044 [astro-ph.HE]

Siegel DM (2022) r-Process nucleosynthesis in gravitational-wave and other explosive astrophysical events. Nat Rev Phys 2522–5820. https://doi.org/10.1038/s42254-022-00439-1

Siegel DM, Metzger BD (2017) Three-dimensional general-relativistic magnetohydrodynamic simulations of remnant accretion disks from neutron star mergers: outflows and *r*-process nucleosynthesis. Phys Rev Lett 119:231102. https://doi.org/10.1103/PhysRevLett.119.231102

Siegel DM, Metzger BD (2018) Three-dimensional GRMHD simulations of neutrino-cooled accretion disks from neutron star mergers. Astrophys J 858:52. https://doi.org/10.3847/1538-4357/aabaec

Siegel DM, Barnes J, Metzger BD (2019) Collapsars as a major source of r-process elements. Nature 569:241–244. https://doi.org/10.1038/s41586-019-1136-0

Sieverding A, Langanke K, Martínez-Pinedo G, Bollig R, Janka HT, Heger A (2019) The *ν*-process with fully time-dependent supernova neutrino emission spectra. Astrophys J 876(2):151. https://doi.org/10.3847/1538-4357/ab17e2. arXiv:1902.06643 [astro-ph.HE]

Smith MS, Kawano LH, Malaney RA (1993) Experimental, computational, and observational analysis of primordial nucleosynthesis. Astrophys J Suppl 85:219–247. https://doi.org/10.1086/191763

Sneden C, Cowan JJ, Gallino R (2008) Neutron-capture elements in the early galaxy. Annu Rev Astron Astrophys 46:241–288. https://doi.org/10.1146/annurev.astro.46.060407.145207

Suda T, Katsuta Y, Yamada S, Suwa T, Ishizuka C, Komiya Y, Sorai K, Aikawa M, Fujimoto MY (2008) Stellar abundances for the galactic archeology (SAGA) database–compilation of the characteristics of known extremely metal-poor stars. Publ Astron Soc Jpn 60:1159. https://doi.org/10.1093/pasj/60.5.1159

Sukhbold T, Ertl T, Woosley SE, Brown JM, Janka HT (2016) Core-collapse supernovae from 9 to 120 solar masses based on neutrino-powered explosions. Astrophys J 821:38. https://doi.org/10.3847/0004-637X/821/1/38

Surman R, McLaughlin GC (2004) Neutrinos and nucleosynthesis in gamma-ray burst accretion disks. Astrophys J 603(2):611–623. https://doi.org/10.1086/381672.. arXiv:astro-ph/0308004 [astro-ph]

Surman R, McLaughlin GC, Hix WR (2006) Nucleosynthesis in the outflow from gamma-ray burst accretion disks. Astrophys J 643(2):1057–1064. https://doi.org/10.1086/501116. arXiv:astro-ph/0509365 [astro-ph]

Takahashi K, Witti J, Janka HT (1994) Nucleosynthesis in neutrino-driven winds from protoneutron stars II. The r-process. Astron Astrophys 286:857–869

Takiwaki T, Kotake K, Sato K (2009) Special relativistic simulations of magnetically dominated jets in collapsing massive stars. Astrophys J 691(2):1360–1379. https://doi.org/10.1088/0004-637X/691/2/1360. arXiv:0712.1949 [astro-ph]

Talbot J, Raymond J, Arnett WD (1971) The evolution of galaxies. I. Formulation and mathematical behavior of the one-zone model. Astrophys J 170:409. https://doi.org/10.1086/151228

Thielemann FK, Applegate JH, Cowan JJ, Wiescher M (1991) Production of heavy elements in inhomogeneous cosmologies. In: Oberhummer H (ed) Nuclei in the cosmos. Graduate texts in contemporary physics. Springer, Berlin, Heidelberg, pp 147–177. https://doi.org/10.1007/978-3-642-48840-5_8

Thielemann FK, Diehl R, Heger A, Hirschi R, Liebendoerfer M (2018a) Massive stars and their supernovae. In: Diehl R, Hartmann DH, Prantzos N (eds) Astrophysics with radioactive isotopes. Astrophysics and space science library, vol 453. Springer, Cham, pp 173–286. https://doi.org/10.1007/978-3-319-91929-4_4

Thielemann FK, Isern J, Perego A, von Ballmoos P (2018) Nucleosynthesis in supernovae. Space Sci Rev 214(3):62. https://doi.org/10.1007/s11214-018-0494-5

Thielemann FK, Nomoto K, Yokoi K (1986) Explosive nucleosynthesis in carbon deflagration models of Type I supernovae. Astron Astrophys 158(1–2):17–33

Thielemann FK, Eichler M, Panov IV, Wehmeyer B (2017) Neutron star mergers and nucleosynthesis of heavy elements. Annu Rev Nucl Part Sci 67:253–274. https://doi.org/10.1146/annurev-nucl-101916-123246

Thielemann FK, Wehmeyer B, Wu MR (2020) r-Process sites, their ejecta composition, and their imprint in galactic chemical evolution. J Phys Conf Ser 1668:012044. https://doi.org/10.1088/1742-6596/1668/1/012044

Thielemann FK, Farouqi K, Rosswog S, Kratz KL (2022) r-Process contributions to low-metallicity stars. Eur Phys J Web Conf 260:09002. https://doi.org/10.1051/epjconf/202226009002

Thompson TA, Burrows A, Meyer BS (2001) The physics of proto-neutron star winds: implications for r-process nucleosynthesis. Astrophys J 562:887–908. https://doi.org/10.1086/323861

Timmes FX (1999) Integration of nuclear reaction networks for stellar hydrodynamics. Astrophys J Suppl 124:241–263. https://doi.org/10.1086/313257

Tinsley BM (1968) Evolution of the stars and gas in galaxies. Astrophys J 151:547. https://doi.org/10.1086/149455

Tinsley BM (1972) Galactic evolution. Astron Astrophys 20:383

Tinsley BM (1980) Evolution of the stars and gas in galaxies. Front Cosmic Phys 5:287–388

Travaglio C, Gallino R, Arnone E, Cowan J, Jordan F, Sneden C (2004) Galactic evolution of Sr, Y, And Zr: a multiplicity of nucleosynthetic processes. Astrophys J 601:864–884

Travaglio C, Röpke FK, Gallino R, Hillebrandt W (2011) Type Ia supernovae as sites of the p-process: two-dimensional models coupled to nucleosynthesis. Astrophys J 739(2):93. https://doi.org/10.1088/0004-637X/739/2/93. arXiv:1106.0582 [astro-ph.SR]

Travaglio C, Gallino R, Rauscher T, Röpke FK, Hillebrandt W (2015) Testing the role of SNe Ia for galactic chemical evolution of p-nuclei with two-dimensional models and with s-process seeds at different metallicities. Astrophys J 799(1):54. https://doi.org/10.1088/0004-637X/799/1/54. arXiv:1411.2399 [astro-ph.SR]

Travaglio C, Rauscher T, Heger A, Pignatari M, West C (2018) Role of core-collapse supernovae in explaining solar system abundances of p nuclides. Astrophys J 854(1):18. https://doi.org/10.3847/1538-4357/aaa4f7. arXiv:1801.01929 [astro-ph.SR]

Truran JW, Cameron AGW (1971) Evolutionary models of nucleosynthesis in the galaxy. Astrophys Space Sci 14(1):179–222. https://doi.org/10.1007/BF00649203

Truran JW, Hansen CJ, Cameron AGW, Gilbert A (1966) Thermonuclear reactions in medium and heavy nuclei. Can J Phys 44:151. https://doi.org/10.1139/p66-011

Tsujimoto T, Nishimura N (2018) Early chemical evolution of Zn driven by magnetorotational supernovae and the pathway to the solar Zn composition. Astrophys J Lett 863(2):L27. https://doi.org/10.3847/2041-8213/aad86b. arXiv:1808.02524 [astro-ph.GA]

Tur C, Heger A, Austin SM (2009) Dependence of s-process nucleosynthesis in massive stars on triple-alpha and $^{12}C(\alpha,\gamma)^{16}O$ reaction rate uncertainties. Astrophys J 702(2):1068–1077. https://doi.org/10.1088/0004-637X/702/2/1068. arXiv:0809.0291 [astro-ph]

Ugliano M, Janka HT, Marek A, Arcones A (2012) Progenitor-explosion connection and remnant birth masses for neutrino-driven supernovae of iron-core progenitors. Astrophys J 757(1):69. https://doi.org/10.1088/0004-637X/757/1/69. arXiv:1205.3657 [astro-ph.SR]

Ulrich RK, Scalo JM (1972) A model for the chemical evolution of S and N star envelopes. Astrophys J Lett 176:L37. https://doi.org/10.1086/181015

van de Voort F, Pakmor R, Grand RJJ, Springel V, Gómez FA, Marinacci F (2020) Neutron star mergers and rare core-collapse supernovae as sources of r-process enrichment in simulated galaxies. MNRAS 494(4):4867–4883. https://doi.org/10.1093/mnras/staa754. arXiv:1907.01557 [astro-ph.GA]

Varma V, Mueller B, Schneider FRN (2022) 3D Simulations of strongly magnetised non-rotating supernovae: explosion dynamics and remnant properties. arXiv e-prints arXiv:2204.11009 [astro-ph.HE]

Vartanyan D, Coleman MSB, Burrows A (2022) The collapse and three-dimensional explosion of three-dimensional massive-star supernova progenitor models. MNRAS 510(4):4689–4705. https://doi.org/10.1093/mnras/stab3702. arXiv:2109.10920 [astro-ph.SR]

Vasini A, Matteucci F, Spitoni E (2022) Chemical evolution of ^{26}Al and ^{60}Fe in the Milky Way. arXiv e-prints arXiv:2204.00510 [astro-ph.GA]

Vescovi D, Reifarth R (2021) s-Processing in asymptotic giant branch stars in the light of revised neutron-capture cross sections. Universe 7(7):239. https://doi.org/10.3390/universe7070239

Vescovi D, Cristallo S, Palmerini S, Abia C, Busso M (2021) Magnetic-buoyancy-induced mixing in AGB stars: fluorine nucleosynthesis at different metallicities. Astron Astrophys 652:A100. https://doi.org/10.1051/0004-6361/202141173. arXiv:2106.08241 [astro-ph.SR]

Villar VA, Cowperthwaite PS, Berger E, Blanchard PK, Gomez S, Alexander KD, Margutti R, Chornock R, Eftekhari T, Fazio GG, Guillochon J, Hora JL, Nicholl M, Williams PKG (2018) Spitzer Space Telescope infrared observations of the binary neutron star merger GW170817. Astrophys J Lett 862:L11. https://doi.org/10.3847/2041-8213/aad281

Wagoner RV, Fowler WA, Hoyle F (1967) On the synthesis of elements at very high temperatures. Astrophys J 148:3. https://doi.org/10.1086/149126

Walker TP, Steigman G, Schramm DN, Olive KA, Kang HS (1991) Primordial nucleosynthesis redux. Astrophys J 376:51–69. https://doi.org/10.1086/170255

Wanajo S (2006) The rp-process in neutrino-driven winds. Astrophys J 647:1323–1340. https://doi.org/10.1086/505483

Wanajo S, Sekiguchi Y, Nishimura N, Kiuchi K, Kyutoku K, Shibata M (2014) Production of all the r-process nuclides in the dynamical ejecta of neutron star mergers. Astrophys J 789:L39. https://doi.org/10.1088/2041-8205/789/2/L39

Wanajo S, Müller B, Janka HT, Heger A (2018) Nucleosynthesis in the innermost ejecta of neutrino-driven supernova explosions in two dimensions. Astrophys J 852(1):40. https://doi.org/10.3847/1538-4357/aa9d97. arXiv:1701.06786 [astro-ph.SR]

Watson D, Hansen CJ, Selsing J, Koch A, Malesani DB, Andersen AC, Fynbo JPU, Arcones A, Bauswein A, Covino S, Grado A, Heintz KE, Hunt L, Kouveliotou C, Leloudas G, Levan AJ, Mazzali P, Pian E (2019) Identification of strontium in the merger of two neutron stars. Nature 574:497–500. https://doi.org/10.1038/s41586-019-1676-3

Weaver TA, Zimmerman GB, Woosley SE (1978) Presupernova evolution of massive stars. Astrophys J 225:1021–1029. https://doi.org/10.1086/156569

Webbink RF (1984) Double white dwarfs as progenitors of R Coronae Borealis stars and type I supernovae. Astrophys J 277:355–360. https://doi.org/10.1086/161701

Wehmeyer B, Pignatari M, Thielemann FK (2015) Galactic evolution of rapid neutron capture process abundances: the inhomogeneous approach. MNRAS 452:1970–1981. https://doi.org/10.1093/mnras/stv1352.. arXiv:1501.07749

Weinberg S (1972) Gravitation and cosmology: principles and applications of the general theory of relativity. Wiley-VCH

Weinberger C, Diehl R, Pleintinger MMM, Siegert T, Greiner J (2020) ^{44}Ti ejecta in young supernova remnants. Astron Astrophys 638:A83. https://doi.org/10.1051/0004-6361/202037536. arXiv:2004.12688 [astro-ph.HE]

Wheeler JC, Sneden C, Truran JW Jr (1989) Abundance ratios as a function of metallicity. Annu Rev Astron Astrophys 27:279–349. https://doi.org/10.1146/annurev.aa.27.090189.001431

Wiescher M, Gorres J, Thielemann FK, Ritter H (1986) Explosive hydrogen burning in novae. Astron Astrophys 160:56–72

Wiescher M, Azuma RE, Gasques L, Görres J, Pignatari M, Simpson E (2006) Charged particle reaction rates from stellar H to C burning. Mem SAIt 77:910

Wiescher M, Käppeler F, Langanke K (2012) Critical reactions in contemporary nuclear astrophysics. Annu Rev Astron Astrophys 50:165–210. https://doi.org/10.1146/annurev-astro-081811-125543

Winteler C, Käppeli R, Perego A, Arcones A, Vasset N, Nishimura N, Liebendörfer M, Thielemann FK (2012) Magnetorotationally driven supernovae as the origin of early galaxy r-process elements? Astrophys J Lett 750:L22. https://doi.org/10.1088/2041-8205/750/1/L22

Witt M, Psaltis A, Yasin H, Horn C, Reichert M, Kuroda T, Obergaulinger M, Couch SM, Arcones A (2021) Post-explosion evolution of core-collapse supernovae. Astrophys J 921(1):19. https://doi.org/10.3847/1538-4357/ac1a6d. arXiv:2107.00687 [astro-ph.HE]

Witze A (2019) How long do neutrons live? Physicists close in on decades-old puzzle. Nature 568 (7753):442–443. https://doi.org/10.1038/d41586-019-01203-9

Wongwathanarat A, Janka HT, Müller E, Pllumbi E, Wanajo S (2017) Production and distribution of ^{44}Ti and ^{56}Ni in a three-dimensional supernova model resembling Cassiopeia A. Astrophys J 842(1):13. https://doi.org/10.3847/1538-4357/aa72de. arXiv:1610.05643 [astro-ph.HE]

Woosley SE, Bloom JS (2006) The supernova gamma-ray burst connection. Annu Rev Astron Astrophys 44(1):507–556. https://doi.org/10.1146/annurev.astro.43.072103.150558.. arXiv:astro-ph/0609142 [astro-ph]

Woosley SE, Heger A (2006) The progenitor stars of gamma-ray bursts. Astrophys J 637:914–921. https://doi.org/10.1086/498500. arXiv:astro-ph/0508175

Woosley SE, Howard WM (1978) The p-processes in supernovae. Astrophys J Suppl 36:285–304. https://doi.org/10.1086/190501

Woosley SE, Weaver TA (1986) The physics of supernova explosions. Annu Rev Astron Astrophys 24:205–253. https://doi.org/10.1146/annurev.aa.24.090186.001225

Woosley SE, Weaver TA (1995) The evolution and explosion of massive stars. II. Explosive hydrodynamics and nucleosynthesis. Astrophys. J. Suppl. 101:181. https://doi.org/10.1086/192237

Woosley SE, Fowler WA, Holmes JA, Zimmerman BA (1978) Semiempirical thermonuclear reaction-rate data for intermediate-mass nuclei. At Data Nucl Data Tables 22:371. https://doi.org/10.1016/0092-640X(78)90018-9

Woosley SE, Taam RE, Weaver TA (1986) Models for type I supernova. I. Detonations in white dwarfs. Astrophys J 301:601. https://doi.org/10.1086/163926

Woosley SE, Hartmann DH, Hoffman RD, Haxton WC (1990) The *v*-process. Astrophys J 356:272–301. https://doi.org/10.1086/168839

Woosley SE, Wilson JR, Mathews GJ, Hoffman RD, Meyer BS (1994) The r-process and neutrino-heated supernova ejecta. Astrophys J 433:229–246. https://doi.org/10.1086/174638

Wu MR, Fischer T, Huther L, Martínez-Pinedo G, Qian YZ (2014) Impact of active-sterile neutrino mixing on supernova explosion and nucleosynthesis. Phys Rev D 89:061303(R). https://doi.org/10.1103/PhysRevD.89.061303

Wu MR, Fernández R, Martínez-Pinedo G, Metzger BD (2016) Production of the entire range of r-process nuclides by black hole accretion disc outflows from neutron star mergers. MNRAS 463:2323–2334. https://doi.org/10.1093/mnras/stw2156

Wu MR, et al. (2017) unpublished

Wu MR, Barnes J, Martínez-Pinedo G, Metzger BD (2019) Fingerprints of heavy-element nucleosynthesis in the late-time lightcurves of kilonovae. Phys Rev Lett 122:062701. https://doi.org/10.1103/PhysRevLett.122.062701

Xu Y, Takahashi K, Goriely S, Arnould M, Ohta M, Utsunomiya H (2013) NACRE II: an update of the NACRE compilation of charged-particle-induced thermonuclear reaction rates for nuclei with mass number $A < 16$. Nucl Phys A 918:61–169. https://doi.org/10.1016/j.nuclphysa.2013.09.007. arXiv:1310.7099 [nucl-th]

Yang J, Turner MS, Steigman G, Schramm DN, Olive KA (1984) Primordial nucleosynthesis–a critical comparison of theory and observation. Astrophys J 281:493–511. https://doi.org/10.1086/162123

Yeh TH, Olive KA, Fields BD (2021) The impact of new d(p,γ)3 rates on big bang nucleosynthesis. J Cosmol Astropart Phys 3:046. https://doi.org/10.1088/1475-7516/2021/03/046. arXiv:2011.13874 [astro-ph.CO]

Yeh TH, Shelton J, Olive KA, Fields BD (2022) Probing physics beyond the standard model: limits from BBN and the CMB independently and combined. J Cosmol Astropart Phys 10:046. https://doi.org/10.1088/1475-7516/2022/10/046. arXiv:2207.13133 [astro-ph.CO]

Zha S, Leung SC, Suzuki T, Nomoto K (2019) Evolution of ONeMg Core in super-AGB stars toward electron-capture supernovae: effects of updated electron-capture rate. Astrophys J 886(1):22. https://doi.org/10.3847/1538-4357/ab4b4b. arXiv:1907.04184 [astro-ph.HE]

Zhu Y et al (2018) Californium-254 and kilonova light curves. Astrophys J 863:L23. https://doi.org/10.3847/2041-8213/aad5de

Zhu YL, Lund KA, Barnes J, Sprouse TM, Vassh N, McLaughlin GC, Mumpower MR, Surman R (2021) Modeling kilonova light curves: dependence on nuclear inputs. Astrophys J 906(2):94. https://doi.org/10.3847/1538-4357/abc69e. arXiv:2010.03668 [astro-ph.HE]

Zingale M, Almgren AS, Barrios Sazo MG, Beckner VE, Bell JB, Friesen B, Jacobs AM, Katz MP, Malone CM, Nonaka AJ, Willcox DE, Zhang W (2018) Meeting the challenges of modeling astrophysical thermonuclear explosions: castro, maestro, and the AMReX astrophysics suite. J Phys Conf Ser 1031:012024. https://doi.org/10.1088/1742-6596/1031/1/012024. arXiv:1711.06203 [astro-ph.IM]

Zinner E (1998) Isotopic abundances in presolar grains from meteorites: implications for stellar nucleosynthesis. In: Mezzacappa A (ed) Stellar evolution, stellar explosions, and galactic chemical evolution. Institute of Physics Publishing, p 345

Zinner E (2008a) Stardust in meteorites: a link between stars and the Solar System. In: Kwok S, Sanford S (eds) Organic Matter in Space. IAU Symposium, vol 251. pp 341–342. https://doi.org/10.1017/S174392130802190X

Zinner E (2008) Stardust in the laboratory. Publ Astron Soc Aust 25(1):7–17. https://doi.org/10.1071/AS07039

Zinner E, Amari S (1999) Presolar grains from meteorites: AGB star matter in the laboratory. In: Le Bertre T, Lebre A, Waelkens C (eds) Asymptotic Giant Branch Stars. IAU Symposium, vol 191. Astronomical Society of the Pacific, p 59

Publisher's Note Springer Nature remains neutral with regard to jurisdictional claims in published maps and institutional affiliations.

Authors and Affiliations

Almudena Arcones[1,2] · Friedrich-Karl Thielemann[2,3]

✉ Friedrich-Karl Thielemann
f-k.thielemann@unibas.ch

Almudena Arcones
almudena.arcones@physik.tu-darmstadt.de

[1] Institut für Kernphysik, Technische Universität Darmstadt, 64289 Darmstadt, Germany

[2] GSI Helmholtzzentrum für Schwerionenforschung GmbH, 64291 Darmstadt, Germany

[3] Department of Physics, University of Basel, Klingelbergstrasse 82, 4056 Basel, Switzerland